Public Disclosure Authorized

Public Disclosure Authorized

Public Disclosure Authorized

THE WORLD BANK
IBRD • IDA | WORLD BANK GROUP

ESMAP
Energy Sector Management Assistance Program

SOLAR RESOURCE AND PV POTENTIAL OF THE MALDIVES

24 MONTH SOLAR RESOURCE REPORT

September 2018

This report was prepared by Solargis, under contract to The World Bank.

It is one of several outputs from the solar resource mapping component of the activity "Renewable Energy Resource Mapping and Geospatial Planning – Maldives" [Project ID: P146018]. This activity is funded and supported by the Energy Sector Management Assistance Program (ESMAP), a multi-donor trust fund administered by The World Bank, under a global initiative on Renewable Energy Resource Mapping. Further details on the initiative can be obtained from the ESMAP website.

This document is a **final output** from the above-mentioned project, and the content is the sole responsibility of the consultant authors. Users are strongly advised to exercise caution when utilizing the information and data contained, as this may include preliminary data and/or findings, and the document has not been subject to full peer review. Final outputs from this project will be marked as such, and any improved or validated solar resource data will be incorporated into the Global Solar Atlas.

Copyright © 2018 THE WORLD BANK
Washington DC 20433
Telephone: +1-202-473-1000
Internet: www.worldbank.org

The World Bank, comprising the International Bank for Reconstruction and Development (IBRD) and the International Development Association (IDA), is the commissioning agent and copyright holder for this publication. However, this work is a product of the consultants listed, and not of World Bank staff. The findings, interpretations, and conclusions expressed in this work do not necessarily reflect the views of The World Bank, its Board of Executive Directors, or the governments they represent.

The World Bank does not guarantee the accuracy of the data included in this work and accept no responsibility for any consequence of their use. The boundaries, colors, denominations, and other information shown on any map in this work do not imply any judgment on the part of The World Bank concerning the legal status of any territory or the endorsement or acceptance of such boundaries.

The material in this work is subject to copyright. Because The World Bank encourages dissemination of its knowledge, this work may be reproduced, in whole or in part, for non-commercial purposes as long as full attribution to this work is given. Any queries on rights and licenses, including subsidiary rights, should be addressed to World Bank Publications, The World Bank Group, 1818 H Street NW, Washington, DC 20433, USA; fax: +1-202-522-2625; e-mail: pubrights@worldbank.org. Furthermore, the ESMAP Program Manager would appreciate receiving a copy of the publication that uses this publication for its source sent in care of the address above, or to esmap@worldbank.org.

Annual Solar Resource Report

for solar meteorological stations after completion of 24 months of measurements

Republic of Maldives

Reference No. 129-07/2018

Date: 26 September 2018

Customer

World Bank
Energy Sector Management Assistance Program
Contact: Mr. Sandeep Kohli
1818 H St NW, Washington DC, 20433, USA
Phone: +1-202-361-0033
E-mail: skohli@worldbank.org
http://www.esmap.org/RE_Mapping

Consultant

Solargis s.r.o.
Contact: Mr. Marcel Suri
Mytna 48, 811 07 Bratislava, Slovakia
Phone +421 2 4319 1708
E-mail: marcel.suri@solargis.com
http://solargis.com

TABLE OF CONTENTS

Table of contents **4**
Acronyms **6**
Glossary **7**
1 Introduction **9**
1.1 Background 9
1.1 Delivered data sets 9
1.2 Information included in this report 10
2 Position of solar meteorological sites **11**
3 Ground measurements in Maldives **13**
3.1 Instruments and measured parameters 13
3.2 Station operation and instruments' field verification 14
3.3 Quality control of measured solar resource data 17
3.3.1 Hanimaadhoo Airport 17
3.3.2 Hulhulé Airport 21
3.3.3 Kadhdhoo Airport 25
3.3.4 Gan Airport 29
3.4 Recommendations on the operation and maintenance of the sites 33
3.5 Instruments re-calibration at the end of measurement campaign 33
4 Solar resource model data **36**
4.1 Solar model 36
4.2 Site adaptation of the solar model – method 37
4.3 Results of the model adaptation at four sites 39
5 Meteorological model data **46**
5.1 Meteorological model 46
5.2 Validation of meteorological data 46
5.2.1 Air temperature at 2 metres 47
5.2.2 Relative humidity 49
5.2.3 Wind speed and wind direction at 10 metres 52
5.2.4 Atmospheric pressure 54
5.3 Uncertainty of meteorological model data 54
6 Solar resource: uncertainty of longterm estimates **56**
6.1 Uncertainty of solar resource yearly estimate 56
6.2 Uncertainty due to interannual variability of solar radiation 57
6.3 Combined uncertainty 59
7 Time series and Typical Meteorological Year data **62**
7.1 Delivered data sets 62
7.2 TMY method 63
7.3 Results 63
8 Conclusions **68**
Annex 1: Site related data statistics **69**

© 2018 Solargis

Yearly summaries of solar and meteorological parameters....69
Monthly summaries of solar and meteorological parameters....71
Frequency of occurrence of GHI and DNI daily model values for a period 1999 to 2017....73
Frequency of occurrence of GHI and DNI 30-minute model values for a period 1999 to 2017....77
Frequency of occurrence of GHI and DNI measured and model values....81
List of figures....87
List of tables....89
References....91
Support information....93
Background on Solargis....**Error! Bookmark not defined.**
Legal information....**Error! Bookmark not defined.**

ACRONYMS

AP	Atmospheric Pressure
CFSR	Climate Forecast System Reanalysis. The meteorological model operated by the US service NOAA (National Oceanic and Atmospheric Administration)
CFS v2	Climate Forecast System Version 2 CFSv2 model is the operational extension of the CFSR (NOAA, NCEP)
DIF	Diffuse Horizontal Irradiation, if integrated solar energy is assumed. Diffuse Horizontal Irradiance, if solar power values are discussed
DNI	Direct Normal Irradiation, if integrated solar energy is assumed. Direct Normal Irradiance, if solar power values are discussed.
GFS	Global Forecast System. The meteorological model operated by the US service NOAA (National Oceanic and Atmospheric Administration)
GHI	Global Horizontal Irradiation, if integrated solar energy is assumed. Global Horizontal Irradiance, if solar power values are discussed.
MACC	Monitoring Atmospheric Composition and Climate – meteorological model operated by the European service ECMWF (European Centre for Medium-Range Weather Forecasts)
Meteosat IODC (MFG)	Meteosat satellites operated by EUMETSAT organization. MFG: Meteosat First Generation. For this report the data from the Meteosat IODC are used. The satellite is positioned over the Indian Ocean.
PWAT	Precipitable water (water vaour)
QC	Quality control
RH	Relative Humidity at 2 metres
TEMP	Air Temperature at 2 metres
WD	Wind Direction at 10 metres
WS	Wind Speed at 10 metres

© 2018 Solargis

GLOSSARY

Aerosols	Small solid or liquid particles suspended in air, for example desert sand or soil particles, sea salts, burning biomass, pollen, industrial and traffic pollution.
All-sky irradiance	The amount of solar radiation reaching the Earth's surface is mainly determined by Earth-Sun geometry (the position of a point on the Earth's surface relative to the Sun which is determined by latitude, the time of year and the time of day) and the atmospheric conditions (the level of cloud cover and the optical transparency of atmosphere). All-sky irradiance is computed with all factors taken into account
Bias	Represents systematic deviation (over- or underestimation) and it is determined by systematic or seasonal issues in cloud identification algorithms, coarse resolution and regional imperfections of atmospheric data (aerosols, water vapour), terrain, sun position, satellite viewing angle, microclimate effects, high mountains, etc.
Clear-sky irradiance	The clear sky irradiance is calculated similarly to all-sky irradiance but without taking into account the impact of cloud cover.
Long-term average	Average value of selected parameter (GHI, DNI, etc.) based on multiyear historical time series. Long-term averages provide a basic overview of solar resource availability and its seasonal variability.
P50 value	Best estimate or median value represents 50% probability of exceedance. For annual and monthly solar irradiation summaries it is close to average, since multiyear distribution of solar radiation resembles normal distribution.
P90 value	Conservative estimate, assuming 90% probability of exceedance (with the 90% probability the value should be exceeded). When assuming normal distribution, the P90 value is also a lower boundary of the 80% probability of occurrence. P90 value can be calculated by subtracting uncertainty from the P50 value. In this report, we apply a simplified assumption of normal distribution of yearly values.
Root Mean Square Deviation (RMSD)	Represents spread of deviations given by random discrepancies between measured and modelled data and is calculated according to this formula: $$RMSD = \sqrt{\frac{\sum_{k=1}^{n}\left(X^{k}{}_{measured} - X^{k}_{modeled}\right)^{2}}{n}}$$ On the modelling side, this could be low accuracy of cloud estimate (e.g. intermediate clouds), under/over estimation of atmospheric input data, terrain, microclimate and other effects, which are not captured by the model. Part of this discrepancy is natural - as satellite monitors large area (of approx. 3.3 x 3.4 km for MSG satellite), while sensor sees only micro area of approx. 1 sq. centimetre. On the measurement side, the discrepancy may be determined by accuracy/quality and errors of the instrument, pollution of the detector, misalignment, data loggers, insufficient quality control, etc.
Solar irradiance	Solar power (instantaneous energy) falling on a unit area per unit time [W/m^2]. Solar resource or solar radiation is used when considering both irradiance and irradiation.
Solar irradiation	Amount of solar energy falling on a unit area over a stated time interval [Wh/m^2 or kWh/m^2].
Uncertainty of estimate, U_{est}	Is a parameter characterizing the possible dispersion of the values attributed to an estimated irradiance/irradiation values. In this report, uncertainty assessment of the solar resource model estimate is based on a detailed understanding of the achievable accuracy of the solar radiation model and its data inputs (satellite, atmospheric and other data), which is confronted by an extensive data validation experience. The second source of uncertainty is ground measurements. Their quality depends on accuracy of instruments, their maintenance and data quality control. Third contribution to the

© 2018 Solargis

uncertainty is from the site adaptation method where ground-measured and satellite-based data are correlated.

© 2018 Solargis

1 INTRODUCTION

1.1 Background

This report is prepared within Phase 2 of the project *Renewable Energy Resource Mapping for the Republic of the Maldives*. This part of the project focuses on solar resource mapping and measurement services as part of a technical assistance in the renewable energy development implemented by the World Bank in Maldives. It is being undertaken in close coordination with the Ministry of Environment and Energy (MEE) of Maldives, the World Bank's primary country counterpart for this project. This project is funded by the *Energy Sector Management Assistance Program* (ESMAP) and *Asia Sustainable and Alternative Energy Program* (ASTAE), both administered by the World Bank and supported by bilateral donors.

This report summarizes results of two years of the measuring campaign by the project ESMAP at four solar meteorological stations, installed in Maldives as part of the World Bank's ESMAP mission in Maldives. This report describes delivery of site-specific data, site adaptation of solar model, data uncertainty and statistical summary.

This report accompanies delivery of site-specific solar resource and meteorological data for four sites, where solar meteorological stations have been operated. As a result of high-quality operation of the meteorological sits, and site adaptation the Solargis model, reliable historical time series and TMY data is computed. **The delivered time series and Typical Meteorological Year data is ready for use for bankable evaluation of solar energy projects.**

The measurements at four sites, located in Maldives, are provided by Suntrace company (Germany) with assistance of local company Renewable Energy Maldives (REM). The model data for the same sites and related works, together with this report are supplied by Solargis (Slovakia).

1.1 Delivered data sets

The site specific data, provided as part of this delivery, include:

- Solar and meteorological ground measurements, after second level quality assessment (first level delivered by Suntrace), representing period of minimum two years 12/2015 – 12/2017 (extended until 03/2018 and 04/2018)
- Time series, representing last 19 years (01/1999 to 12/2017)
- Typical Meteorological Year data, also representing last 19 calendar years (01/1999 to 12/2017)

The data is delivered in formats ready to use in energy simulation software. This report provides detailed insight of the methodologies and reuslts.

Table 1.1 Delivered data characteristics

Feature	Time coverage	Primary time step	Delivered files
Measurements (Suntrace)	Dec 2015 to Dec 2017* * Planned two-year period extended until March 2018 on sites where threshold 95% of quality data was not reached	1 minute	Quality controlled measurements – 1- minute
Model data – original (Solargis)	Jan 1999 to Dec 2017	30 minutes	Time series – hourly Time series – monthly Time series – yearly
Model data – site adapted (Solargis)	Jan 1999 to Dec 2017	30 minutes	Time series – hourly Time series – monthly Time series – yearly
Model data – site adapted (Solargis)	Jan 1999 to Dec 2017	hourly	Typical Meteorological Year P50 Typical Meteorological Year P90

© 2018 Solargis

Table 1.2 Parameters in the delivered site-adapted time series and TMY data (hourly time step)

Parameter	Acronym	Unit	TS	TMY P50	TMY P90
Global horizontal irradiance	GHI	W/m^2	X	X	X
Direct normal irradiance	DNI	W/m^2	X	X	X
Diffuse horizontal irradiance	DIF	W/m^2	X	X	X
Global tilted irradiance (at optimum angle)	GHI	W/m^2	X	-	-
Solar azimuth	SA	°	X	X	X
Solar elevation	SE	°	X	X	X
Air temperature at 2 metres	TEMP	°C	X	X	X
Wind speed at 10 metres	WS	m/s	X	X	X
Wind direction at 10 metres	WD	°	X	X	X
Relative humidity	RH	%	X	X	X
Air Pressure	AP	hPa	X	X	X
Precipitable Water	PWAT	kg/m^2	X	X	X

1.2 Information included in this report

This report presents:

- Solar resource and meteorological measurements after 24 months of operation
  - Review and quality check of the measured data
  - Calibration procedures and results
  - List and explanation of the occurred disturbances and failures
- Comparison of the measurements to the model and uncertainty analysis
  - Comparison of solar and meteo measurements with the model data
  - Site adaptation of satellite data based on ground measurements and uncertainty estimate
  - Estimate of data uncertainty
- Data analysis (measured vs. modelled)
  - Monthly summaries of solar and meteorological parameters captured at the site
  - Variability of measured solar parameters
  - Frequency of occurrence of GHI and DNI 1-minute and 30-minute values
  - Frequency of occurrence of GHI and DNI 1-minute and 30-minute ramps

© 2018 Solargis

2 POSITION OF SOLAR METEOROLOGICAL SITES

In Maldives, four measuring stations were installed within the ESMAP Solar initiative. All of them have been located at the airports within the premises of Maldives Meteorological Service (Figure 2.1, Table 2.1).

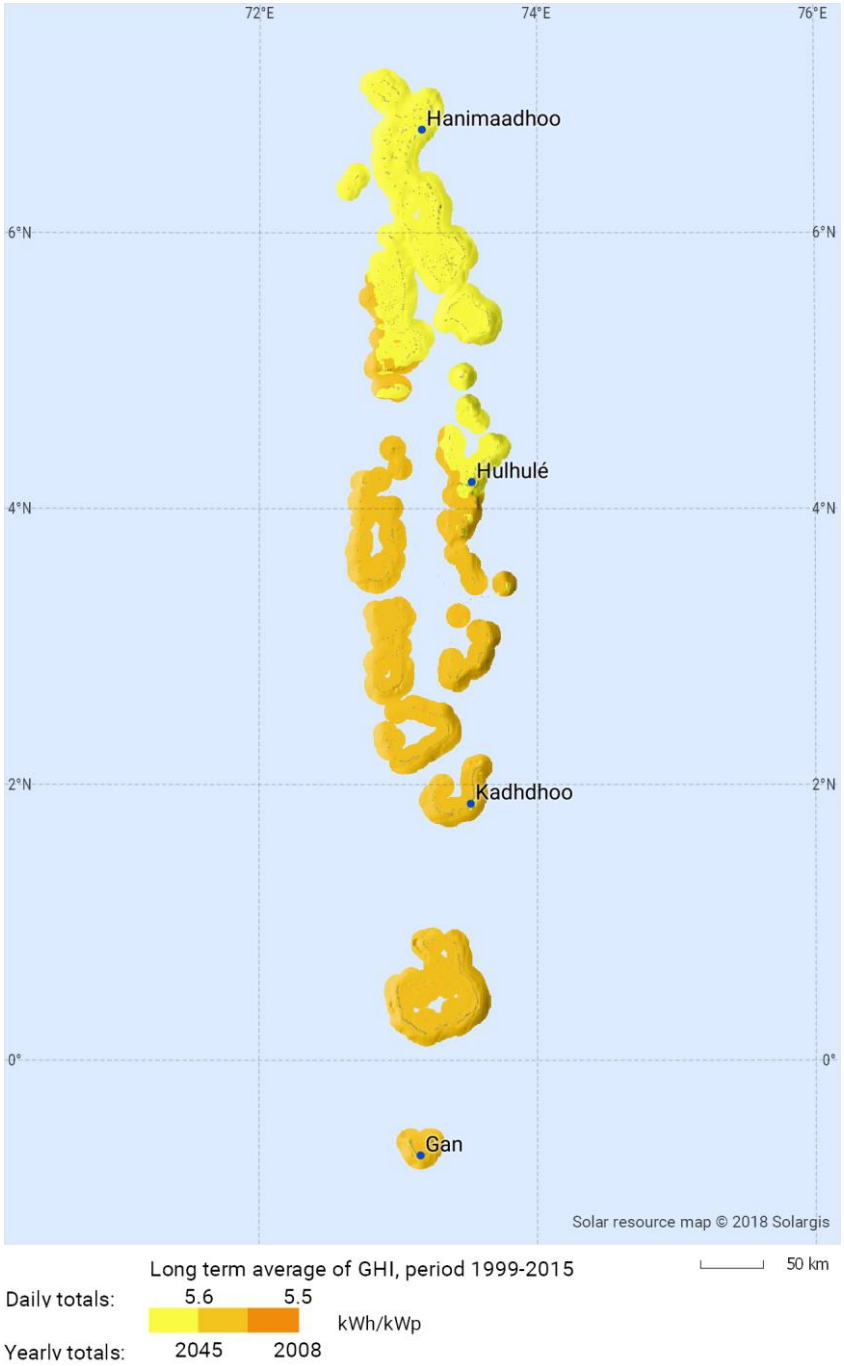

Figure 2.1: Position of solar meteorological stations in Maldives
Map of global horizontal irradiation in the background

Table 2.1 Overview information on the solar meteorological stations installed in Maldives

Site name (airport)	Site ID	Latitude [°]	Longitude [°]	Altitude [m a.s.l.]	Measurement station host
Hanimaadhoo	MVHAQ	6.7482°	73.1696°	2	Hanimaadhoo International Airport
Hulhulé	MVMLE	4.1927°	73.5281°	2	Male International Airport
Kadhdhoo	MVKDO	1.8599°	73.5203°	2	Kadhdhoo Airport
Gan	MVGAN	-0.6911°	73.1599°	2	Gan International Airport

Besides the good geographical distribution within the territory of Maldives, the locations fit well to the population centres, where solar installations can be primarily deployed.

In addition to geographical and socio-economic criteria, the sites fulfil the criteria for the operation and maintenance of the solar measuring stations:

- Availability of free horizon,
- Availability of GSM networks,
- Availability of local work force for maintenance,
- Easy to access and high level of security

During the two years of the measurements, the measured data was analysed and harmonized with the objective to acquire reference solar radiation data for reducing the uncertainty of the model Chapter 6). The quality data from four Tier-2 meteorological stations are available for this assessment (Chapter 3).

Position and detailed information about measurement sites is available also on Global Solar Atlas website: http://globalsolaratlas.info/?c=4.850154,73.146973,6&e=1

© 2018 Solargis

3 GROUND MEASUREMENTS IN MALDIVES

3.1 Instruments and measured parameters

Basic information about measurements sites is in Table 3.1. Solar parameters at all stations are measured by high (SR20, for measurements of GHI) and medium (RSP, for GHI, DNI and DIF) accuracy equipment (Table 3.2 and 3.3). The measurement campaign in Maldives has been performed by Suntrace GmbH company, Germany.

Table 3.1 Overview information on measurement stations operated in the region

ID	Site name (airport)	Site ID	Latitude [°]	Longitude [°]	Altitude [m a.s.l.]	Station type	Installation date
1	Hanimaadhoo	MVHAQ	6.7482°	73.1696°	2	TIER 2	10 Dec 2015
2	Hulhulé	MVMLE	4.1927°	73.5281°	2	TIER 2	08 Dec 2015
3	Kadhdhoo	MVKDO	1.8599°	73.5203°	2	TIER 2	14 Dec 2015
4	Gan	MVGAN	-0.6911°	73.1599°	2	TIER 2	13 Dec 2015

Table 3.2 Instruments installed at the solar meteorological stations

Site name	GHI 1	GHI 2	DNI	DIF	Temp	RH	WS	AP
Hanimaadhoo	SR20 - T1	RSP 4G	RSP 4G	RSP 4G	DKRF 400	DKRF 400	First Class	-
Hulhulé	SR20 - T1	RSP 4G	RSP 4G	RSP 4G	DKRF 400	DKRF 400	First Class	-
Kadhdhoo	SR20 - T1	RSP 4G	RSP 4G	RSP 4G	DKRF 400	DKRF 400	First Class	-
Gan	SR20 - T1	RSP 4G	RSP 4G	RSP 4G	DKRF 400	DKRF 400	First Class	-

Table 3.3 Technical parameters and accuracy class of the instruments

Parameter	Instrument	Type	Manufacturer	Uncertainty
GHI 1	Secondary standard pyranometer	SR20 - T1	Hukseflux	< ±2.0 % (daily)
GHI 2	Rotating Shadowband Irradiometer	RSP 4G	Reichert GmbH	Indicatively ±5 %
DIF	Rotating Shadowband Irradiometer	RSP 4G	Reichert GmbH	Indicatively ±8 %
DNI	Rotating Shadowband Irradiometer	RSP 4G	Reichert GmbH	Indicatively ±5 %
TEMP	Temperature probe	DKRF 400	Driesen und Kern	± 1.5 °C
RH	Relative humidity probe	DKRF 400	Driesen und Kern	± 3.5 % RH
WS	Wind speed sensor (WS at 3.0 m height)	First Class	Thies Clima	< ±1 %
AP	Barometric pressure sensor	Not provided	-	-
-	Data logger	Blueberry	Wilmers GmbH	-

© 2018 Solargis

3.2 Station operation and instruments' field verification

In this report, a complete set of data from of planned 2-year measurement campaign is analysed. As the measurement stations have been installed during December 2015, the regular envisaged period for the data analysis starts in January 2016 and ends in December 2017. However, the limit of 95% of high quality data availability within 2-years period was not fulfilled at three stations (Tab. 3.5). Therefore, the measurement campaign was extended for three to four months more (in Kadhdhoo and Gan until April 2018) to reach this criterion. Overview of the data availability (recovery rate), time step and measured parameters is shown in Table 3.4 to 3.6.

Table 3.4 Overview information on solar meteorological stations operating in the region

Site name(airport)	Site ID	Measurement period	Primary time step
Hanimaadhoo	MVHAQ	11 Dec 2015 to 31 Mar 2018	1 minute
Hulhulé	MVMLE	09 Dec 2015 to 31 Mar 2018	1 minute
Kadhdhoo	MVKDO	15 Dec 2015 to 30 Apr 2018	1 minute
Gan	MVGAN	14 Dec 2015 to 30 Apr 2018	1 minute

Table 3.5 shows data recovery statistics for 2-years period for each station. In this statistics, only serious technical issues (missing data for a longer period, erroneous data - initial installation problem or shading ring problem) are accounted. Short-term and other operational issues (surrounding shading, morning instrument dew, etc.) are not included. *Data loss* column represents amount of missing data or data excluded during quality control process due to technical issues. *Percentage* share is calculated from daytime values and *days* represent cumulative amount of missing data (one day may be composed from several shorter missing data periods). *Influenced days* column represents number of days with fully or partially missing data or days excluded by quality control process. It has to be noted that acceptance criteria were not achieved only for DNI and DIF measured by RSR4 instrument mainly due to shadow ring issue. The GHI measurements for all station fulfilled the requirements.

Table 3.5 Data recovery statistics of the two-year measurement campaign period

Maldives	Data loss*			Influenced days**		Acceptance criteria			
measurement period	Erroneous + missing data			Total	Length of individual periods	DNI, DIF		GHI	
01/2016 - 12/2017	[%]	[days]	Description	[days]	(days)	95%	10+ days	95%	10+ days
Hanimaadhoo	3.6	**26**	shading ring problem	**92**	24, 68	OK	FAIL	OK	OK
Hulhule	7.4	**54**	shading ring problem and missing data	**156**	2, 66, 88	FAIL	FAIL	OK	OK
Kadhdoo	10	**73**	shading ring problem	**172**	64, 108	FAIL	FAIL	OK	OK
Gan	15	**110**	shading ring problem (DNI, DIF) and missing data	**249**	14, 31, 35, 4, 91, 74	FAIL	FAIL	OK	OK

The measurement campaign continued for three to four months more, and measurements were used together with the initial period (December 2015) to re-evaluate the 2-years recovery rate (availability) criteria for DNI and DIF (Table 3.6). First, the data was quality controlled; the measurements affected by serious technical issues were excluded. The most influenced were the measurements from Gan station, where shading ring issue reduced amount of available DNI and DIF data from the extension period, the GHI data was not affected. The valid data from the extension period was added to the valid data from the 2-years period and the 2-years recovery statistics was recalculated for each station. The results (Table 3.6) show that prolonged measurement campaign helped to significantly exceed required 95% recovery rate at all four stations.

© 2018 Solargis

Table 3.6 Data recovery statistics of the measurement campaign period including prolongation

	Two years period (2016-2017)		Measurements extension (2015, 2018)			Recovery rate (Availability)			Acceptance criteria
	Excluded* [%]	Missing to 95% threshold [%]	Length [days]	Excluded* [%]	Valid [days]	two years [%]	extension [%]	two years + extension [%]	95%
Hanimaadhoo	3.6	1.4	111	0.0	111	96.4	15.2	111.6	OK
Hulhule	7.4	-2.4	113	6.5	106	92.6	14.5	107.1	OK
Kadhdoo	10.0	-5.0	136	1.2	134	90.0	18.4	108.4	OK
Gan	15.0	-10.0	137	30.2	96	85.0	13.1	98.1	OK

** Excluded due to technical issues*

Table 3.7 Period of measurements analysed in this report

Year, month Parameter	2015												2016												2017												2018											
	1	2	3	4	5	6	7	8	9	10	11	12	1	2	3	4	5	6	7	8	9	10	11	12	1	2	3	4	5	6	7	8	9	10	11	12	1	2	3	4	5	6	7	8	9	10	11	12
Hanimaadhoo																																															
Hulhulé																																															
Kadhdhoo																																															
Gan																																															

During the measurement campaign, local staff of Maldives Meteorological Service, which was trained by Suntrace, participated on inspection and cleaning of instruments. The local partner Renewable Energy Maldives performed detailed visits and station maintenance after 6 months of meteorological stations operation.

Field verification of instruments was performed by Suntrace GmbH after first year of operation. In particular, one day long comparative measurements of solar radiation parameters has been cross checked with the instruments from the spare parts to proof that sensitivities (calibration constants) remained stable within the instrument specifications,.

According to the results of filed verification of the instruments, the calibration coefficients at Gan, Kadhdhoo and Hulhulé meteorological stations has been updated. Detailed results and discussion is supplied in *Annual maintenance visit reports* delivered separately for each meteorological station in February 2017.

Table 3.8 Meteorological stations maintenance and instruments field verification

Hanimaadhoo - MVHAQ		**Comments and issues**
Station type	Tier 2	• Shading of the pyranometer by wind mast during some minutes in the afternoon in May 2016 – July 2016 and in June 2017. GHI values are replaced by GHI values from the RSP. • TEMP and RH sensor malfunction - on 14.06.2017 the stopped measuring RH and on 22.11.2017 also stopped measuring TEMP. The missing values of RH were replaced by measurements from the MMS meteorological measurement station (distance approx. 10 m) in period June 2017 – March 2018 and missing values of TEMP were replaced in period November 2017 – March 2018.
Instruments cleaning interval [days]	Average: 1.0 Longest: 2	
Verification visits date	31 May 2016 23 Nov 2016 23 Jun 2017 3 to 10 April 2018	
Instruments field verification	GHI – reference SR 20 – T1 DHI 2 – reference RSP 4G DIF – reference RSP 4G DNI – reference RSP 4G	
Hulhulé - MVMLE		**Comments and issues**
Station type	Tier 2	• Incorrect measurements during noontime in period 15.05.2016 – 01.06.2016 until RSR shadowband adaptation • Shading of the pyranometer from wind mast during some minutes in the afternoon in May 2016 – July 2016 and June – August 2017. GHI values are replaced by GHI values from the RSP. • No station cleaning in July 2016
Instruments cleaning interval [days]	Average: 3.9 Longest: 31	
Verification visits date	1 Jun 2016 22 Nov 2016 29 Jun 2017 3 to 10 April 2018	

© 2018 Solargis

Instruments field verification	GHI – reference SR 20 – T1 DHI 2 – reference RSP 4G DIF – reference RSP 4G DNI – reference RSP 4G	• Malfunction of TEMP and RH sensor in 1 – 22 November 2016. The missing values were replaced by 10-minute measurements from the MMS meteorological measurement station (distance approx. 2 m) interpolated to 1-minute resolution. • Replacement of RSR on 29.06.2017 by new calibrated unit, then incorrect measurements during noontime until shadowband adaptation (20.07.2017).
Kadhdhoo - MVKDO		**Comments and issues**
Station type	Tier 2	• The pyranometer is influenced by shading from the wind mast during some minutes in the afternoon in period June – July 2016 and June – July 2017. These values are replaced by GHI values from the RSI. • Malfunction of TEMP and RH sensor in February – April 2018. The missing values were replaced measurements from the MMS meteorological station (distance approx. 10 m). • solar radiation sensors with void calibration February 2018 – April 2018
Instruments cleaning interval [days]	Average: 1.1 Longest: 3	
Verification visits date	30 May 2016 27 Nov 2016 24 Jun 2017 3 to 10 April 2018	
Instruments field verification	GHI – reference SR 20 – T1 DHI 2 – reference RSP 4G DIF – reference RSP 4G DNI – reference RSP 4G	
Gan - MVGAN		**Comments and issues**
Station type	Tier 2	• Incorrect measurements during noontime in period 14.12.2015 – 13.01.2016, then in May 2016, June 2017 – July 2017 and November 2017 – January 2018, due to sun position. • Shading of the pyranometer from wind mast in December 2015 – March 2016, then in October 2016 – December 2016, March 2017 and November 2017 – March 2018. GHI values are replaced by GHI values from the RSP. • Malfunction of TEMP and RH sensor in 01.09.2016 – 13.10.2016 and 23.04.2017 - 27.04.2017. The missing values were replaced by 10-minute measurements from the MMS meteorological measurement station (distance approx. 10 m) interpolated to 1-minute resolution. • RSR measurements outage due to low battery voltage in period from 16.12.2016 to 19.12.2016 • February 2018 – April 2018 solar radiation sensors with void calibration
Instruments cleaning interval [days]	Average: 1.2 Longest: 5	
Verification visits date	28 May 2016 25 Nov 2016 25 June 2017 3 to 10 April 2018	
Instruments field verification	GHI – reference SR 20 – T1 DHI 2 – reference RSP 4G DIF – reference RSP 4G DNI – reference RSP 4G	

At the end of measurement campaign, the re-calibration of instruments and handing-over of measurement stations to local authority is planned. These tasks will be performed by Suntrace, procedures are described in detail in Chapter 3.5.

© 2018 Solargis

3.3 Quality control of measured solar resource data

Prior to correlation with satellite-based solar data, the ground-measured solar radiation was quality-controlled by Solargis. Quality control (QC) was based on methods defined in SERI QC procedures and Younes et al. [1, 2] and the in-house developed tests. The ground measurements were inspected also visually, mainly for identification of shading and other error patterns such as RSP shading ring malfunction.

Figures 3.1 to 3.12 show results of quality control for individual stations. The colours in Figures 3.1, 3.3, 3.6 and 3.9 indicate the following flags:

- Blue: data excluded by visual inspection - mainly shading, shading ring issues
- Green: data passed all tests
- Grey: sun below horizon
- White and brown strips: missing data
- Red: GHI, DNI and DIF consistency problem
- Violet and cyan: physical limit problem.

The data records not passing the quality control test were flagged and excluded from the further processing (Tables 3.10, 3.13, 3.16 and 3.19). The results show relatively small amount of excluded GHI data readings, mainly due to local shading occurring in the early morning and late afternoon. The amount of excluded DNI data samples is considerably higher, mainly due to shadowband issues and shading.

3.3.1 Hanimaadhoo Airport

Table 3.9 Occurrence of data readings for Hanimaadhoo meteorological station

Data availability	GHI SR20		GHI, DNI RSP	
Sun below horizon	602,004	49.7%	602,004	49.7%
Sun above horizon	610,415	50.3%	610,415	50.3%
Total data readings	1,212,419	100.0%	1,212,419	100.0%

Table 3.10 Excluded ground measurements after quality control (Sun above horizon) in Hanimaadhoo

Type of test	Occurrence of data samples (Sun above horizon)					
	GHI SR20		DNI RSP		GHI RSP	
Physical limits test	431	0.1%	0	0.0%	2,631	0.4%
Consistency test (GHI – DNI – DIF)	-	-	149	0.0%	149	0.0%
Visual test (incorrect data)	43,072	7.1%	62,451	10.2%	41,536	6.8%
Other (non valid data)	98	0.0%	166	0.0%	166	0.0%
Total excluded data samples	43,601	7.1%	62,766	10.3%	44,482	7.3%
Total samples	610,415	100.0%	610,415	100.0%	610,415	100.0%

© 2018 Solargis

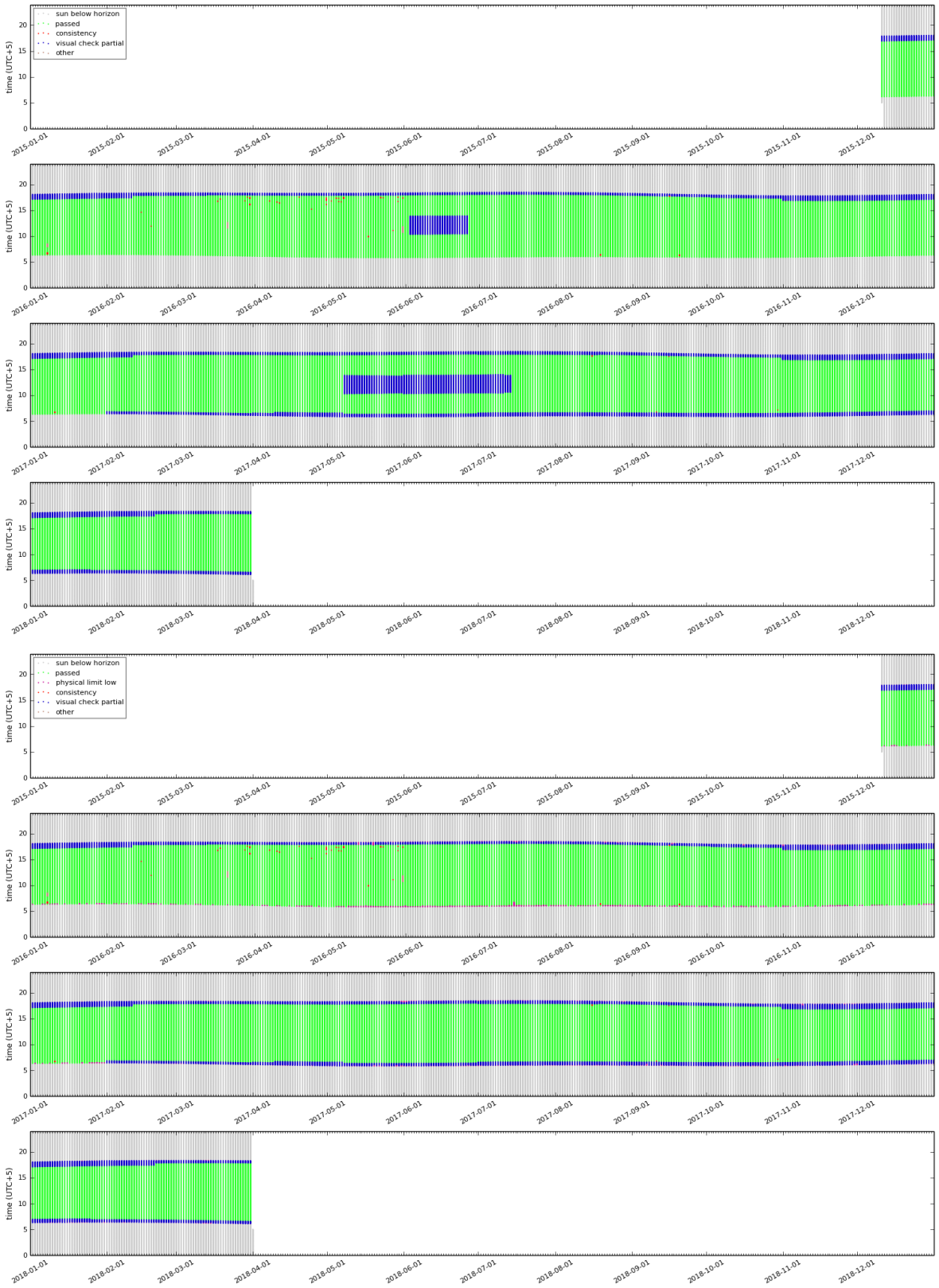
sun below horizon
passed
consistency
visual check partial
other
time (UTC+5)
sun below horizon
passed
physical limit low
consistency
visual check partial
other
time (UTC+5)

Figure 3.1 Results of DNI and GHI quality control in Hanimaadhoo.
Green – data passing all tests; grey – sun below horizon; red – consistency issue,
violet and cyan – physical limit, blue excluded by visual inspection.
Top: DNI (RSP); middle: GHI (RSP); bottom: GHI (SR20)

Main findings:

- Shadowband malfunction. Due to location of measurement station close to the Equator the rotating shadowband did not in some periods sufficiently shade the sensor. This insufficient shading results in incorrect DNI and DIF measurements. This problem was identified for period from 3 to 26 June 2016 and 8 May to 14 July 2017 around the noon. Approximately 3.1% of DNI and DIF measurements were excluded.
- A systematic difference between GHI measurements from secondary standard pyranometer SR20-T1 and RSP (Figure 3.4). GHI from SR20 is in average higher by 5.3% than GHI from RSP. In the noon time, it can exceed 7%. The overall difference in 2016 was 4.5% while in 2017 it was 5.7%.
- Late afternoon shading from surrounding objects. Since February 2017 also early morning shading.
- GHI measurements from SR20 were replaced by data from RSP in case of shading from wind mast (see Table 3.8).

© 2018 Solargis

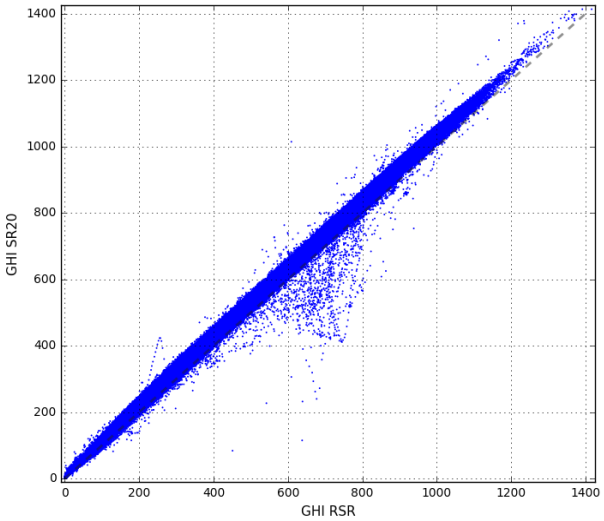

Figure 3.2 Systematic difference between GHI from SR20 and RSP – Hanimaadhoo.

Table 3.11 Quality control summary – Hanimaadhoo

Indicator	Flag	Description
Station description, metadata		Installation report available
Instrument accuracy		1x Secondary standard pyranometer SR20-T1 (GHI)
		1x Rotating Shadowband Radiometer RSP 4G(GHI, DIF, DNI)
Instrument calibration		Instruments were calibrated
Data structure		Clear
Cleaning and maintenance information		Cleaning log available Diligent cleaning
Time reference		Correct and clear time reference
Quality control complexity		RSP G4 data, full QC comparison of GHI from RSP and SR20
Quality control results		Except for period of ca 3 months (noontime), dues to shadowband malfunction Early morning and late afternoon shading Inconsistency between of RSP and SR20 measurements – increasing in time
Availability of high quality data		More than 27 months, DNI ca 26 months due to shadowband malfunction
Other issues		

Legend: Quality flag

Very good	Good	Sufficient	Problematic	Insufficient	Not specified

3.3.2 Hulhulé Airport

Table 3.12 Occurrence of data readings for Hulhulé meteorological station

Data availability	GHI SR20		GHI, DNI RSP	
Sun below horizon	603,061	49.6%	603,061	49.6%
Sun above horizon	612,238	50.4%	612,238	50.4%
Total data readings	1,215,299	100.0%	1,215,299	100.0%

Table 3.13 Excluded ground measurements after quality control (Sun above horizon) in Hulhulé

Type of test	Occurrence of data samples (Sun above horizon)					
	GHI SR20		DNI RSP		GHI RSP	
Physical limits test	498	0.1%	3	0.0%	2,540	0.4%
Consistency test (GHI – DNI – DIF)	-	-	576	0.1%	576	0.1%
Visual test (incorrect data)	29,425	4.8%	62,727	10.2%	33,313	5.4%
Other (non valid data)	101	0.0%	11,356	1.9%	910	0.1%
Total excluded data samples	30,024	4.9%	74,662	12.2%	37,339	6.1%
Total samples	612,238	100.0%	612,238	100.0%	612,238	100.0%

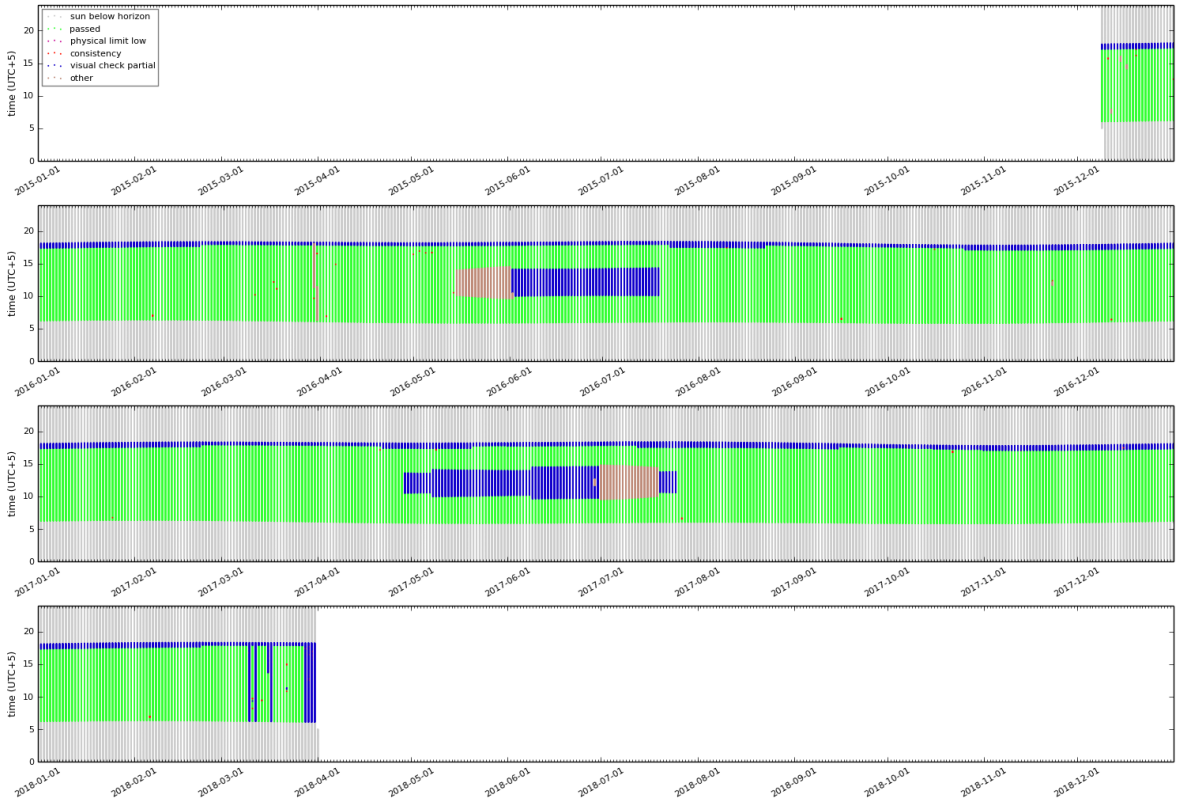

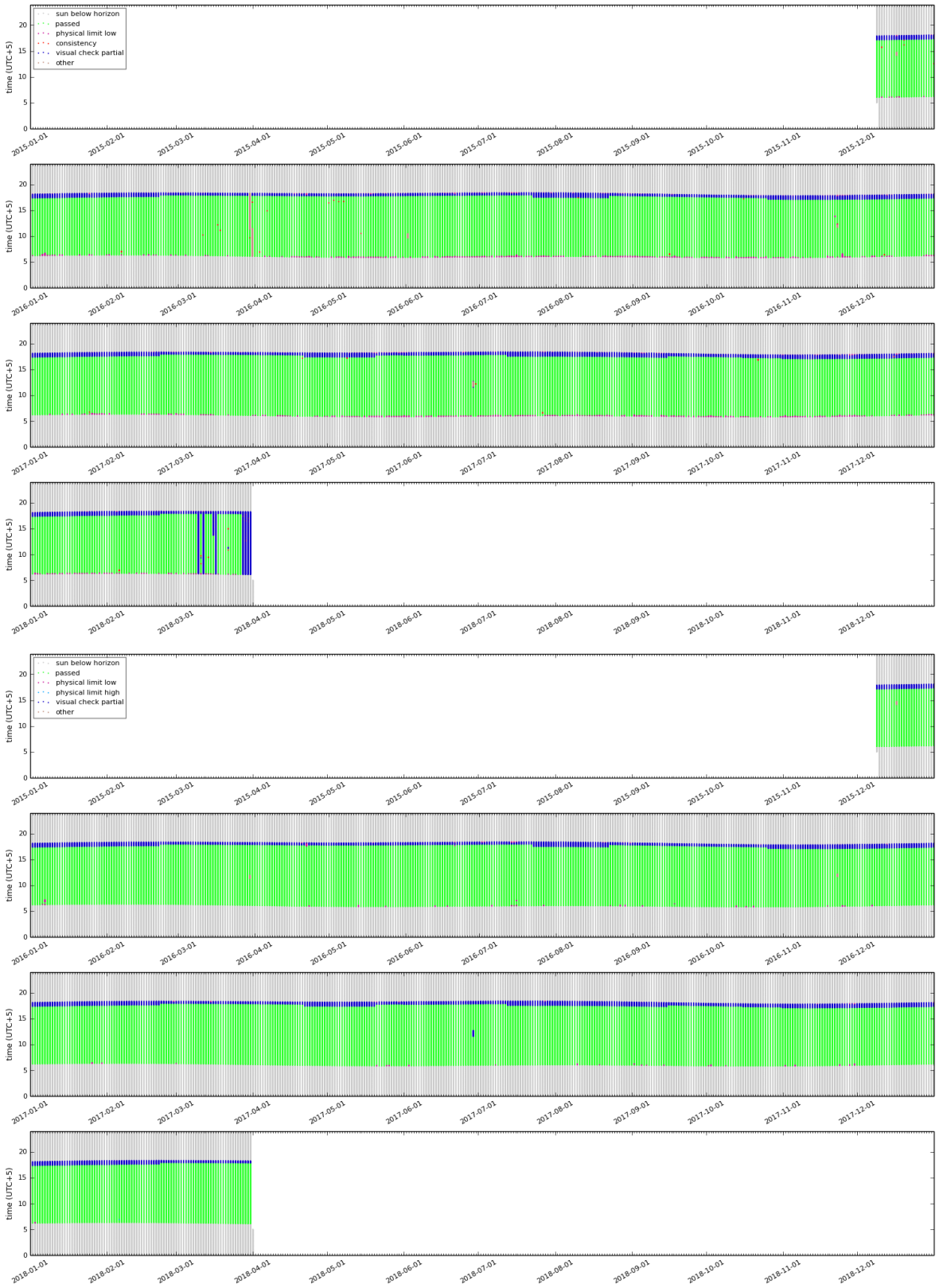

Figure 3.3 Results of DNI and GHI quality control in Hulhulé.
Green – data passing all tests; grey – sun below horizon; red – consistency issue,
cyan and violet – physical limit issue, blue excluded by visual inspection; brown – missing data.
Top: DNI (RSP); middle: GHI (RSP); bottom: GHI (SR20)

Main findings:

- Shadowband malfunction (Figure 3.4). This issue was identified for a period from 15 May to 19 July 2016 and from 29 April to 25 July 2017 around the noon. Affected data readings in May 2016 and July 2017 were excluded by data provider, remaining affected readings were excluded by quality control. Approximately 5.6% of DNI and DIF measurements were excluded in total.
- A systematic difference between GHI measurements from secondary standard pyranometer SR20-T1 and RSP (Figure 3.5). GHI from SR20 is in average higher by 7.4% than GHI from RSP. In the noontime the difference can exceed 10%. The overall difference in 2016 was 6.8% while in 2017 it was 8.1%.
- Late afternoon shading from surrounding objects
- GHI measurements from SR20 were replaced by data from RSP in case of shading from wind mast (see Table 3.8).
- Malfunction of RSP instrument (GHI, DNI, DIF) in the end of March 2018.

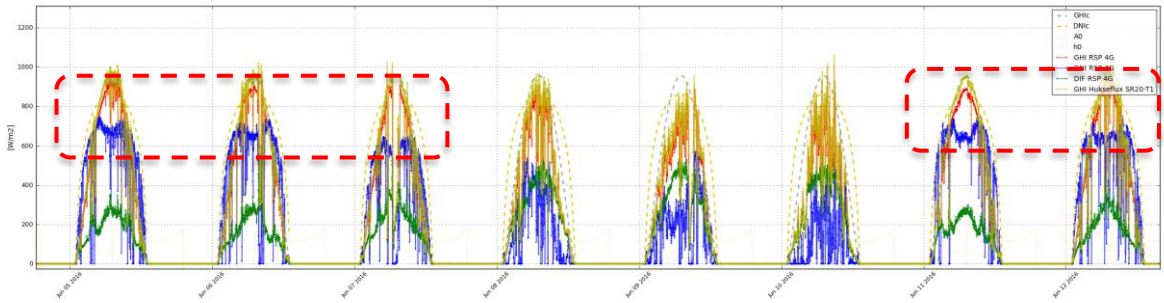

Figure 3.4 Effect of RSP shadowband issues – drop of DNI in Hulhulé.
Blue: DNI RSP; yellow: GHI SR20; red: GHI RSP; green: DIF RSP; dashed: theoretical clear-sky profile

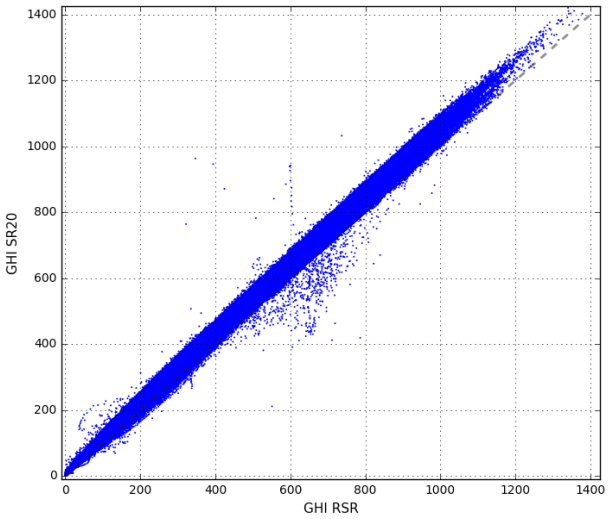

Figure 3.5 Systematic difference between GHI from SR20 and RSP - Hulhulé.

Table 3.14 Quality control summary – Hulhulé

Indicator	Flag	Description
Station description, metadata		Installation report available
Instrument accuracy		1x Secondary standard pyranometer SR20-T1 (GHI)
		1x Rotating Shadowband Radiometer RSP 4G (GHI, DIF, DNI)
Instrument calibration		Instruments were calibrated
Data structure		Clear
Cleaning and maintenance information		Cleaning log available No cleaning in July 2016
Time reference		Correct and clear time reference
Quality control complexity		RSP G4 data, full QC comparison of GHI from RSP and SR20
Quality control results		Shadowband malfunction (ca 5 months noontime) Inconsistency between of RSP and SR20 measurements – increasing in time
		Early morning and late afternoon shading Malfunction of RSP in March 2018
Availability of high-quality data		More than 27 months, DNI ca 25 months due to shadowband malfunction
Other issues		

Legend: Quality flag

Very good	Good	Sufficient	Problematic	Insufficient	Not specified

© 2018 Solargis

3.3.3 Kadhdhoo Airport

Table 3.15 Occurrence of data readings for Kadhdhoo meteorological station

Data availability	GHI SR20		GHI, DNI RSP	
Sun below horizon	619,617	49.6%	619,617	49.6%
Sun above horizon	630,242	50.4%	630,242	50.4%
Total data readings	1,249,859	100.0%	1,249,859	100.0%

Table 3.16 Excluded ground measurements after quality control (Sun above horizon) in Kadhdhoo

Type of test	Occurrence of data samples (Sun above horizon)					
	GHI SR20		DNI RSP		GHI RSP	
Physical limits test	803	0.1%	0	0.0%	2,260	0.4%
Consistency test (GHI – DNI – DIF)	-	-	190	0.0%	190	0.0%
Visual test (incorrect data)	55,844	8.9%	110,959	17.6%	54,448	8.6%
Other (non valid data)	48	0.0%	102	0.0%	101	0.0%
Total excluded data samples	56,695	9.0%	111,251	17.7%	56,999	9.0%
Total samples	630,242	100.0%	630,242	100.0%	630,242	100.0%

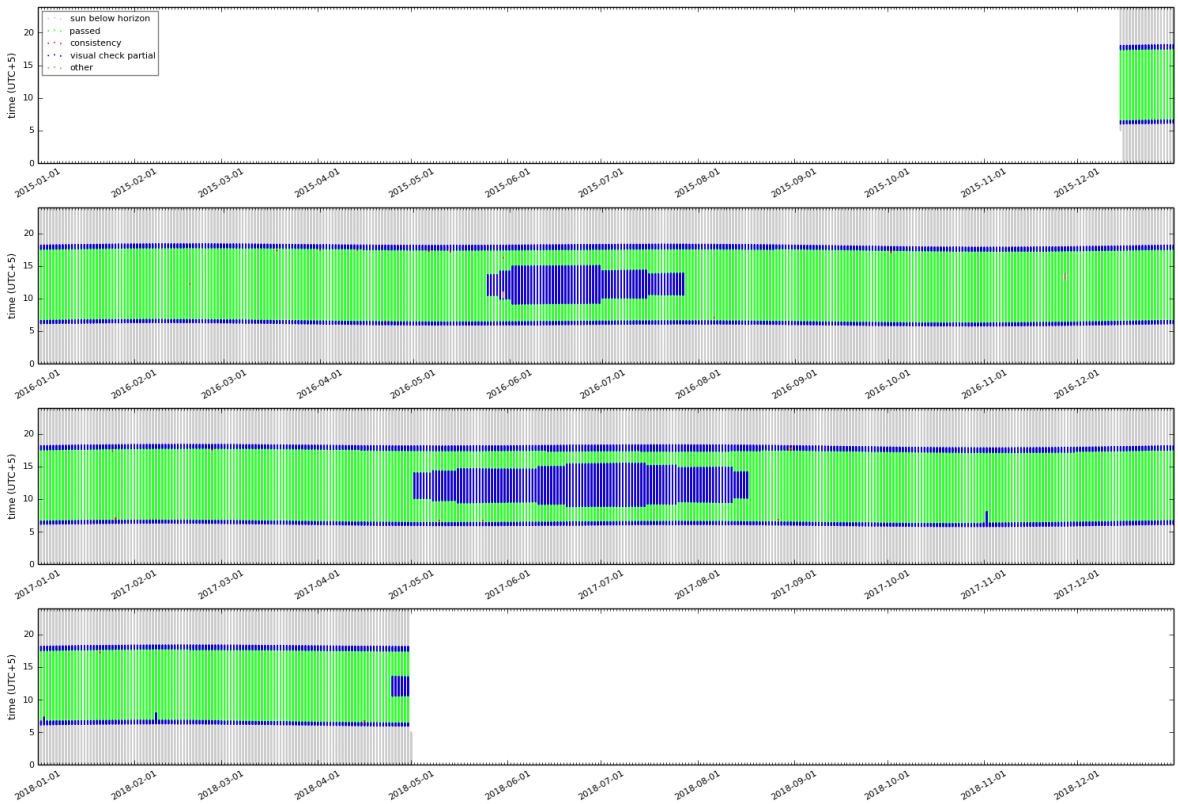

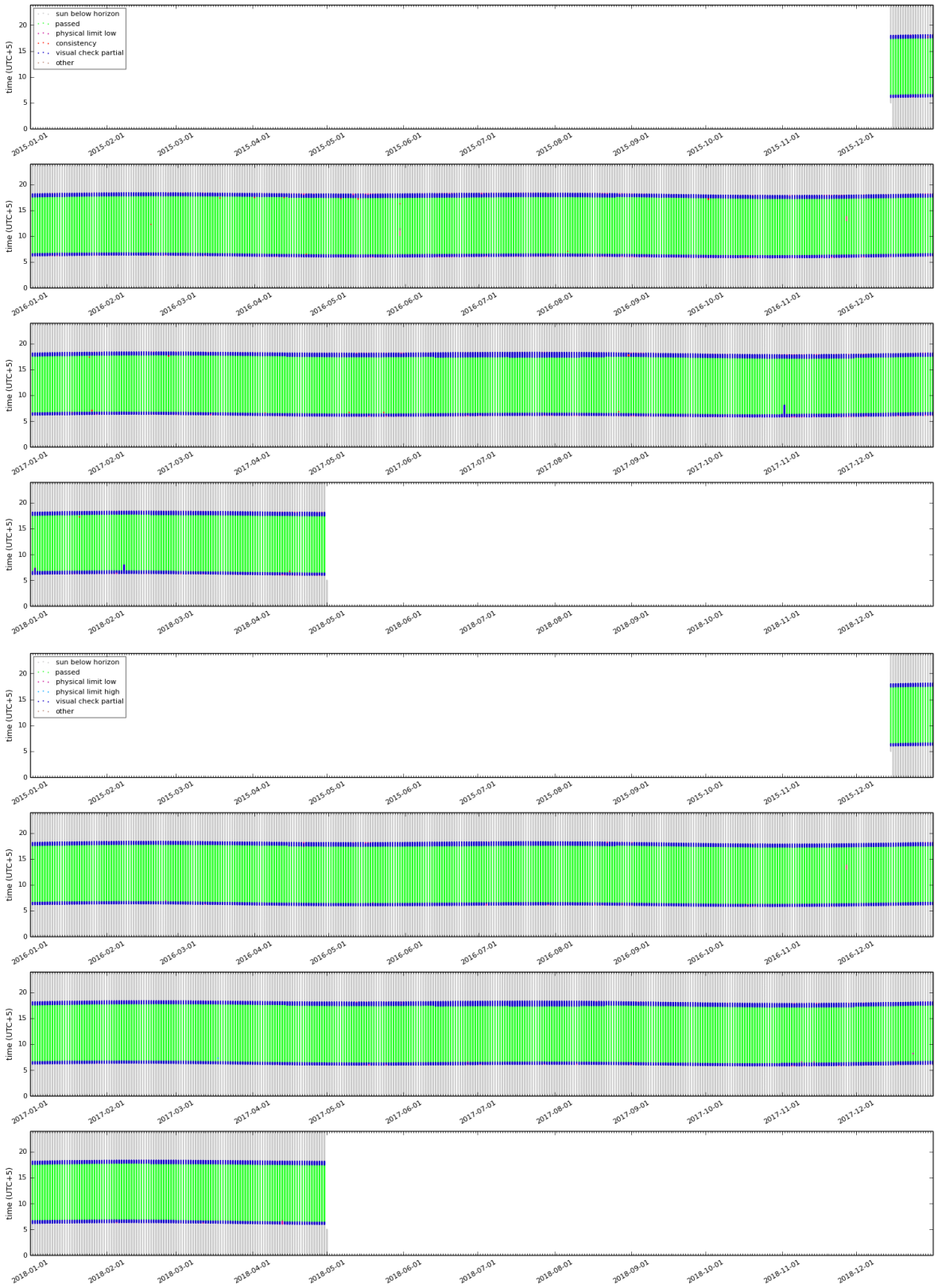

Figure 3.6 Results of DNI and GHI quality control – Kadhdhoo.
Green – data passing all tests; grey – sun below horizon; red – consistency issue, violet – physical limit issue, blue excluded by visual inspection. Top: DNI (RSP); middle: GHI (RSP); bottom: GHI (SR20)

Main findings:

- Shadowband malfunction (Figure 3.7). This issue was identified for a period from 25 May to 27 July 2016, from 2 May to 17 August 2017 and 25 April to 30 April 2018 around the noon. Affected data readings were excluded by quality control. Approximately 9.0% of DNI and DIF measurements were excluded in total.
- A systematic difference between GHI measurements from secondary standard pyranometer SR20-T1 and RSP (Figure 3.8). GHI from SR20 is in average higher by 4.9% than GHI from RSP. In the noon time it can exceed 7%. The overall difference in 2016 was 4.5% while in 2017 it was 5.0%.
- Late afternoon and early morning shading from surrounding objects
- GHI measurements from SR20 were replaced by data from RSP in case of shading from wind mast (see Table 3.8).

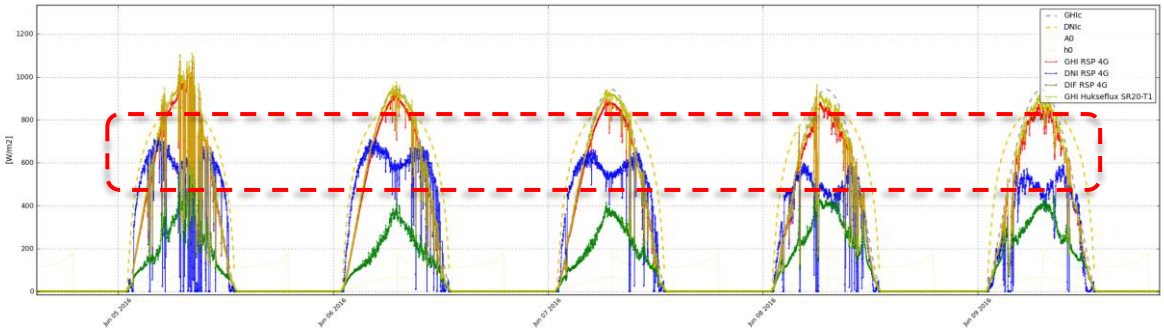

Figure 3.7 Effect of RSP shadowband issues – drop of DNI in Kadhdhoo.
Blue: DNI RSP; yellow: GHI SR20; red: GHI RSP; green: DIF RSP; dashed: theoretical clear-sky profile

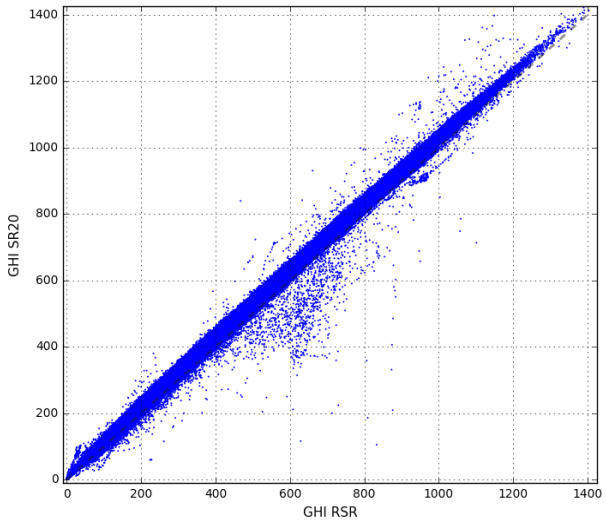

Figure 3.8 Systematic difference between GHI from SR20 and RSP – Kadhdhoo.

© 2018 Solargis

Table 3.17 Quality control summary – Kadhdhoo

Indicator	Flag	Description
Station description, metadata		Installation report available
Instrument accuracy		1x Secondary standard pyranometer SR20-T1 (GHI)
		1x Rotating Shadowband Radiometer RSP 4G (GHI, DIF, DNI)
Instrument calibration		Instruments were calibrated up to January 2018, then 2 months were measured with void calibration
Data structure		Clear
Cleaning and maintenance information		Cleaning log available Diligent cleaning
Time reference		Correct and clear time reference
Quality control complexity		RSP G4 data, full QC comparison of GHI from RSP and SR20
Quality control results		Shadowband malfunction (ca 5.5 months noontime)
		Early morning and late afternoon shading
		Inconsistency between of RSP and SR20 measurements – increasing in time
Availability of high-quality data		More than 28 months, DNI ca 25 months due to shadowband malfunction
Other issues		

Legend: Quality flag

Very good	Good	Sufficient	Problematic	Insufficient	Not specified

© 2018 Solargis

3.3.4 Gan Airport

Table 3.18 Occurrence of data readings for Gan meteorological station

Data availability	GHI SR20		GHI, DNI RSP	
Sun below horizon	619 976	49.5%	619 976	49.5%
Sun above horizon	631 323	50.5%	631 323	50.5%
Total data readings	1 251 299	100.0%	1 251 299	100.0%

Table 3.19 Excluded ground measurements after quality control (Sun above horizon) in Gan

Type of test	Occurrence of data samples (Sun above horizon)					
	GHI SR20		DNI RSP		GHI RSP	
Physical limits test	753	0.1%	0	0.0%	2 387	0.4%
Consistency test (GHI – DNI – DIF)	-	-	234	0.0%	234	0.0%
Visual test (incorrect data)	0	0.0%	47 487	7.5%	16	0.0%
Other (non valid data)	98	0.0%	63 418	10.0%	328	0.1%
Total excluded data samples	851	0.1%	111 139	17.6%	2 965	0.5%
Total samples	631 323	100.0%	631 323	100.0%	631 323	100.0%

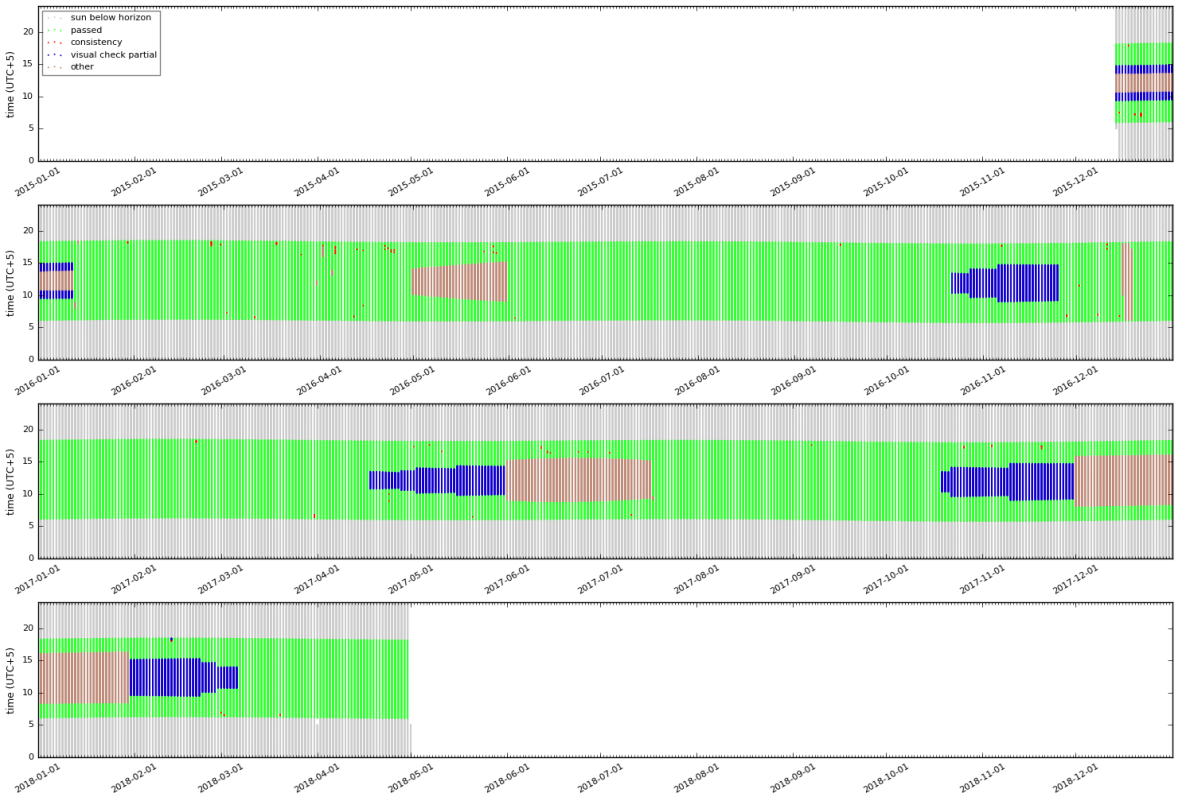

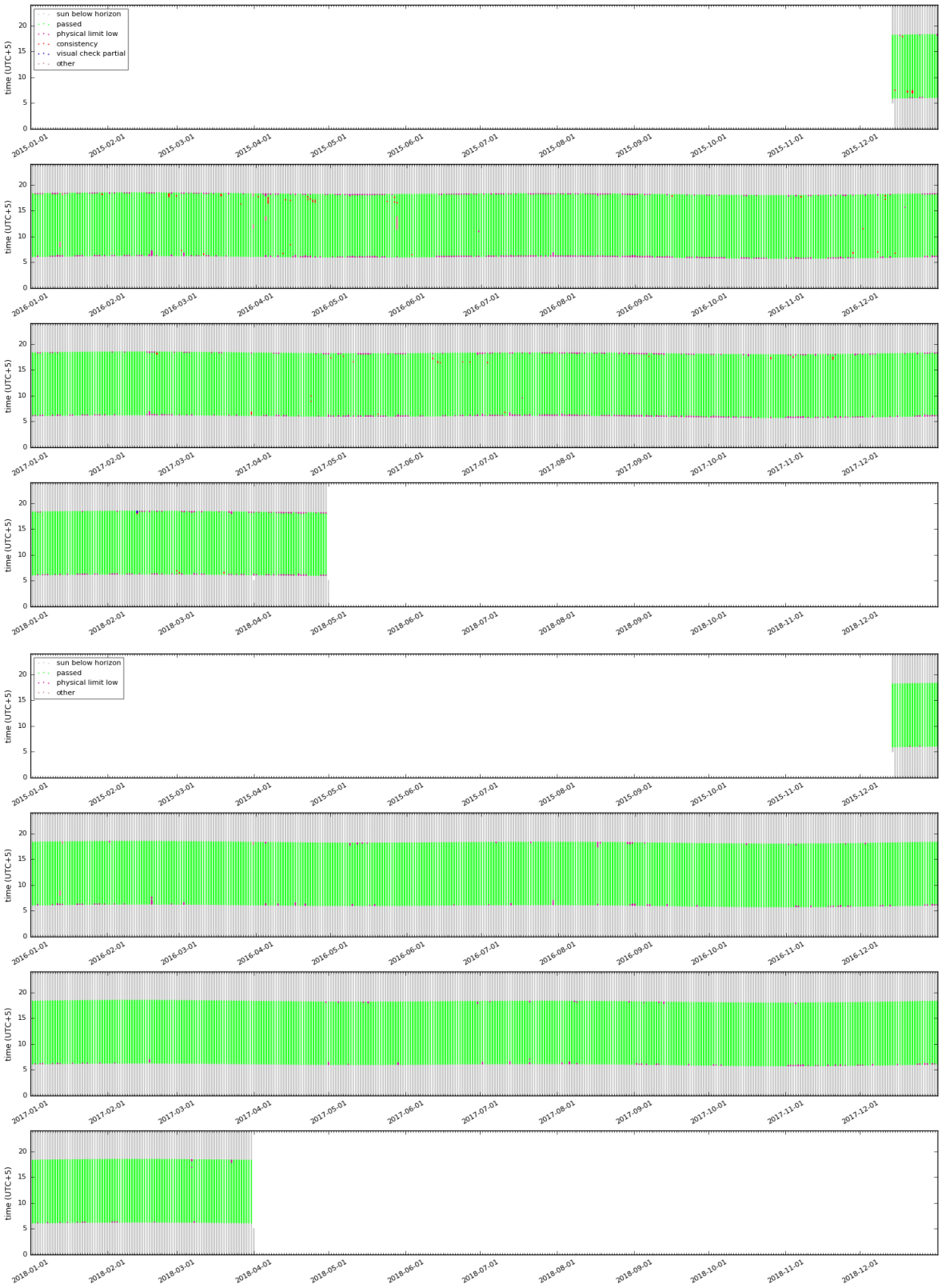

Figure 3.9 Results of DNI and GHI quality control – Gan.
Green – data passing all tests; grey – sun below horizon; red – consistency issue, violet – physical limit issue, blue excluded by visual inspection; brown – missing data.
Top: DNI (RSP); middle: GHI (RSP); bottom: GHI (SR20)

Main findings:

- Shadowband malfunction (Figure 3.10). This issue was identified for several periods (from 14 December 2015 to 12 January 2016; from 1 May to 31 May 2016, from 22 October to 25 November 2016, from 17 April to 17 July 2017, from 18 October 2017 to 6 March 2018) around the noon. Affected data readings were excluded partly by data provider and partly by quality control. Approximately 17.5% of DNI and DIF measurements were excluded in total.
- A systematic difference between GHI measurements from secondary standard pyranometer SR20-T1 and RSP (Figure 3.11). GHI from SR20 is in average higher by 5.3% than GHI from RSP. In the noon time it can exceed 7%. The overall difference in 2016 was 4.7% while in 2017 it was 5.8%.
- GHI measurements from SR20 were replaced by data from RSP in case of shading from wind mast (Figure 3.12).

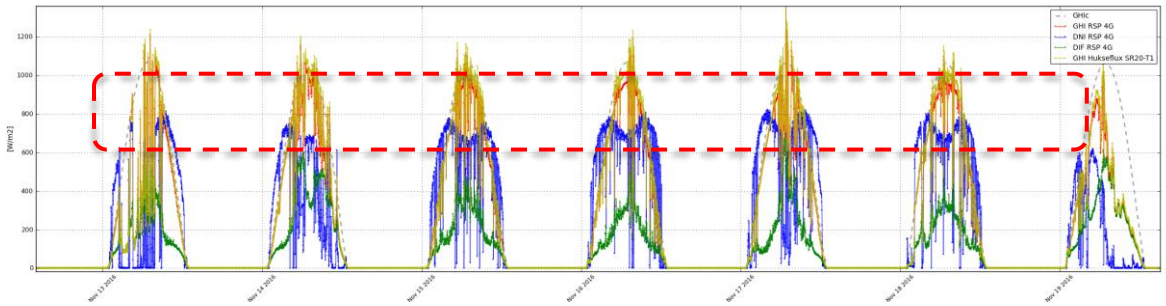

Figure 3.10 Effect of RSP shadowband issues – drop of DNI in Gan.
Blue: DNI RSP; yellow: GHI SR20; red: GHI RSP; green: DIF RSP; dashed: theoretical clear-sky profile

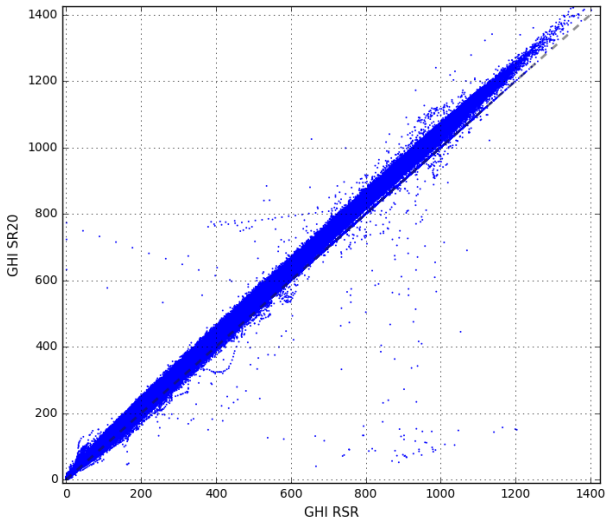

Figure 3.11 Systematic difference between GHI from SR20 and RSP - Gan.

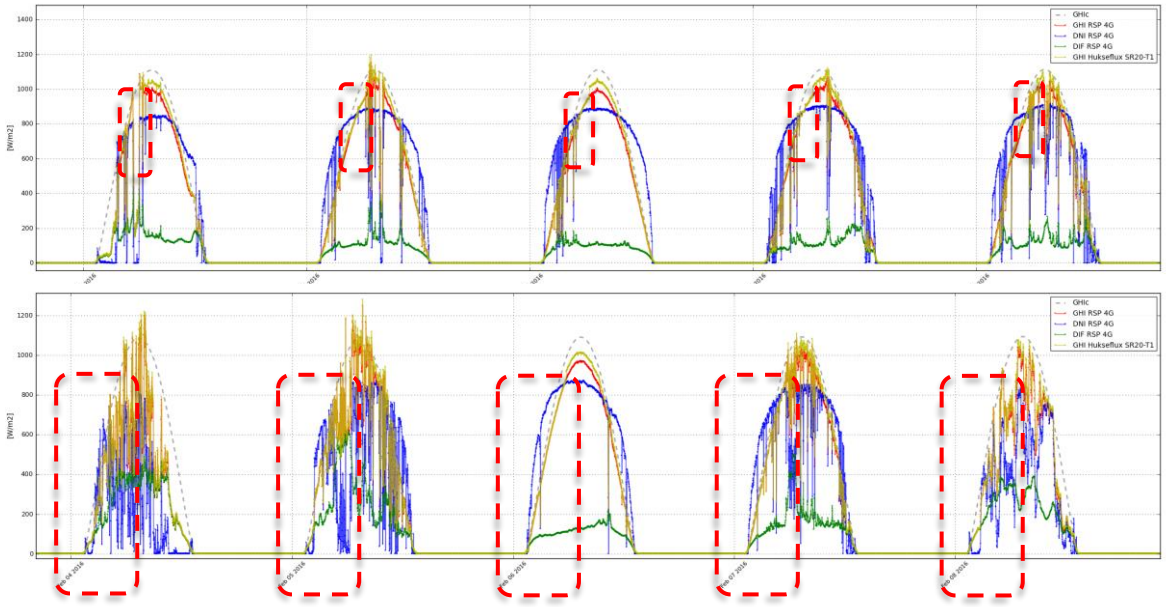

Figure 3.12 Replacement of SR20 GHI by RSP GHI due to wind mast shading in Gan.
Blue: DNI RSP; red: GHI RSP yellow: GHI SR20; green: DIF RSP; dashed: theoretical clear-sky profile

Table 3.20 Quality control summary – Gan

Indicator	Flag	Description
Station description, metadata		Installation report available
Instrument accuracy		1x Secondary standard pyranometer SR20-T1 (GHI)
		1x Rotating Shadowband Radiometer RSP 4G (GHI, DIF, DNI)
Instrument calibration		Instruments were calibrated up to January 2018, then 2 months measured with void calibration
Data structure		Clear
Cleaning and maintenance information		Cleaning log available Diligent cleaning
Time reference		Correct and clear time reference
Quality control complexity		RSP G4 data, full QC comparison of GHI from RSP and SR20
Quality control results		Shadowband malfunction (ca 10.5 months noontime)
		Inconsistency between of RSP and SR20 measurements – increasing in time
Availability of high-quality data		More than 28.5 months for GHI, more than 23.5 months DNI and DIF (reduction due to shadowband malfunction)
Other issues		

Legend: Quality flag

Very good	Good	Sufficient	Problematic	Insufficient	Not specified

© 2018 Solargis

3.4 Recommendations on the operation and maintenance of the sites

Based on the results of quality control (Table 3.11, 3.14, 3.17 and 3.20), we conclude that the solar radiation measurements come from the high (SR20) and medium (RSP) accuracy equipment that is professionally operated and maintained. Some issues were identified during the data quality control of the whole period of ground measurement campaign:

- Incorrect DNI and DIF measurements due to shadowband malfunction. These data were flagged and excluded from further processing. Most influenced are measurements from Gan station, where ca 17.5% of DNI and DIF data was excluded due to this issue for full period of measurements (15% for 2-years period).
- Higher systematic difference between GHI from SR20 and RSP (up to 7.4% in Hulhulé). The difference between the instruments increasing within the second year at all stations (6.8% for 2016 and 8.1% for 2017 in Hulhulé). This is known effect that should relate mainly to GHI instrument calibration. Due to this issue, the GHI from RSP was not considered for site-adaptation. The effect of this issue on the measured DNI is unknown as the data from higher accuracy reference instrument was not available. It is expected that the effect will not be extremely high, because both initial measurements (GHI and DIF) used for the calculation of the DNI are affected in the same way and should at the end in some extent eliminate each other. Unfortunately there is no direct proof for this behaviour. Therefore, a higher uncertainty of DNI measurements should be considered.

For future operation and maintenance of the measuring stations by local provider we recommend:

- Adopt measures to avoid the shadowband problems, where possible.
- Identify and fix source of systematic difference between SR20 and RSP

3.5 Instruments re-calibration at the end of measurement campaign

Methodology

At the end of 2-years measurement campaign all solar sensors should be re-calibrated upon the hand-over to a local organization. Suntrace originally proposed a “round robin" re-calibration strategy using the one set of spare sensors: one thermopile pyranometer and one RSI, which both still hold valid calibration certificates as they have not been exposed to sunlight over the 2 years of operations and thus, according to the manufacturer, can be still regarded as newly calibrated. After exchange at the first site (MVMLE – Male International Airport), the 2 used sensors were returned to Europe for re-calibration. The re-calibrated sensors should have been then installed at site no. 2. This procedure should have been repeated at all other stations, until the sensors of all 4 stations were re-calibrated.

Reasons for improved re-calibration:

- When proposing the re-calibration plan for the ESMAP measurement campaign in Maldives in 2014, Suntrace assumed that following the findings of [24] a duration of 4 weeks for re-calibrating the RSI instruments provides sufficient quality. In the course of the project DLR published a paper [25], which comes to the conclusion that the long term-outdoor calibration at PSA should last at least 60 days and during winter 90 days are needed to reach good results. This causes that the calibration of the RSI instruments at PSA takes about 2 to 3 times longer than originally planned.
- Latest findings on the quality of remote calibration of RSI using PSA as the reference station [26] indicate relatively large differences for sites in more humid regions. An RSI instrument calibrated at PSA and operated in India shows significant differences compared to the reference station operated at the same site. These systematic differences are likely due to much higher water vapor at the site in India compared to PSA site, which is located in an arid climate. As all 4 sites in Maldives are in humid tropical climate, we have to assume that the remote calibration at PSA may be also leading to significant deviations there.

The “round robin” re-calibration actually started in July 2017 with exchanging the RSI and SR20 sensor with the spare parts at MVMLE. The dismantled RSI was then sent for re-calibration to Spain (PSA calibration) and the SR20 to the Netherlands. The round-trip transport time turned out to be 6 weeks longer than planned due to customs organization etc.

© 2018 Solargis

The duration for shipping and re-calibration of these sensors turns out to be far too lengthy - one swap was taking 3 months instead of only 6 weeks as originally planned due to administration required from different parties. Therefore, and for the increase of accuracy of the RSI calibration, Suntrace is proposing an improved re-calibration method. This proposed new time schedule of improved re-calibration is shown in Table 3.21. This time schedule may change, depending on the decisions taken.

Summary of proposed re-calibration and check of solar radiation sensors (Table 3.22):

- Thermopile pyranometers: all 5 pyranometers will be exchanged by a new or refurbished/re-calibrated pyranometers of same type or better.
- RSI: Instead of shipping to Europe and performing a long-term calibration against a reference station (3 months in summer or 6 months in winter) re-calibrated thermopile pyranometers at each site will be used and applied an in-situ calibration. This calibration (improved calibration based on [27]) has the advantage that it is more site- and time-specific, as it considers the actual aerosol and water vapor conditions at the site, whereas the long-term calibration against a reference station would be optimized to the local climate of that location. Especially in tropical regions this can lead to significant offsets. The advanced calibration method takes the local weather conditions of the last weeks and the measurements of the precise thermopile pyranometer into account to calibrate the RSI. In order to achieve this, all 5 data loggers will be additionally exchanged with new data loggers including the in-situ calibration algorithm.
- Silicon photodiode: Check of proper horizontal levelling within specs, comparison with thermopile pyranometer during the past 2 years and after replacement against a newly calibrated one. Calculation of degradation and in case of significant sensitivity changes derivation and implementation of a new calibration constant.

Re-calibration and check of auxiliary meteorological sensors:

- Temperature/humidity probe: Exchange of the sensor head against a new one.
- Radiation shield: Cleaning of the surface to guarantee continued low albedo for minimizing errors due to heating up under strong sunlight.
- Barometric pressure: Comparison of the barometric pressure during the site visit with another barometer of equal of better quality.
- Wind speed: Anemometer function will be checked during site visit.
- Wind direction: Wind vane readings will be verified by compass bearings during site visit.

Table 3.21 Updated re-calibration schedule proposed by Suntrace

Period	Main tasks
04.06. – 10.06.2018	Receive python prototype algorithm
11.06. – 15.07.2018	Validation and documentation of algorithm
16.07. – 29.07.2018	Install test station on roof of university building in Hamburg Implement C-code into data logger of clone station
30.07. – 26.08.2018	Test run
27.08. – 09.09.2018	Verify proper operation in data logger
10.09. – 23.09.2018	Shipping to Maldives
24.09. – 07.10.2018	Installations on all 4 Islands in Maldives
08.10. – 14.10.2018	Hand-over of stations to MMS and final workshop

© 2018 Solargis

Table 3.22 Overview of instruments to be re-calibrated and/or exchanged with new/refurbished instruments

No.	Site Code	Instrument	Manufacturer	Model	Serial No.	Requires re-calibration	To be exchanged
1	MVMLE	Thermo-hygro sensor	Driesen und Kern	DKRF 400	K04496	Yes	Yes
2	MVMLE	Data Logger	Wilmers Messtechnik GmbH	Blueberry COMPACT	1125	No	Yes
3	MVHAQ	RSI	Reichert GmbH	RSP 4G	14-11	Yes	No
4	MVHAQ	Pyranometer	Hukseflux	SR20-T1	4485	Yes	Yes
5	MVHAQ	Thermo-hygro sensor	Driesen und Kern	DKRF 400	K04495	Yes	Yes
6	MVHAQ	Data Logger	Wilmers Messtechnik GmbH	Blueberry COMPACT	1124	No	Yes
7	MVKDO	RSI	Reichert GmbH	RSP 4G	14-07	Yes	No
8	MVKDO	Pyranometer	Hukseflux	SR20-T1	4383	Yes	Yes
9	MVKDO	Thermo-hygro sensor	Driesen und Kern	DKRF 400	K04498	Yes	Yes
10	MVKDO	Data Logger	Wilmers Messtechnik GmbH	Blueberry COMPACT	1122	No	Yes
11	MVGAN	RSI	Reichert GmbH	RSP 4G	14-03	Yes	No
12	MVGAN	Pyranometer	Hukseflux	SR20-T1	4384	Yes	Yes
13	MVGAN	Thermo-hygro sensor	Driesen und Kern	DKRF 400	K04497	Yes	Yes
14	MVGAN	Data Logger	Wilmers Messtechnik GmbH	Blueberry COMPACT	1121	No	Yes

Comments:

Additionally, one re-calibrated RSI, pyranometer, thermo-hygro sensor and one new data logger will be provided as spare parts.

© 2018 Solargis

4 SOLAR RESOURCE MODEL DATA

4.1 Solar model

Solar radiation is calculated by Solargis model, which is parameterized by a set of inputs characterizing the cloud transmittance, state of the atmosphere and terrain conditions. A comprehensive **overview of the Solargis model** is made available in the recent book publication [3]. The methodology is also described in [4, 5]. The related uncertainty and requirements for bankability are discussed in [6, 7].

In Solargis approach, the **clear-sky irradiance** is calculated by the simplified SOLIS model [8]. This model allows fast calculation of clear-sky irradiance from the set of input parameters. Sun position is deterministic parameter, and it is described by the algorithms with satisfactory accuracy. Stochastic variability of clear-sky atmospheric conditions is determined by changing concentrations of atmospheric constituents, namely aerosols, water vapour and ozone. Global atmospheric data, representing these constituents, are routinely calculated by world atmospheric data centres:

- In Solargis, the new generation **aerosol data set** representing Atmospheric Optical Depth (AOD) is used. The calculation accuracy is strongly determined by quality of aerosols, especially for cloudless conditions. The aerosol data implemented by MACC-II/CAMS and MERRA-2 projects are used [9, 10].
- **Water vapour** is also highly variable in space and time, but it has lower impact on the values of solar radiation, compared to aerosols. The GFS and CFSR databases (NOAA NCEP) are used in Solargis, and the data represent the daily variability from 1999 to the present time [11, 12, 13].
- **Ozone** absorbs solar radiation at wavelengths shorter than 0.3 μm, thus having negligible influence on the broadband solar radiation.

The clouds are the most influencing factor, modulating clear-sky irradiance. Effect of clouds is calculated from the satellite data in the form of a **cloud index** (cloud transmittance). The cloud index is derived by relating radiance recorded by the satellite in spectral channels and surface albedo to the cloud optical properties. In Solargis, the modified calculation scheme of Cano has been adopted to retrieve cloud optical properties from the satellite data [14].

To calculate **all-sky irradiance** in each time step, the clear-sky global horizontal irradiance is coupled with cloud index. Direct Normal Irradiance (DNI) is calculated from Global Horizontal Irradiance (GHI) using modified Dirindex model [15]. Diffuse irradiance for tilted surfaces, which is calculated by Perez model [16]. The calculation procedure includes also terrain disaggregation, the spatial resolution is enhanced with use of the digital terrain model to 250 meters [17]. Solargis model version 2.1 has been used. Table 4.1 summarizes technical parameters of the model inputs and of the primary data outputs.

Table 4.1 Input data used in the Solargis and related GHI and DNI outputs for Maldives

Inputs into the Solargis model	Source of input data	Time representation	Original time step	Approx. grid resolution
Cloud index	Meteosat MFG IODC Meteosat MSG IODC satellites (EUMETSAT)	1999 to 2016 2017 to date	30 minutes 15 minutes	2.8 x 3.2 km 3.1 x 3.5 km
Atmospheric optical depth (aerosols)*	MACC-II/CAMS* (ECMWF) MERRA-2 (NASA)	2003 to date 1999 to 2002	3 hours 1 hour	75 km and 125 km 50 km
Water vapour	CFSR/GFS (NOAA)	1999 to date	1 hour	35 and 55 km
Elevation and horizon	SRTM-3 (SRTM)	-	-	250 m
Solargis primary data outputs (GHI and DNI)	-	1999 to date	30 minutes	250 m

** Aerosol data for 2003-2012 come from the reanalysis database; the data representing years 2013-present are derived from near-real time operational model*

© 2018 Solargis

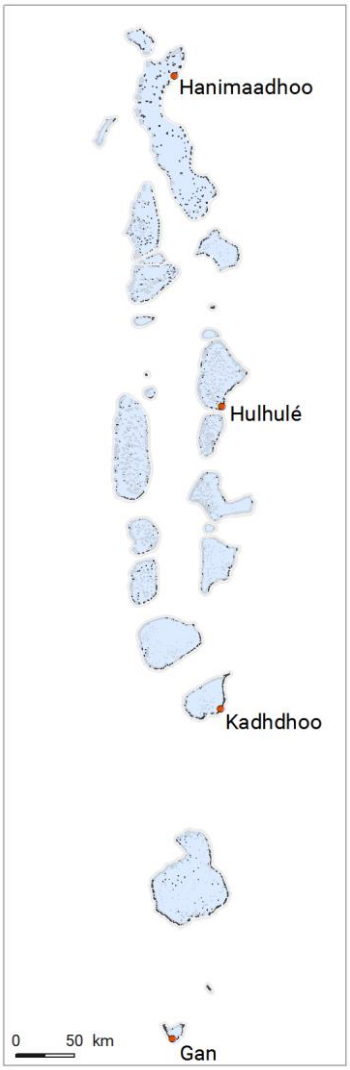

Figure 4.1: Sites with solar meteorological stations used for site adaptation of Solargis model in Maldives

4.2 Site adaptation of the solar model – method

This chapter describes accuracy improvement of the delivered model time series for four sites. This improvement has been achieved by site adaptation of the model, based on the use of 2+ years of local measurements.

The fundamental difference between a satellite observation and a ground measurement is that signal received by the satellite radiometer integrates a large area, while a ground station represents a pinpoint measurement. This results in a mismatch when comparing instantaneous values from these two observation instruments, mainly during intermittent cloudy weather and changing aerosol load. Nearly half of the hourly Root Mean Square Deviation (RMSD) for GHI and DNI can be attributed to this mismatch (value at sub-pixel scale), which is also known as the "nugget effect" [18].

The satellite pixel is not capable describing the inter-pixel variability in complex regions, where within one pixel diverse natural conditions mix-up (e.g. fog in narrow valleys or along the coast). In addition, the coarse spatial resolution of atmospheric databases such as aerosols or water vapour is not capable to describe local patterns of the state of atmosphere. These features can be seen in the satellite DNI data by increased bias due to imperfect description of aerosol load. Satellite data have inherent inaccuracies, which have certain degree of geographical and time variability.

© 2018 Solargis

Especially DNI is strongly sensitive to variability of cloud information, aerosols, water vapour, and terrain shading. The relation between uncertainty of global and direct irradiance is nonlinear. Often, a negligible error in global irradiance may have high counterpart in the direct irradiance component.

The solar energy projects require representative and accurate GHI and DNI time series. The satellite-derived databases are used to describe long-term solar resource for a specific site. However, their problem when compared to the high-quality ground measurements is a slightly higher bias and partial disagreement of frequency distribution functions, which may limit their potential to record the occurrence of extreme situations (e.g. very low atmospheric turbidity resulting in a high DNI and GHI). A solution is to correlate satellite-derived data with ground measurements to understand the source of discrepancy and subsequently to improve the accuracy of the resulting time series.

The Solargis satellite-derived data are correlated with ground measurement data with two objectives:

- Improvement of the overall bias (removal of systematic deviations)
- Improvement of the fit of the frequency distribution of values.

Limited spatial and temporal resolution of the input data and simplified nature of the models results in the occurrence of systematic and random deviations of the model outputs when compared to the ground observations. The deviations in the satellite-computed data, which have *systematic nature*, can be reduced by site adaptation or regional adaptation methods. In this report we apply site-adaptation of the solar model, i.e. adapting the model for the local conditions represented by on-site measurements.

The terminology related to the procedure improving accuracy of the satellite data is not harmonized, and various terms are used:

- Correlation of ground measurements and satellite-based data;
- Calibration of the satellite model (its inputs and parameters);
- Site adaptation or regional adaptation of satellite based data.

The term *site adaptation* is more general and best explains the concept of adapting the satellite-based model (by correlation, calibration, fitting and recalculation) to the ground measured data. **Site adaptation** aims to adapt the characteristics of the satellite-based time series to the site-specific conditions described by local measurements.

Three conditions are important for successful adaptation of the satellite-based model:

1. High quality DNI and GHI ground measurements for at least 12 months must be available; optimally data for 2 or 3 years should be used;
2. High quality satellite data must be used, with consistent quality over the whole period of data;
3. There must be identified a systematic difference between both data sources.

Systematic difference can be measured by two characteristics:

- Bias (offset)
- Systematic deviation in the distribution of hourly or daily values (in the histogram)

Systematic difference can be stable over the year or it can slightly change seasonally for certain meteorological conditions (e.g. typical cloud formation during a day, seasonal air pollution). The data analysis should distinguish systematic differences from those arising at occasional events, such as extreme sand storms or forest fires. The episodically-occurring differences may mislead the results of adaptation, especially if short period of ground measurements is only available.

If one of the three above-mentioned conditions is not fulfilled, site adaptation (regional adaptation) will not provide the expected results. On the contrary, such an attempt may provide worse results.

For the quantitative assessment of the accuracy enhancement procedures, the following metrics is used:

- Metrics based on the comparison of all pairs of the hourly daytime data values: Mean Bias, and Root Mean Square Deviation (RMSD), histogram, in an absolute and relative form (divided by the daytime mean DNI values);
- Metrics based on the difference of the cumulative distribution functions: KSI (Kolmogorov-Smirnov test Integral) [19]

The normalized KSI is defined as an integral of absolute differences of two cumulative distribution functions D normalized by the integral of critical value $a_{critical}$:

$$KSI\% = \frac{\int_{x\,\min}^{x\,\max} D_n dx}{a_{critical}} * 100$$

$$a_{critical} = V_c * (x_{max} - x_{min})$$

$$V_c = \frac{1.63}{\sqrt{N}}, \quad N \geq 35$$

where critical value depends on the number of the data pairs *N*. As the KSI value is dependent on the size of the sample, the KSI measure may be used only for the relative comparison of fit of cumulative distribution of irradiance values.

For the accuracy enhancement of solar resource parameters in this study, a combination of two methods was used. First, systematic deviations due to influence of aerosols were partially removed. Afterwards, to improve the distribution of values, the fitting of cumulative frequency distribution curves of ground measurements and satellite data was used.

The site-adaptation procedure first identifies the sources of discrepancies by comparing the ground-measured data with Solargis model data, for the period of the overlap between both data sets. Based on this analysis, correction coefficients to improve the fit between the measured and the model Solargis data are developed. In the second step, these coefficients are used for the adaptation of the full (19 years) time series.

The satellite data is available in 15 and 30-minute time step and the ground measurements in 1-minute time step. To partially remove the conceptual difference of point and satellite pixel measurements, prior to site adaptation, all the measures are calculated using aggregated data in the hourly time step.

The adaptation was based on measured DNI data from RSP 4G instrument and GHI data from the secondary standard SR20-T1 instrument. GHI measured by the RSP 4G was not used because of higher uncertainty of the measurements (Chapter 3.3).

4.3 Results of the model adaptation at four sites

The original Solargis data show a regional pattern of overestimation, compared to the ground measurements – mainly for DNI. The model adaptation allowed removing large part of mismatch between satellite-based data and ground measurements. The GHI fits the ground measurements very well.

Tables 4.2 to 4.5 summarize results of the site-adaptation for all solar measuring stations.

Table 4.2 Direct Normal Irradiance: bias and KSI before and after model site-adaptation

Meteo station	Original DNI data			DNI after site adaptation		
	Bias	Bias	KSI	Bias	Bias	KSI
	[kWh/m²]	[%]	[-]	[kWh/m²]	[%]	[-]
Hanimaadhoo	19	5.3	104	0	0.0	56
Hulhulé	31	8.4	149	0	0.0	82
Kadhdhoo	29	7.5	148	0	0.0	94
Gan	33	8.4	159	0	0.0	110
Mean	28.0	7.4	140	0.0	0.0	85.5
Standard deviation	6.2	1.5		0.0	0.0	

© 2018 Solargis

Table 4.3 Global Horizontal Irradiance: bias and KSI before and after model site-adaptation

Meteo station	Original GHI data			GHI after site adaptation		
	Bias	Bias	KSI	Bias	Bias	KSI
	[kWh/m²]	[%]	[-]	[kWh/m²]	[%]	[-]
Hanimaadhoo	3	0.7	49	0	0.0	38
Hulhulé	0	0.0	50	0	0.0	42
Kadhdhoo	3	0.7	52	0	0.0	45
Gan	7	1.4	67	0	0.0	44
Mean	3.3	0.7	55	0.0	0.0	42
Standard deviation	2.9	0.5		0.0	0.0	

Table 4.4 Direct Normal Irradiance: RMSD before and after model site-adaptation

Meteo station	RMSD of original DNI data			RMSD of DNI after site adaptation		
	Hourly	Daily	Monthly	Hourly	Daily	Monthly
	[%]	[%]	[%]	[%]	[%]	[%]
Hanimaadhoo	31.8	17.7	6.6	31.6	17.1	4.3
Hulhulé	35.2	20.0	9.1	34.2	18.6	3.5
Kadhdhoo	35.6	19.3	8.1	34.9	18.3	2.9
Gan	35.8	20.1	9.3	35.0	18.7	4.3
Mean	34.6	19.3	8.3	33.9	18.2	3.7

Table 4.5 Global Horizontal Irradiance: RMSD before and after model site-adaptation

Meteo station	RMSD of original GHI data			RMSD of GHI after site adaptation		
	Hourly	Daily	Monthly	Hourly	Daily	Monthly
	[%]	[%]	[%]	[%]	[%]	[%]
Hanimaadhoo	15.3	6.6	2.3	15.3	6.6	2.2
Hulhulé	16.4	7.2	1.8	16.5	7.2	1.8
Kadhdhoo	16.7	7.1	1.3	16.7	7.1	1.2
Gan	16.2	7.2	2.2	16.1	7.0	1.7
Mean	16.2	7.0	1.9	16.1	7.0	1.7

As a result, at the level of individual measurement sites in Maldives, the mean bias of the adapted values was reduced to zero. The values of RMSD and KSI accuracy parameters are also reduced, especially for DNI.

The effect of the site adaptation is presented in a detail for all sites (Figures 4.2 to 4.5). The changes of GHI are very small, as the original data have good fit to ground measurements. The changes of DNI are more significant.

© 2018 Solargis

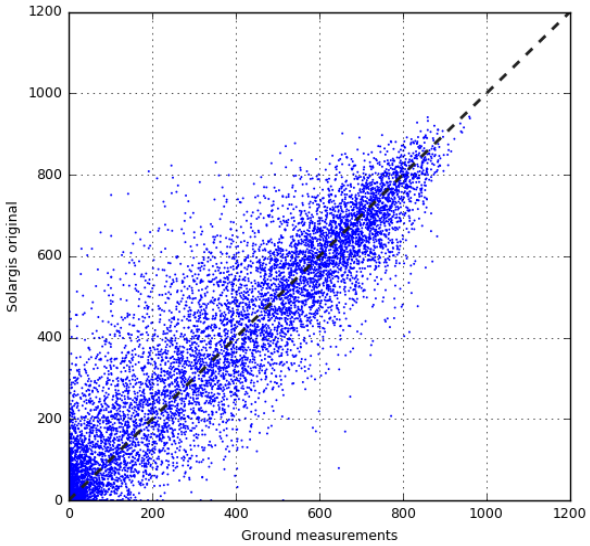

Hanimaadhoo: Original DNI

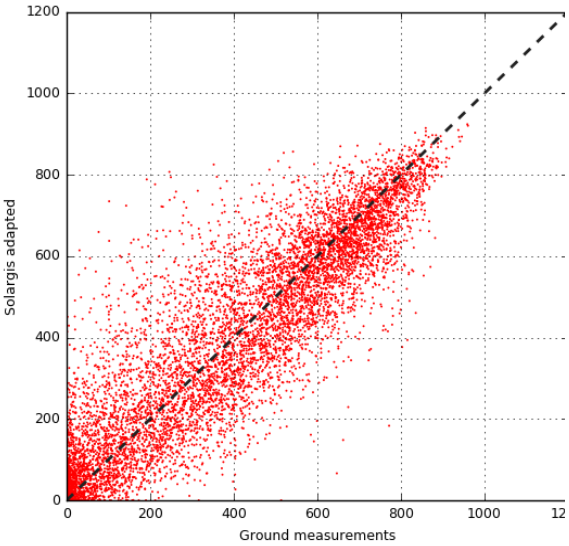

Hanimaadhoo: DNI after adaptation

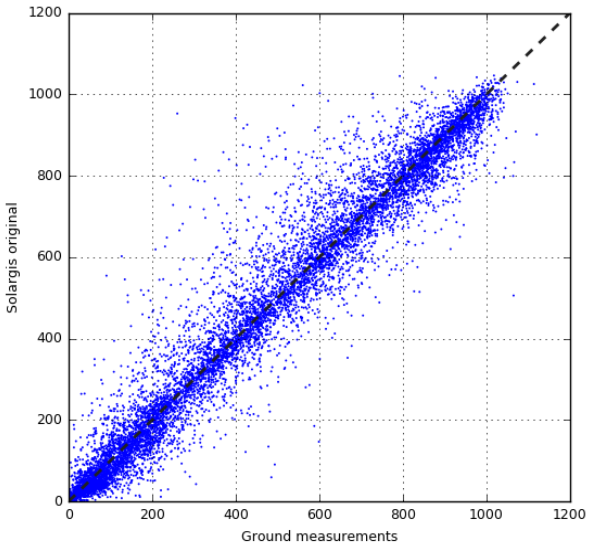

Hanimaadhoo: Original GHI

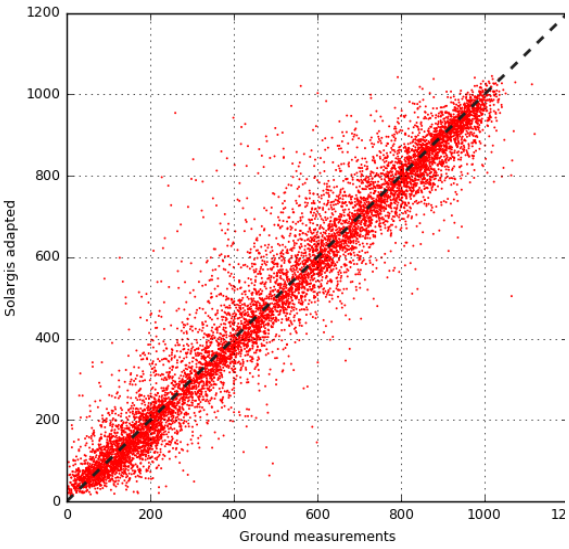

Hanimaadhoo: GHI after adaptation

Figure 4.2: Correction of DNI and GHI hourly values for Hanimaadhoo.
Left: original Solargis data, right: site-adapted Solargis data.
The X-axis represents the measured data and the Y-axis represents the satellite-derived data.

© 2018 Solargis

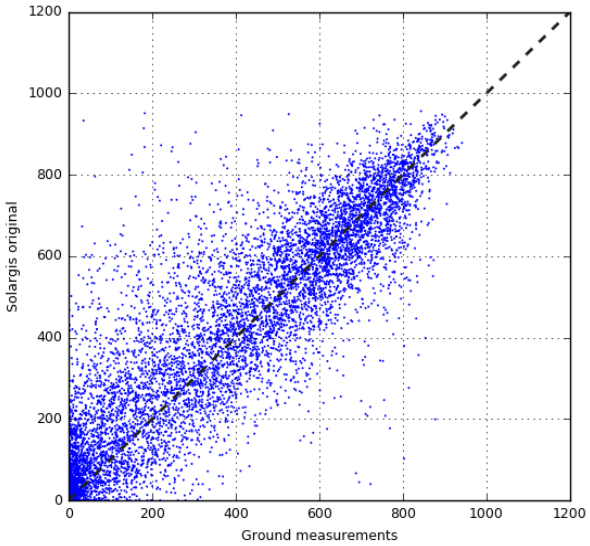

Hulhulé: Original DNI

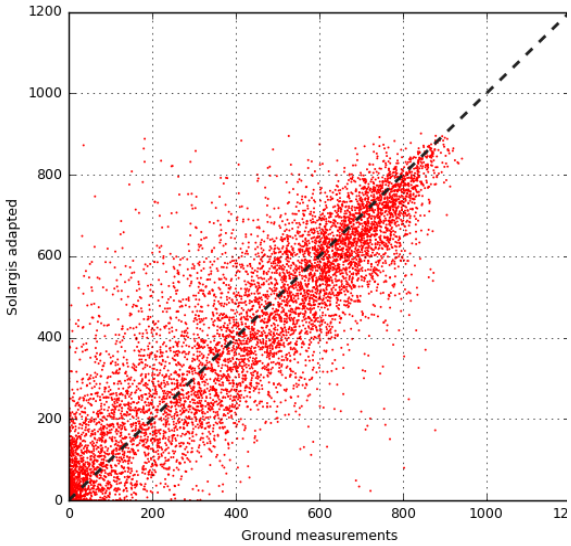

Hulhulé: DNI after adaptation

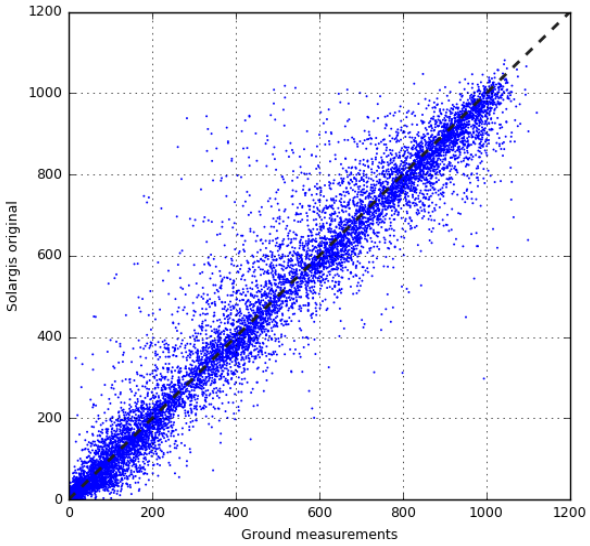

Hulhulé: Original GHI

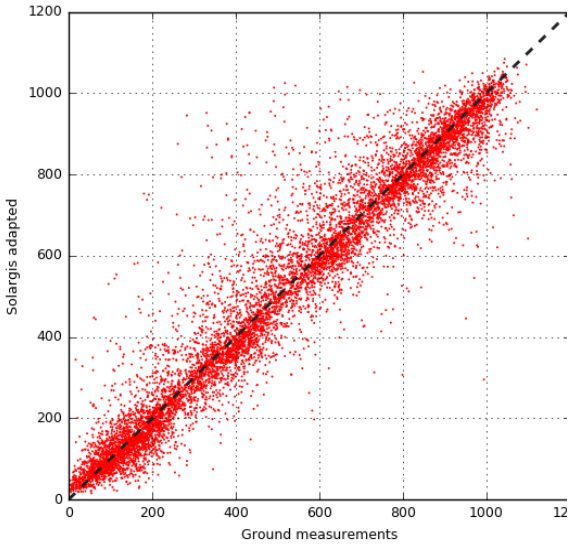

Hulhulé: GHI after adaptation

Figure 4.3: Correction of DNI and GHI hourly values for Hulhulé
Left: original Solargis data, right: site-adapted Solargis data.
The X-axis represents the measured data and the Y-axis represents the satellite-derived data.

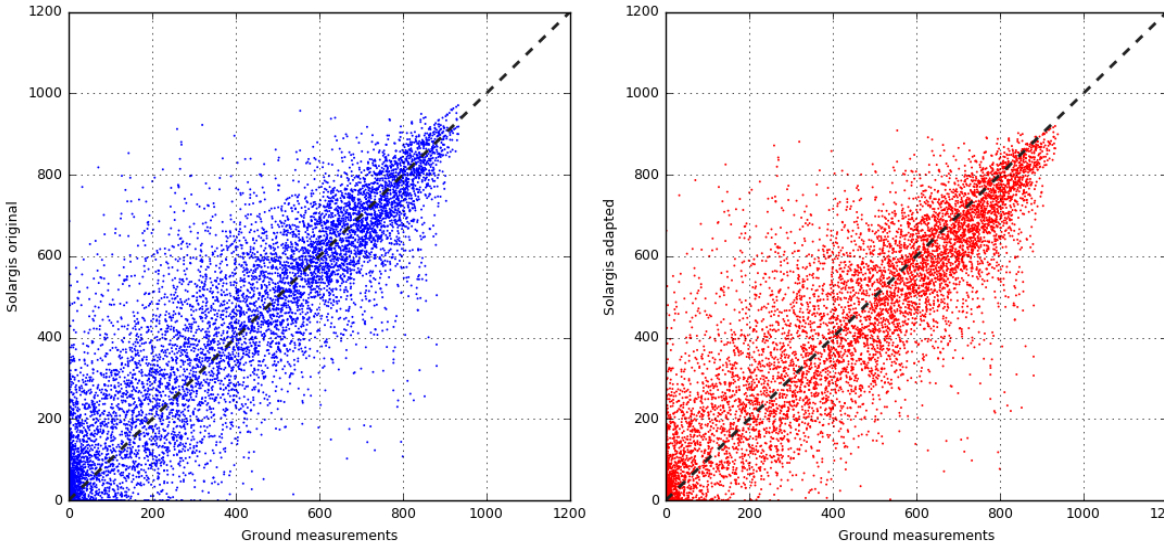

Kadhdhoo: Original DNI

Kadhdhoo: DNI after adaptation

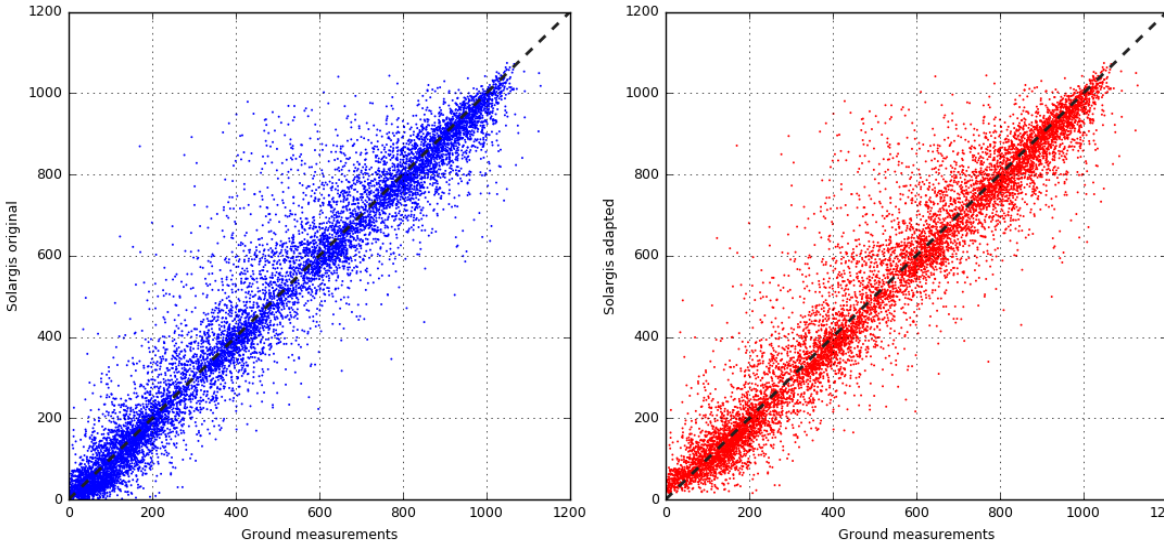

Kadhdhoo: Original GHI

Kadhdhoo: GHI after adaptation

Figure 4.4: Correction of DNI and GHI hourly values for Kadhdhoo.
Left: original Solargis data, right: site-adapted Solargis data.
The X-axis represents the measured data and the Y-axis represents the satellite-derived data.

© 2018 Solargis

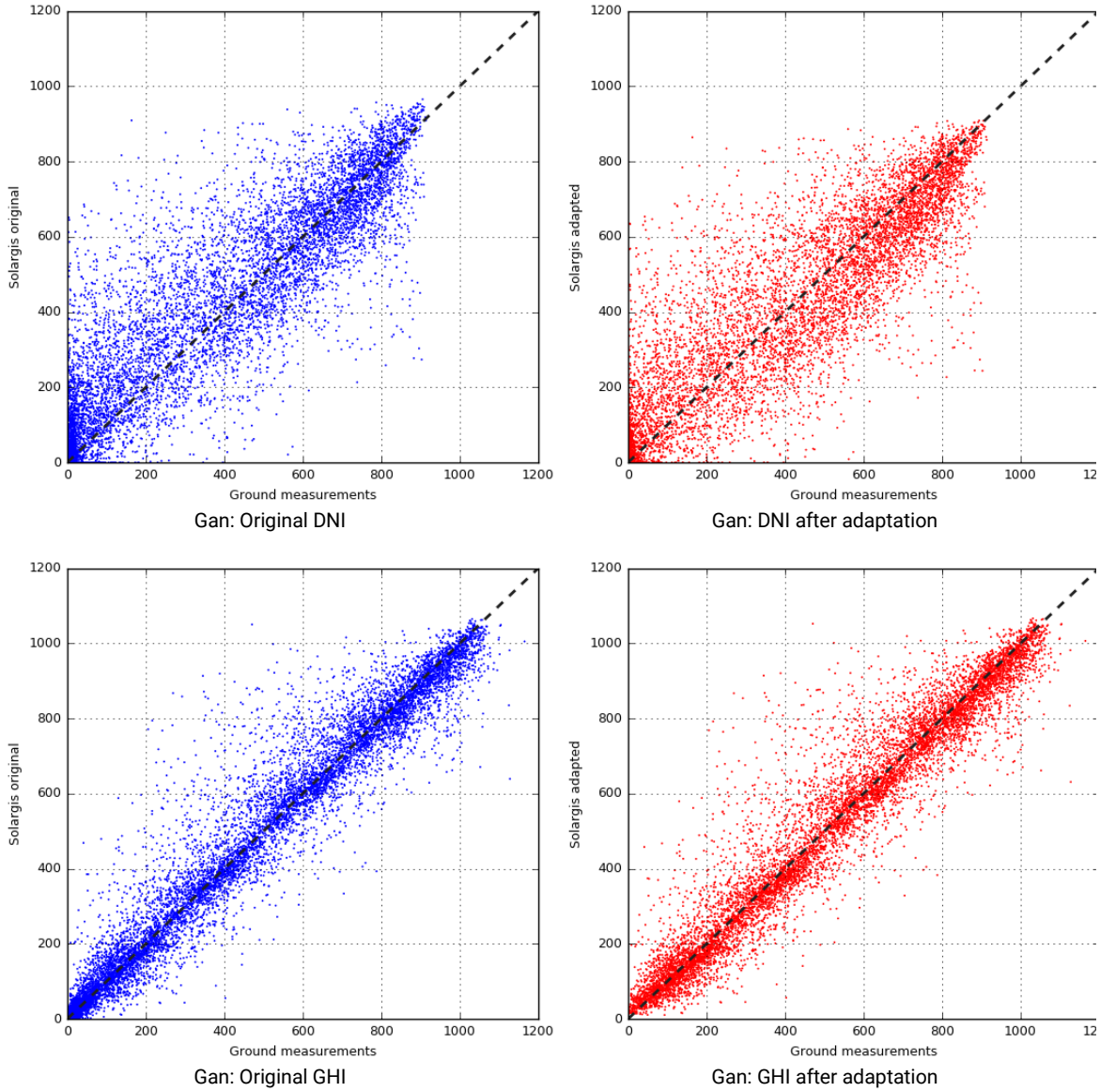

Gan: Original DNI | Gan: DNI after adaptation

Gan: Original GHI | Gan: GHI after adaptation

Figure 4.5: Correction of DNI and GHI hourly values for Gan.
Left: original Solargis data, right: site-adapted Solargis data.
The X-axis represents the measured data and the Y-axis represents the satellite-derived data.

The change of model GHI and DNI after adaptation is presented on an example of Hanimaadhoo (Figure 4.6). The change for GHI is negligible, the adapted DNI is lower than original one. The other sites are very similar (Table 4.6).

The site-adapted model values better represent the geographical characteristics of DNI and GHI solar resource and they also improve the distribution and match of hourly values.

The measurements show that the model performs well in the region, and these results significantly improve the confidence about the reliability of the measured and modelled solar resource data in Maldives.

© 2018 Solargis

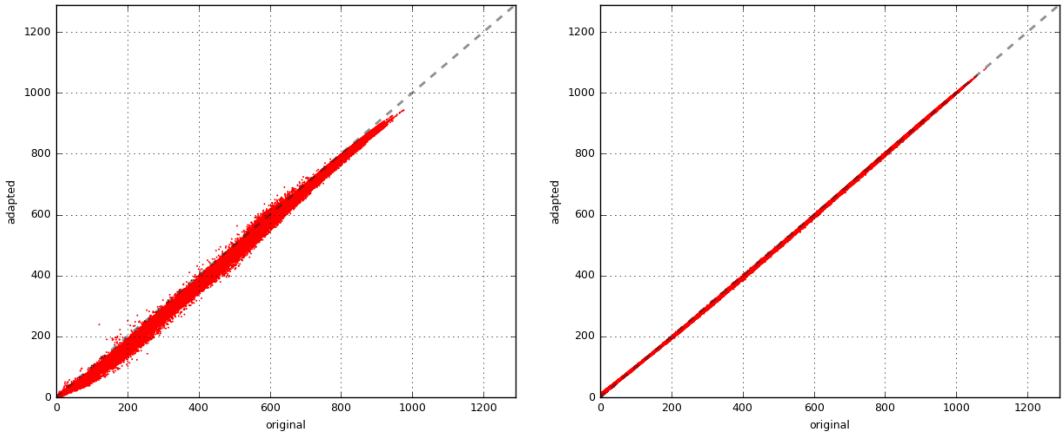

Figure 4.6: Comparison of Solargis original and site-adapted data for Hanimaadhoo site.
Left: DNI; Right: GHI; Data represent years 1999 to 2017.

Table 4.6 Comparison of long-term average of yearly summaries of original and site-adapted values

Meteo station	DNI annual values			GHI annual values		
	Original	Site-adapted	Difference	Original	Site-adapted	Difference
	[kWh/m^2]	[kWh/m^2]	[%]	[kWh/m^2]	[kWh/m^2]	[%]
Hanimaadhoo	1524	1440	-5.5	2030	2018	-0.6
Hulhulé	1619	1485	-8.3	2051	2052	+0.1
Kadhdhoo	1685	1555	-7.7	2058	2046	-0.6
Gan	1748	1609	-8.0	2076	2048	-1.4

© 2018 Solargis

5 METEOROLOGICAL MODEL DATA

5.1 Meteorological model

For the territory of Maldives, the last 19 years of the Solargis model-based meteorological data is derived from the regional models. The meteorological data in Solargis database is derived from the two data sources: CFSR and CFSv2, with original characteristics specified in Table 5.1.

Table 5.1 Original source of Solargis meteorological data: models CFSR and CFSv2.

	Climate Forecast System Reanalysis (CFSR)	Climate Forecast System (CFSv2)
Time period	1999 to 2010	2011 to the present time
Original spatial resolution	30 x 35 km	19 x 22 km
Original time resolution	1 hour	1 hour

Table 5.2 shows meteorological parameters available in Solargis, their specifications and it also indicates, which of them have been delivered within this study. In general, the original spatial resolution of the models is enhanced to 1 km for air temperature and relative humidity by spatial disaggregation and use of the Digital Elevation Model SRTM-3; for Maldives this correction has no effect. The spatial resolution of other parameters is unchanged.

Table 5.2 Solargis meteorological parameters delivered within this project

Meteorological parameter	Acronym	Unit	Time resolution	Spatial representation	Data delivered	Data validated
Air temperature at 2 metres (dry bulb temperature)	TEMP	°C	60 minute	1 km	Yes	Yes
Relative humidity at 2 metres	RH	%	60 minute	1 km	Yes	Yes
Wind speed at 10 metres	WS	m/s^2	60 minute	Original model	Yes	Yes
Wind direction at 10 metres	WD	°	60 minute	Original model	Yes	Yes
Atmospheric pressure	AP	hPa	60 minute	Original model	Yes	Yes
Precipitable water	PWAT		60 minute	Original model	Yes	No

Important note: meteorological parameters are derived from the numerical weather model outputs and they have lower spatial and temporal resolution. Thus, they do not represent the same accuracy as the solar resource data. Especially wind speed data has higher uncertainty, and it provides only overview information for solar energy projects. Thus, the **local microclimate of the site may deviate from the values derived from the global databases.**

5.2 Validation of meteorological data

The validation procedure was carried out to compare the modelled data with ground-measurements from the 4 meteorological stations installed within the ESMAP project: Hanimaadhoo, Hulhulé, Kadhdhoo and Gan. In general, the data from the meteorological models represent larger area, and it is not capable to represent accurately the local microclimate created by small land mass of the islands in the atolls of the Maldives.

© 2018 Solargis

5.2.1 Air temperature at 2 metres

Air temperature is derived from the model outputs of both CSFR and CSFv2 meteorological models and recalculated at the spatial resolution of 1 km (Table 5.3 and Figures 5.1 to 5.4). Considering spatial and time interpolation, the deviation of the modelled values to the ground observations for hourly values can occasionally reach several degrees of Celsius.

Figures 5.1 to 5.4 show graphical representation of the model values accuracy at the meteorological stations. In general, the model matches the ground measurements well. Main issue identified is underestimation of daily temperature amplitude. This is caused by relatively small land mass of the islands (in comparison to the pixel size of the meteorological model). Model air temperature is driven mainly by the air temperature over the ocean, where the daily amplitude is lower than temperature amplitude at individual islands. The limitations of the meteorological models are seen only partially, as the air temperature is changing only a little across the seasons and across the day time.

Table 5.3 Air temperature at 2 m: accuracy indicators of the model outputs [°C].

Meteorological station	CFSv2 model							
	Bias mean	Bias min	Bias max	Bias nigh-time	Bias day-time	RMSD hourly	RMSD daily	RMSD monthly
Hanimaadhoo	-0.9	0.7	-2.5	0.1	-1.7	1.8	1.4	1.0
Hulhulé	-0.9	0.3	-2.3	-0.3	-1.6	1.5	1.1	0.9
Kadhdhoo	-0.5	1.2	-2.3	0.4	-1.4	1.6	0.9	0.6
Gan	-0.4	1.2	-1.9	0.4	-1.3	1.4	0.8	0.5

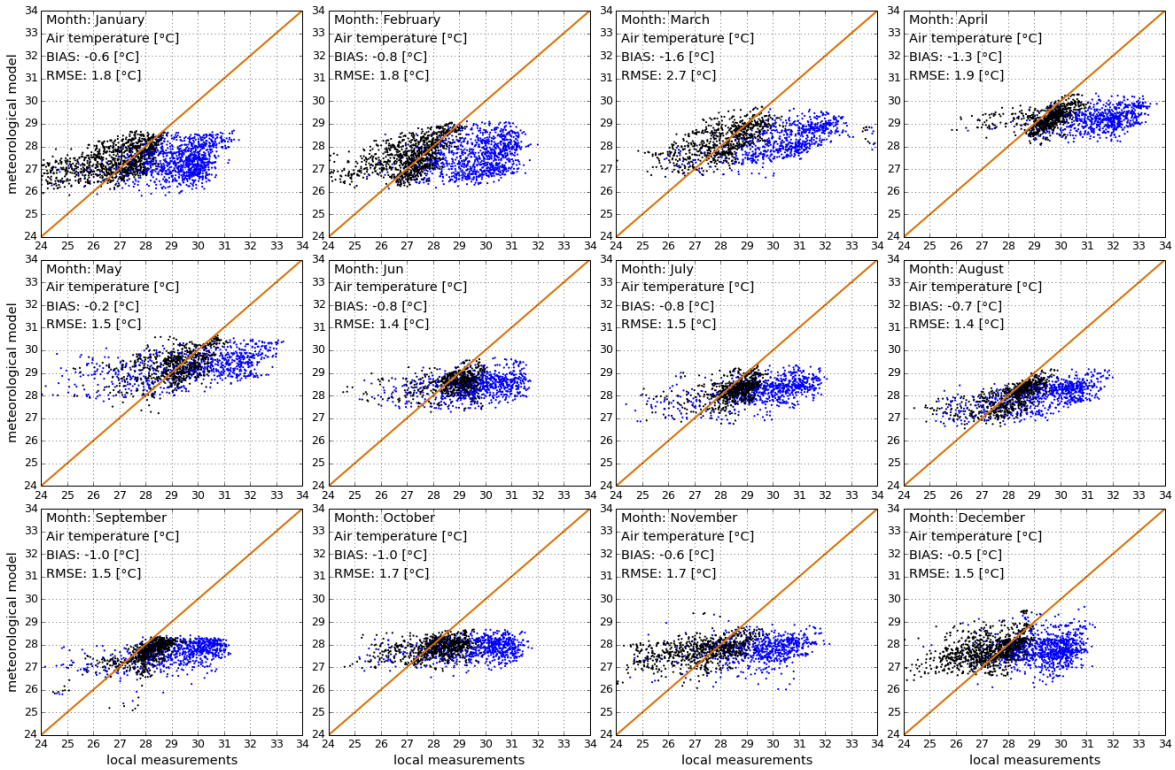

Figure 5.1: Scatterplots of air temperature at 2 m at Hanimaadhoo meteorological station.
Measured values (horizontal axis) and meteorological model values (vertical axis)
Blue: day-time, Black: night-time measurements

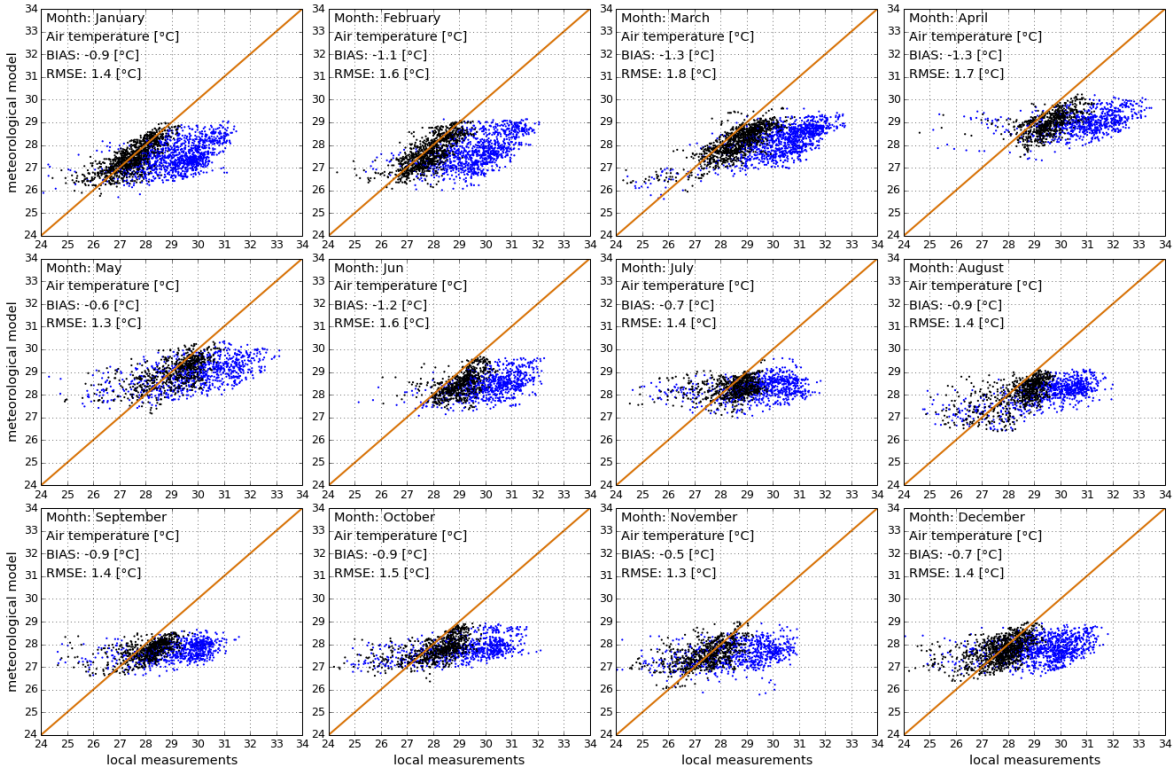

Figure 5.2: Scatterplots of air temperature at 2 m at Hulhulé meteorological station.
Measured values (horizontal axis) and meteorological model values (vertical axis)
Blue: day-time, Black: night-time measurements

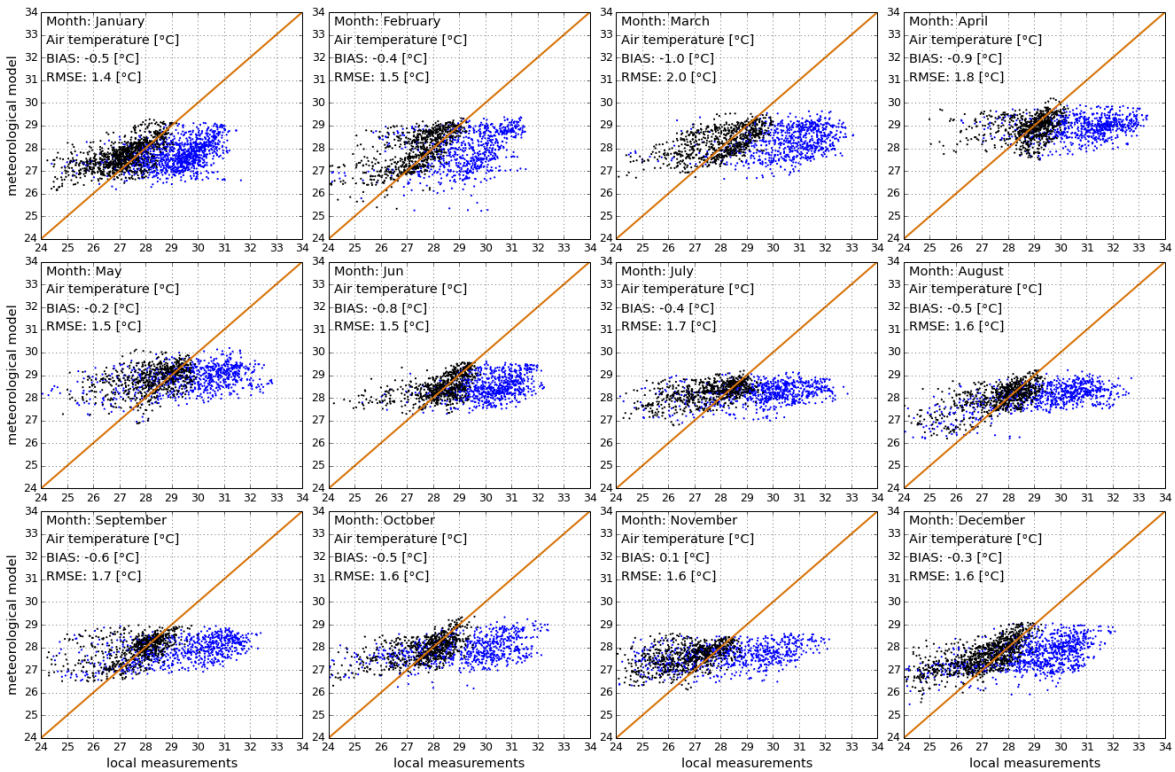

Figure 5.3: Scatterplots of air temperature at 2 m at Kadhdhoo meteorological station.
Measured values (horizontal axis) and meteorological model values (vertical axis)
Blue: day-time, Black: night-time measurements

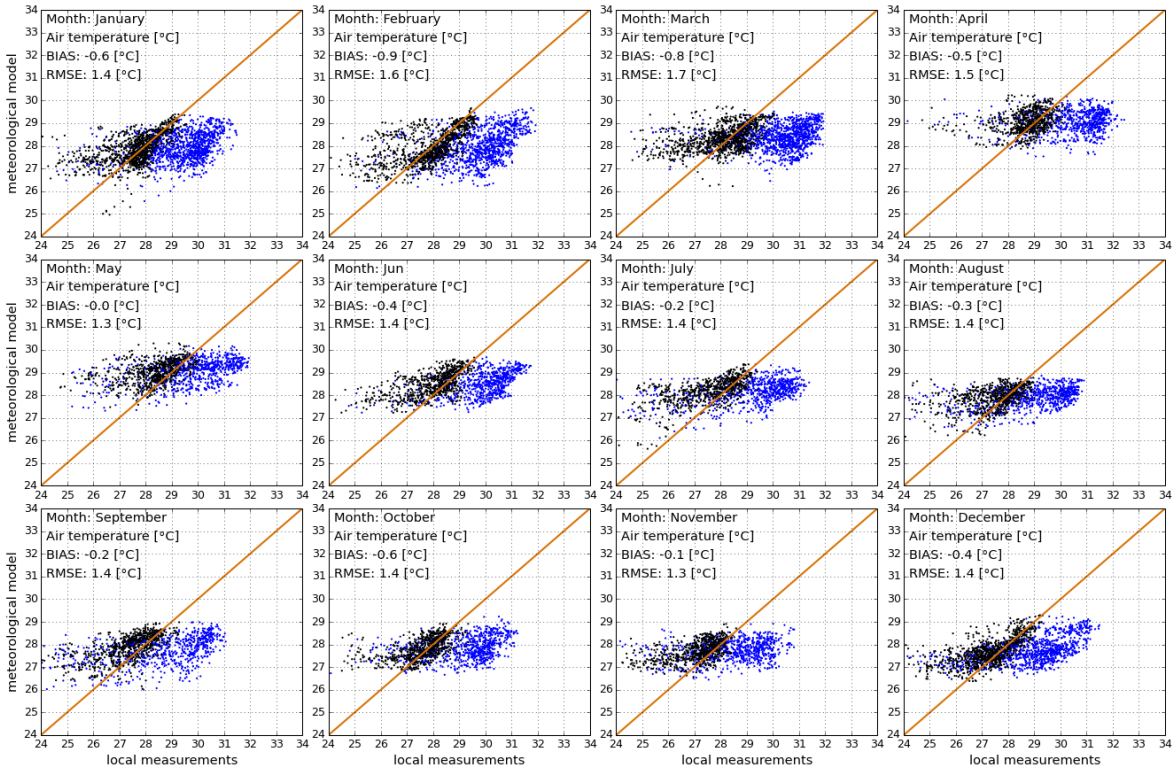

Figure 5.4: Scatterplots of air temperature at 2 m at Gan meteorological station.
Measured values (horizontal axis) and meteorological model values (vertical axis)
Blue: day-time, Black: night-time measurements

5.2.2 Relative humidity

Relative humidity is calculated from the specific humidity, air pressure and the site-adapted air temperature. The comparison of the model values with ground measurements at all 4 meteorological stations is shown in Table 5.4 and Figures 5.5 to 5.8. The issue identified is amplitude reduction of daily relative humidity. Otherwise, relative humidity is quite stable across the seasons and day time.

Table 5.4 Relative humidity: accuracy indicators of the model outputs [%].

Meteorological station	CFSv2 model							
	Bias mean	Bias min	Bias max	Bias nigh-time	Bias day-time	RMSD hourly	RMSD daily	RMSD monthly
Hanimaadhoo	-5	0	-11	-10	-2	11	13	8
Hulhulé	-5	0	-9	-7	-3	7	6	5
Kadhdhoo	-7	-2	-12	-10	-4	9	8	7
Gan	-7	-2	-12	-10	-4	9	8	7

© 2018 Solargis

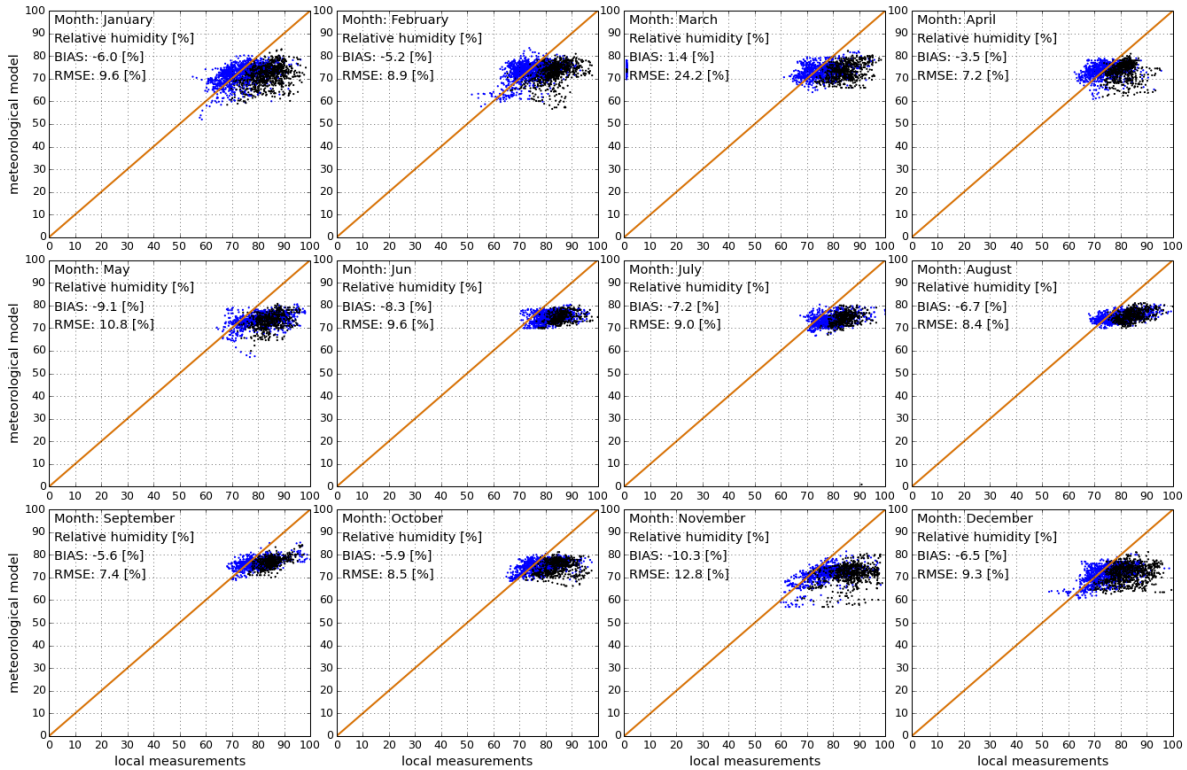

Figure 5.5: Scatterplots of relative humidity at 2 m at Hanimaadhoo meteorological station.
Measured values (horizontal axis) and meteorological model values (vertical axis).
Blue: day-time, black: night-time measurements.

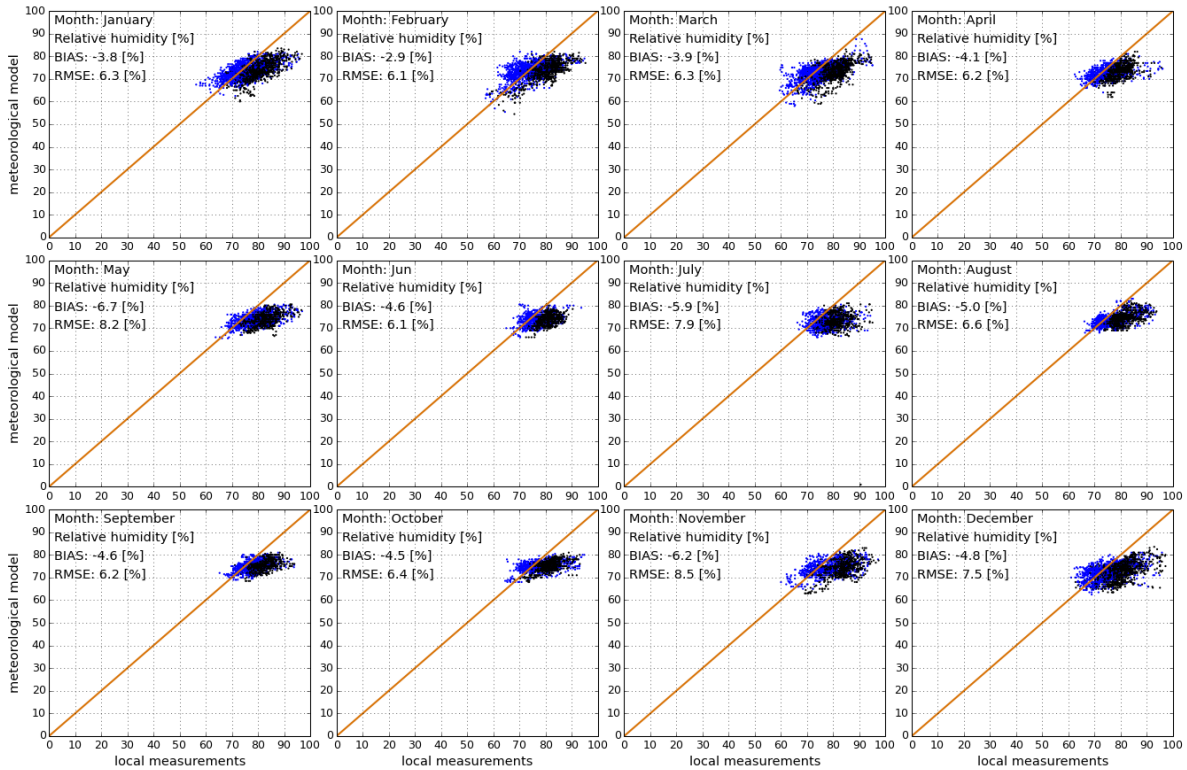

Figure 5.6: Scatterplots of relative humidity at 2 m at Hulhulé meteorological station.
Measured values (horizontal axis) and meteorological model values (vertical axis).
Blue: day-time, black: night-time measurements.

© 2018 Solargis

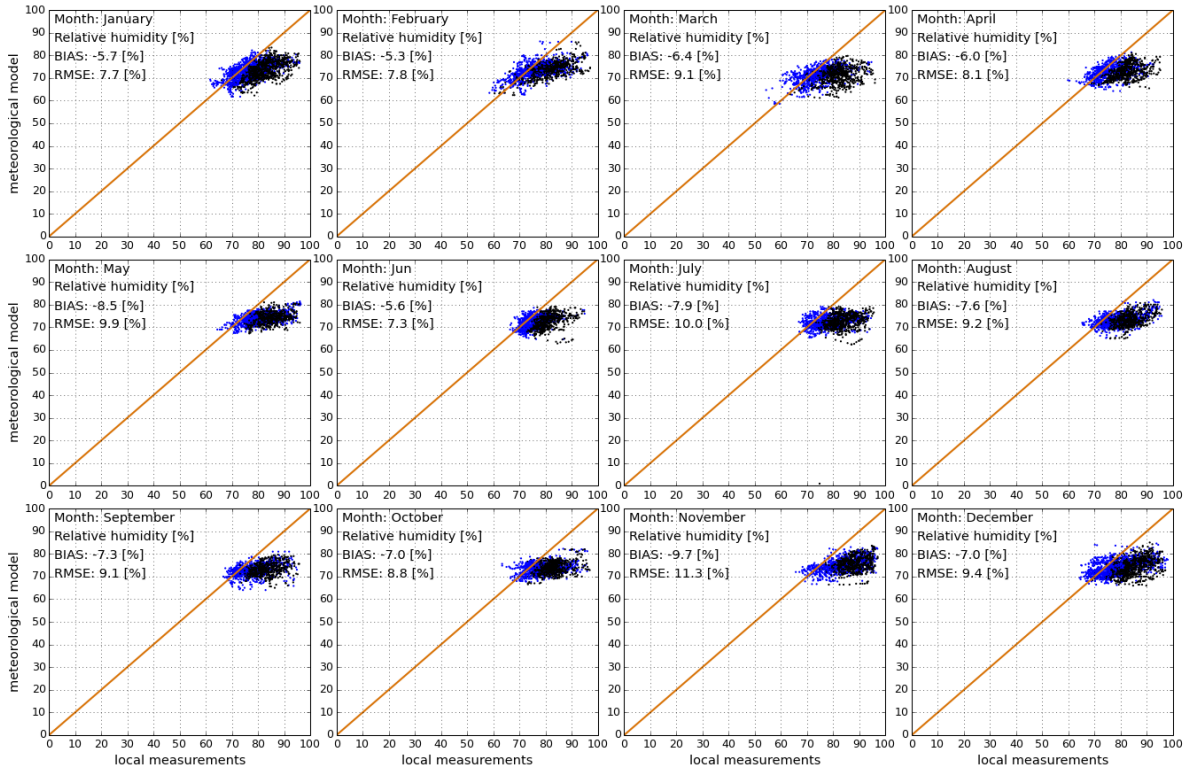

Figure 5.7: Scatterplots of relative humidity at 2 m at Kadhdhoo meteorological station.
Measured values (horizontal axis) and meteorological model values (vertical axis).
Blue: day-time, black: night-time measurements.

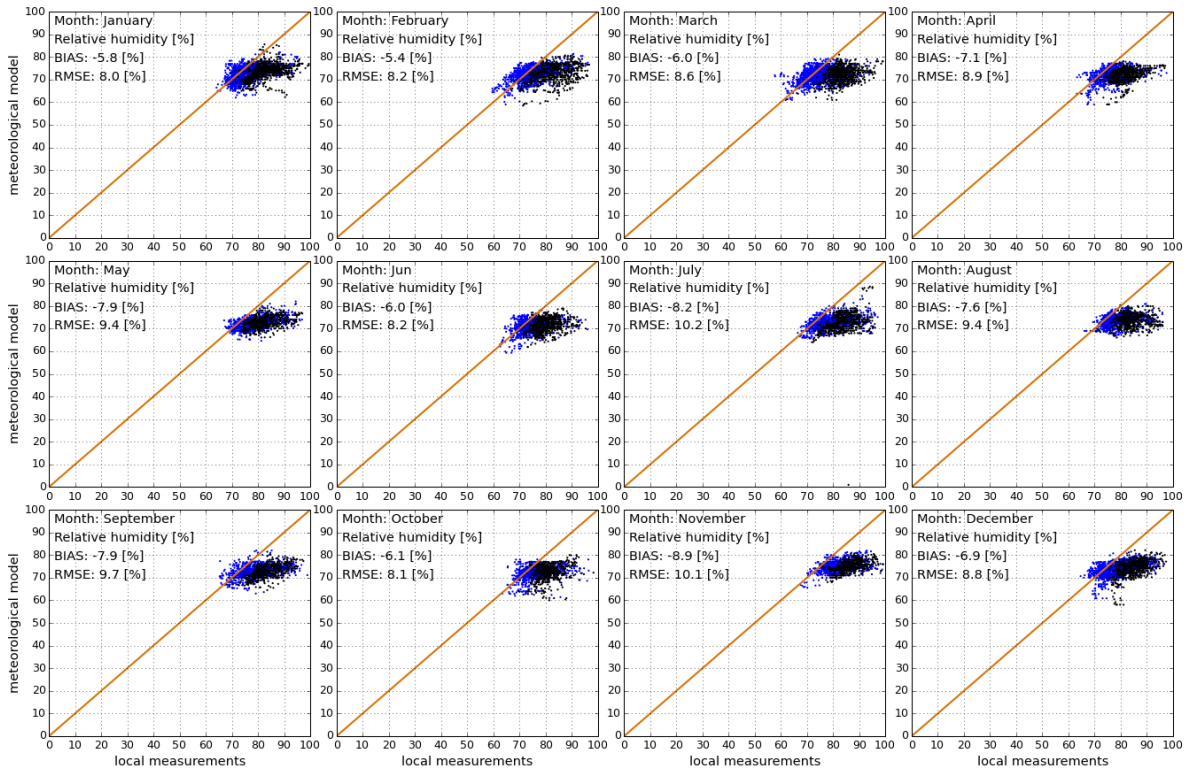

Figure 5.8: Scatterplots of relative humidity at 2 m at Gan meteorological station.
Measured values (horizontal axis) and meteorological model values (vertical axis).
Blue: day-time, black: night-time measurements.

5.2.3 Wind speed and wind direction at 10 metres

Wind speed and direction values delivered within Solargis data represent the height at 10 meters and they are calculated from the CFSR and CFSv2 models, from 10 m wind u- and v- components. The spatial resolution is kept as in the original data. Wind measurements take place **at the height of approx. 3 metres, while the model data represent values at height of 10 m above ground**.

Comparison of the modelled wind speed with ground measurements is shown in Table 5.5 and Figures 5.9 to 5.12. The model values are higher compared to the wind conditions measured at the meteorological stations. Similarly to relative humidity, the data representation for wind speed and wind direction strongly depends on the local conditions; therefore the model values are only indicative and better characterize a larger region rather than the local microclimate. The important source of systematic difference is different height of the installed sensor (3 metres above ground), compared to the model assumptions (10 metres).

Table 5.5 Wind speed: accuracy indicators of the model outputs [m/s].

Meteorological station	CFSR and CFSv2 models							
	Bias mean	Bias min	Bias max	Bias nigh-time	Bias day-time	RMSD hourly	RMSD daily	RMSD monthly
Hanimaadhoo	2.8	2.4	3.1	3.0	2.6	3.3	3.2	3.1
Hulhulé	2.4	2.2	2.4	2.5	2.2	2.9	2.7	2.6
Kadhdhoo	2.8	2.4	3.1	3.0	2.7	3.4	3.2	3.0
Gan	1.5	1.4	1.4	1.8	1.1	2.1	1.8	1.5

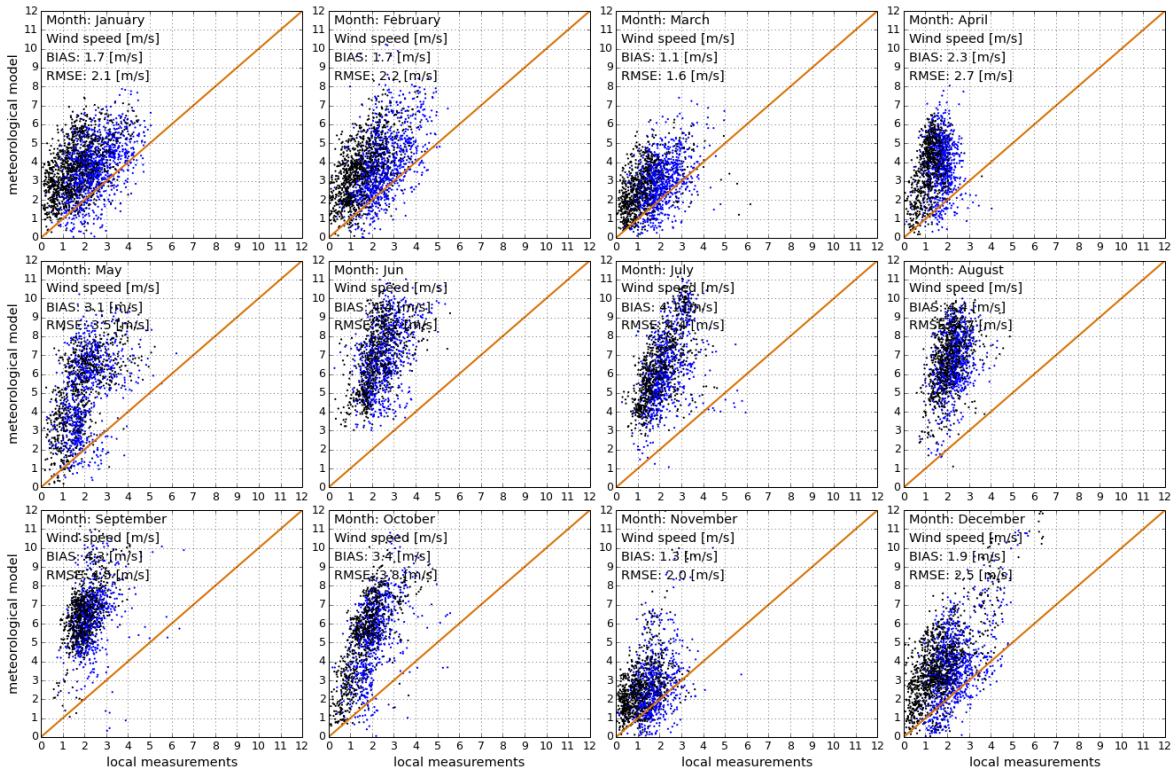

Figure 5.9: Scatterplots of wind speed at Hanimaadhoo meteorological station.
Measured values (horizontal axis) and meteorological model values (vertical axis).
Blue: day-time, black: night-time. (observations at 3 m height and model data at 10 m)

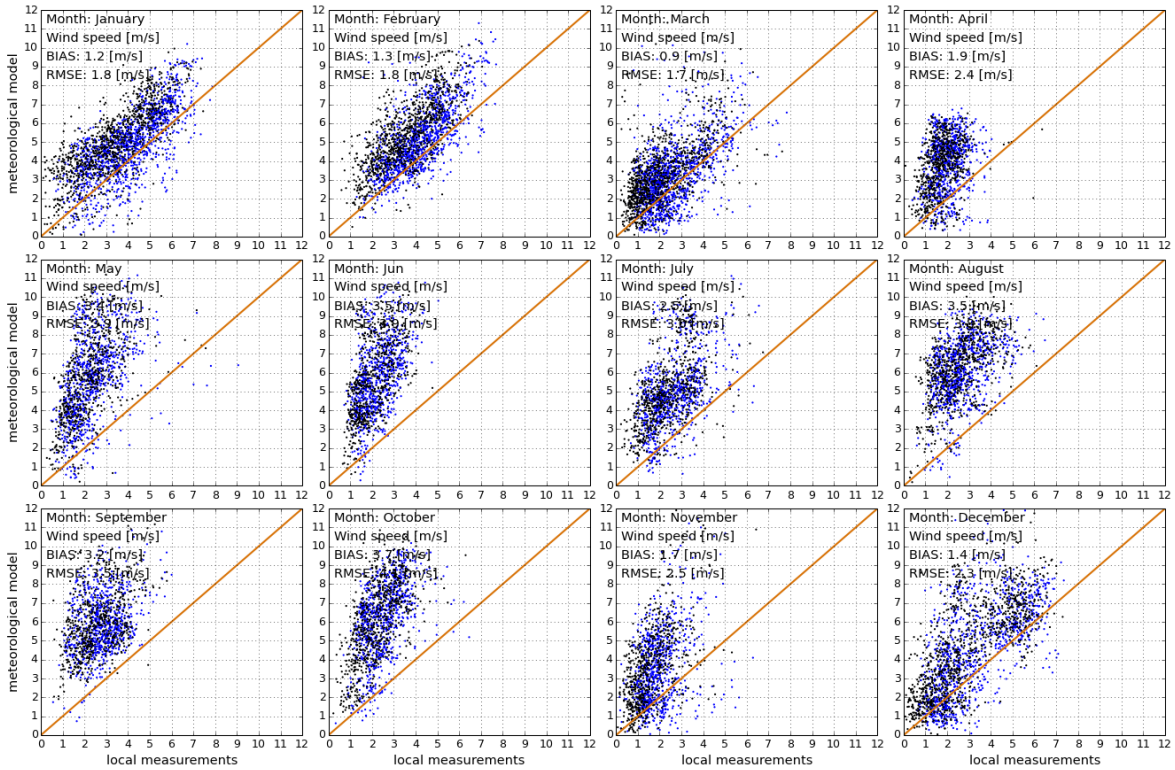

Figure 5.10: Scatterplots of wind speed at Hulhulé meteorological station.
Measured values (horizontal axis) and meteorological model values (vertical axis).
Blue: day-time, black: night-time. (observations at 3 m height and model data at 10 m)

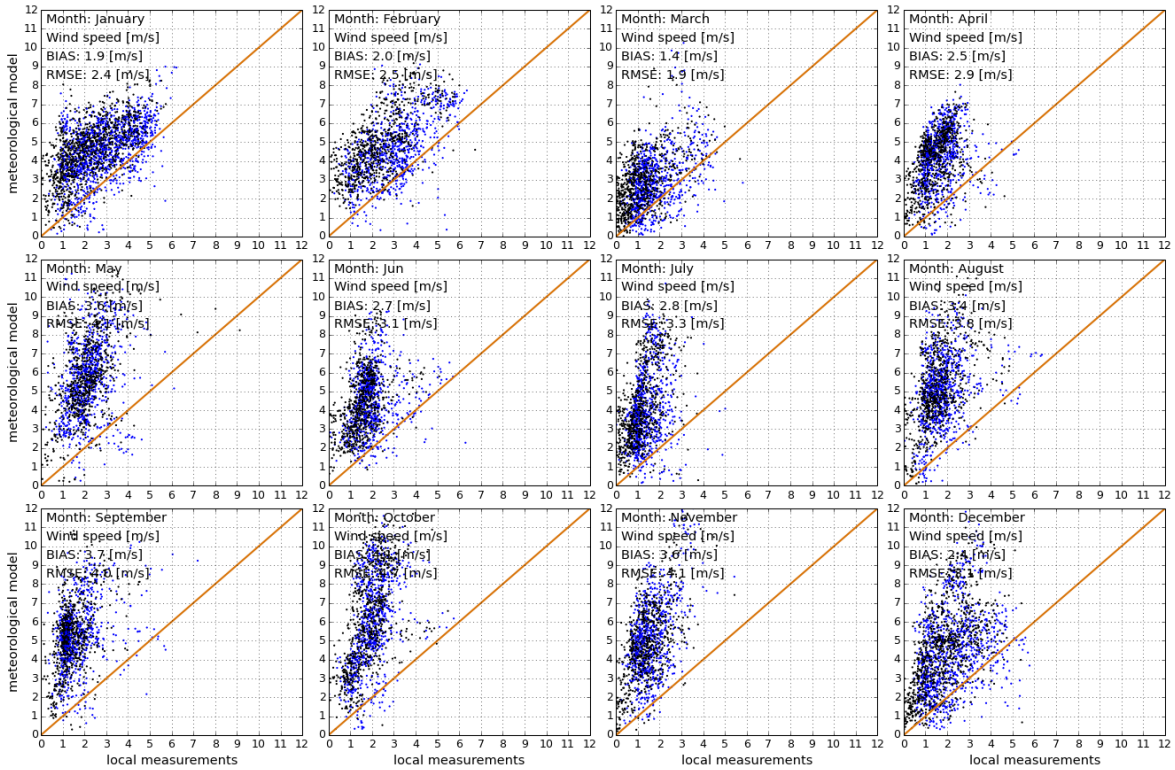

Figure 5.11: Scatterplots of wind speed at Kadhdhoo meteorological station.
Measured values (horizontal axis) and meteorological model values (vertical axis).
Blue: day-time, black: night-time. (observations at 3 m height and model data at 10 m)

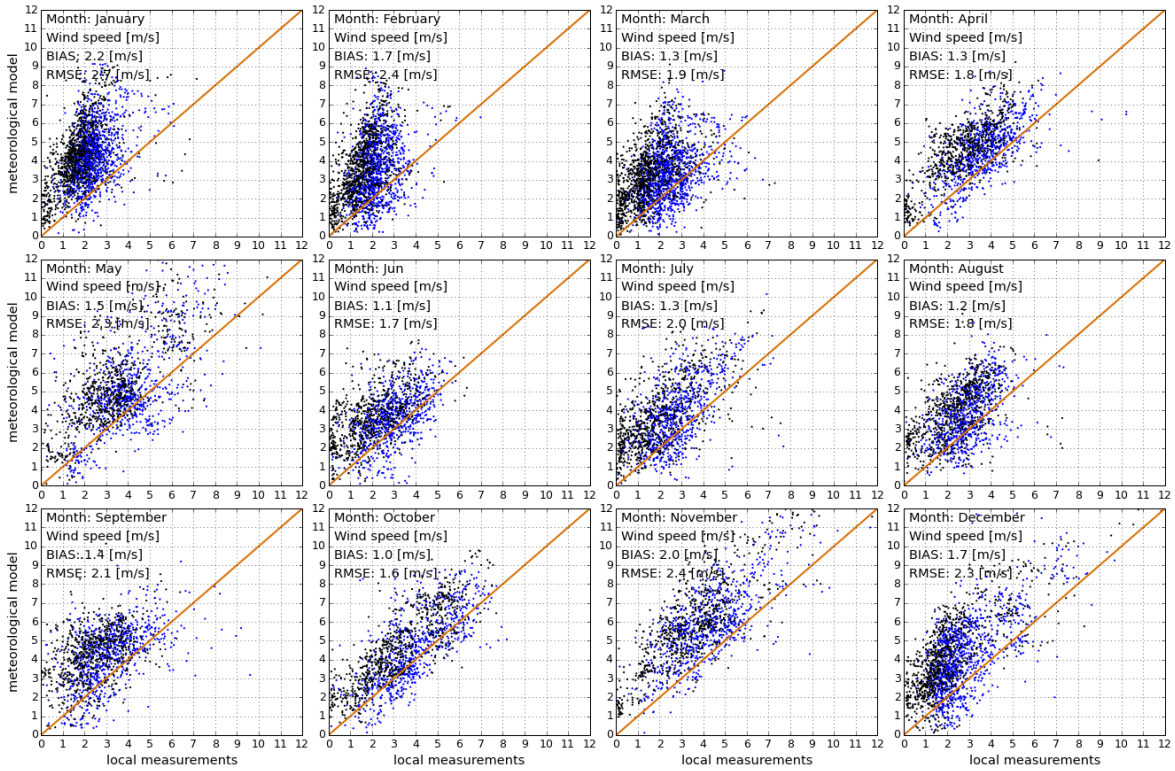

Figure 5.12: Scatterplots of wind speed at Gan meteorological station.
Measured values (horizontal axis) and meteorological model values (vertical axis).
Blue: day-time, black: night-time. (observations at 3 m heigth and model data at 10 m)

5.2.4 Atmospheric pressure

It was found that atmospheric pressure from the model fits well measured data with a very small bias for all stations, not exceeding 2 hPa.

5.3 Uncertainty of meteorological model data

The meteorological parameters are derived from two very similar numerical meteorological models covering periods from 1999 to 2010 (CFSR model) and 2011 to 2017 (CFSv2). Considering the comparison results, the uncertainty of the estimate for the main meteorological parameters is summarised in Table 5.6. The uncertainty expresses 80% probability of occurrence, so that it can be used for calculation of 90% probability of exceedance values.

It was found that the modelled air temperature fits reasonably well the measured data though (logically) due to the spatial resolution, the model daily amplitude is significantly smaller than amplitude of measured data.

Similarly to air temperature, relative humidity from the model exhibits much smaller daily amplitude than measured relative humidity. Wind speed data, obtained from the meteorological model, represents an area of larger region and this data is smoothed, in comparison to the point measurements collected at the meteorological sites. For all stations at Maldives wind speed is overestimated by the meteorological model. The reason is coarse resolution of the model and different elevation (observations at approx. 3 m height and the model data representing 10 m)

© 2018 Solargis

Table 5.6 Expected uncertainty of modelled meteorological parameters at the project site.

	Unit	Annual	Monthly	Hourly
Air temperature at 2 m	°C	±1.0	±1.0	±2.0
Relative Humidity at 2 m	%	±8	±8	±15
Average wind speed at 10 m	m/s	±3.0	±3.5	±4.0

© 2018 Solargis

6 SOLAR RESOURCE: UNCERTAINTY OF LONGTERM ESTIMATES

6.1 Uncertainty of solar resource yearly estimate

The **uncertainty of site-adapted satellite-based GHI and DNI** is determined by the uncertainty of the model and of the ground measurements [7], more specifically it depends on:

1. Parameterization and adaptation of **numerical models integrated in Solargis** for the given data inputs and their ability to generate accurate results for various geographical and time-variable conditions:
    - Data inputs into Solargis model (accuracy of satellite data, aerosols and water vapour and Digital Terrain Model).
    - Clear-sky model and its capability to properly characterize various states of the atmosphere
    - Simulation accuracy of the satellite model and cloud transmittance algorithms, being able to properly distinguish different types of desert surface, clouds, fog, but also snow and ice.
    - Diffuse and direct decomposition models
    - Site adaptation methods.
2. Uncertainty of the **ground-measurements**, which is determined by:
    - Accuracy of the instruments
    - Maintenance practices, including sensor cleaning, calibration
    - Data post-processing and quality control procedures.

Accuracy statistics, such as bias and RMSD (Chapter 4.3) characterize accuracy of Solargis model in the given validation points, relative to the ground measurements. The validation statistics is affected by local geography and by quality and reliability of the ground-measured data. Therefore the validation statistics only indicates performance of the model in the region.

Solargis model uncertainty is compared to the high-quality data measured by the meteorological instruments. Representativeness of such data comparison (satellite and ground-measured) is determined by the precision of the measuring instruments, the maintenance and operational practices, and by quality control of the measured data – in other words, by the measurement accuracy achieved at each meteorological station.

From the user's perspective, the information about the model uncertainty has probabilistic nature. It generalizes the validation accuracy and it has to be considered at different confidence levels. The expert estimate of the calculation uncertainty in this report assumes 80% probability of occurrence of values, so that it is straightforward to calculate P90 exceedance values.

The solar model uncertainty is discussed in Chapters 4 and 6.1. The main findings are summarized in Table 6.1. The site-adaptation procedure reduced uncertainty of estimate of all parameters. Chapter 6.3 evaluates combined uncertainty, in which also interannual variability is included (Chapter 6.2).

Table 6.1 Uncertainty of the model estimates for original and site-adapted annual long-term values (Considers 80% probability of occurrence)

Uncertainty of long-term annual values	Acronym	Uncertainty of the original Solargis model	Uncertainty of the Solargis model after site adaptation	
			After 1st year	After 2nd year
Global Horizontal Irradiation	GHI	±5.0%	±3.5%	±3.0%
Direct Normal Irradiance	DNI	±11.0%	±6.0%	±6.0%

The reduction of the model uncertainty was significant already after site adaptation using one year of ground measurements; and it was further reduced for GHI after second year of measurement campaign (Table 6.1). A higher uncertainty of DNI, measured with lower accuracy RSP instrument, is also a result of some quality issues as well as higher temporal instability of the instrument (Chapter 3.3). As a result, the uncertainty of site-adapted DNI after second year of measurements remained unchanged.

In case of both GHI and DNI parameters, the site adaptation has increased confidence in the model data values.

© 2018 Solargis

6.2 Uncertainty due to interannual variability of solar radiation

Weather changes in cycles and has also stochastic nature. Therefore annual solar radiation in each year can deviate from the long-term average in the range of few percent. The estimation of the interannual variability below shows the magnitude of this change. The uncertainty of GHI and DNI prediction is highest if only one single year is considered, but when averaged for a longer period, weather oscillations even out and approximate to the long-term average.

In this report, the **interannual variability** is calculated from the unbiased standard deviation *stdev* of GHI and DNI over **19 years**, considering, in the long-term, the normal distribution of the annual sums for *n* years, where x_i is any particular year and $\bar{x}$is longterm yearly average. Due to the limited number of years of available data, for the calculation we apply simplified assumption of normal distribution of yearly values:

$$stdev = \sqrt{\frac{1}{n-1}\sum_{i=1}^{n}(x_i - \bar{x})^2}$$

Tables 6.2 and 6.3 show GHI and DNI values that are to be exceeded at P90 for a consecutive number of years. The variability (var_n) for a number of years (n) is calculated from the unbiased standard deviation (*stdev*):

$$var_n = \frac{stdev}{\sqrt{n}}$$

The uncertainty, which characterises 80% probability of *occurrence* (U_{var}), is calculated from the variability (var_n), multiplying it with 1.28155:

$$uncert = 1.28155\ var$$

The lower boundary (negative value) of uncertainty represents 90% probability of *exceedance*, and it is used for calculating the P90 value.

Table 6.2 Annual GHI that should be exceeded with 90% probability in the period of 1 to 10 (25) years

Hanimaadhoo | Years	**1**	**2**	**3**	**4**	**5**	**6**	**7**	**8**	**9**	**10**	**25**
Variability [±%]	1.3	0.9	0.8	0.7	0.6	0.5	0.5	0.5	0.4	0.4	0.3
Uncertainty P90 [±%]	1.7	1.2	1.0	0.8	0.7	0.7	0.6	0.6	0.6	0.5	0.3
Minimum GHI P90	**1984**	**1994**	**1999**	**2001**	**2003**	**2004**	**2005**	**2006**	**2007**	**2007**	**2011**

Hulhulé | Years	**1**	**2**	**3**	**4**	**5**	**6**	**7**	**8**	**9**	**10**	**25**
Variability [±%]	1.5	1.1	0.9	0.8	0.7	0.6	0.6	0.5	0.5	0.5	0.3
Uncertainty P90 [±%]	2.0	1.4	1.1	1.0	0.9	0.8	0.7	0.7	0.7	0.6	0.4
Minimum GHI P90	**2012**	**2023**	**2029**	**2032**	**2034**	**2035**	**2037**	**2038**	**2039**	**2039**	**2044**

Kadhdhoo | Years	**1**	**2**	**3**	**4**	**5**	**6**	**7**	**8**	**9**	**10**	**25**
Variability [±%]	2.1	1.5	1.2	1.0	0.9	0.8	0.8	0.7	0.7	0.6	0.4
Uncertainty P90 [±%]	2.6	1.9	1.5	1.3	1.2	1.1	1.0	0.9	0.9	0.8	0.5
Minimum GHI P90	**1992**	**2007**	**2014**	**2019**	**2021**	**2024**	**2025**	**2026**	**2028**	**2029**	**2035**

Gan | Years	**1**	**2**	**3**	**4**	**5**	**6**	**7**	**8**	**9**	**10**	**25**
Variability [±%]	2.0	1.4	1.2	1.0	0.9	0.8	0.8	0.7	0.7	0.6	0.4
Uncertainty P90 [±%]	2.6	1.8	1.5	1.3	1.2	1.1	1.0	0.9	0.9	0.8	0.5
Minimum GHI P90	**1994**	**2010**	**2017**	**2021**	**2024**	**2026**	**2027**	**2029**	**2030**	**2031**	**2037**

© 2018 Solargis

Table 6.3 Annual DNI that should be exceeded with 90% probability in the period of 1 to 10 (25) years.

Hanimaadhoo | Years	**1**	**2**	**3**	**4**	**5**	**6**	**7**	**8**	**9**	**10**	**25**
Variability [±%]	3.6	2.5	2.1	1.8	1.6	1.5	1.4	1.3	1.2	1.1	0.7
Uncertainty P90 [±%]	4.6	3.3	2.7	2.3	2.1	1.9	1.7	1.6	1.5	1.5	0.9
Minimum DNI P90	**1373**	**1393**	**1401**	**1406**	**1410**	**1412**	**1414**	**1416**	**1417**	**1419**	**1426**

Hulhulé | Years	**1**	**2**	**3**	**4**	**5**	**6**	**7**	**8**	**9**	**10**	**25**
Variability [±%]	4.1	2.9	2.3	2.0	1.8	1.7	1.5	1.4	1.4	1.3	0.8
Uncertainty P90 [±%]	5.2	3.7	3.0	2.6	2.3	2.1	2.0	1.8	1.7	1.6	1.0
Minimum DNI P90	**1408**	**1430**	**1440**	**1446**	**1450**	**1453**	**1456**	**1458**	**1459**	**1460**	**1469**

Kadhdhoo | Years	**1**	**2**	**3**	**4**	**5**	**6**	**7**	**8**	**9**	**10**	**25**
Variability [±%]	4.5	3.2	2.6	2.2	2.0	1.8	1.7	1.6	1.5	1.4	0.9
Uncertainty P90 [±%]	5.8	4.1	3.3	2.9	2.6	2.4	2.2	2.0	1.9	1.8	1.2
Minimum DNI P90	**1466**	**1492**	**1503**	**1510**	**1515**	**1519**	**1521**	**1523**	**1525**	**1527**	**1537**

Gan | Years	**1**	**2**	**3**	**4**	**5**	**6**	**7**	**8**	**9**	**10**	**25**
Variability [±%]	4.3	3.0	2.5	2.1	1.9	1.7	1.6	1.5	1.4	1.4	0.9
Uncertainty P90 [±%]	5.5	3.9	3.2	2.7	2.5	2.2	2.1	1.9	1.8	1.7	1.1
Minimum DNI P90	**1520**	**1546**	**1558**	**1564**	**1569**	**1573**	**1575**	**1577**	**1579**	**1581**	**1591**

We can interpret the above Table 6.2 and 6.3 on the example of Hulhulé site:

i. GHI interannual variability at P90 of 2.0% has to be considered for any single year in Hulhulé. In other words, assuming that the long-term average is 2052 kWh/m^2, it is expected (with 90% probability) that annual GHI exceeds, at any single year, the value of 2012 kWh/m^2.

ii. Within a period of three consecutive years, it is expected at P90 that annual average of GHI exceeds value of 2029 kWh/m^2;

iii. For a period of 25 years, it is expected at 90% probability that due to interannual variability the estimate of the long-term annual DNI average will deviate within the range of ±1.0% in Hulhulé. Thus assuming that the estimate of the long-term average is 1485 kWh/m^2, it can be expected at P90 that *due to variability of weather*, it should be at least 1469 kWh/m^2.

It is to be underlined that prediction of the future irradiation is based on the analysis of the recent historical data (period 1999 to 2017). Future weather changes may include man-induced or natural events such as volcano eruptions, which may have impact on this prediction.

Based on the existing scientific knowledge [20, 21], an effect of **extreme volcano eruptions**, with an emission of large amount of stratospheric aerosols, can be estimated on the example of Pinatubo event in 1991 (the second largest volcano eruption in 20th century). It can be expected that in such a case, the annual DNI in the affected year can decrease by approx. 16% or more, compared to the long-term average, still influencing another two consecutive years. In the same way, the volcano eruption of the comparable size may reduce long-term average estimate of DNI by about 4%. The decrease of GHI is much lower; the annual value in the particular year of eruption could be reduced by about 2% compared to the long-term average.

© 2018 Solargis

6.3 Combined uncertainty

In this Chapter, the combined uncertainty of the annual GHI and DNI values is quantified. Taking into account uncertainties of both types of data (satellite and ground measured), the combined effect of two components of the uncertainty of the site-adapted GHI and DNI values has to be considered.

1. **Uncertainty of the estimate** (U_{est}) of the annual solar resource values, which is ±3.0% for GHI and ±6.0% for DNI (Chapter 6.1);
2. **Interannual variability** (U_{var}) in any particular year, due to changing weather. In four Maldivian sites, it varies from ±1.7% to ±2.6% for GHI and from ±4.6% to ±5.8% for DNI. The uncertainty due to weather variability decreases over the time with square root of the number of years (Chapter 6.2).

The two above-mentioned uncertainties combine in U_c (see Glossary), which represents a conservative expectation of the minimum GHI and DNI assuming various number of years N (Tables 6.4 and 6.5). Considering a simplified assumption of normal distribution of the annual values, probability of exceedance can be calculated at different confidence levels. GHI and DNI minimum annual values expected for combined uncertainty in any single year are shown on Figure 6.2 and 6.3.

Table 6.4 Combined probability of exceedance of annual GHI for uncertainty of the estimate ±3.0%.

Nr. of years	Uncertainty of estimate	Interanual variability	Combined uncertainty	Expected minimum | **Hanimaadhoo** [kWh/m²]								
N	[±%]	N years [±%]	P90 [±%]	P01	P05	P10	P25	P50	P75	P90	P95	P99
1	3.0	1.7	3.4	2144	2107	2087	2055	2018	1982	1949	1929	1892
5	3.0	0.7	3.1	2131	2098	2081	2051	2018	1985	1956	1938	1905
10	3.0	0.5	3.0	2130	2097	2080	2051	2018	1986	1957	1939	1907
25	3.0	0.3	3.0	2129	2096	2079	2050	2018	1986	1957	1940	1908

Nr. of years	Uncertainty of estimate	Interanual variability	Combined uncertainty	Expected minimum | **Hulhulé** [kWh/m²]								
N	[±%]	N years [±%]	P90 [±%]	P01	P05	P10	P25	P50	P75	P90	P95	P99
1	3.0	2.0	3.6	2185	2146	2126	2091	2052	2013	1978	1958	1918
5	3.0	0.9	3.1	2168	2134	2116	2086	2052	2018	1988	1970	1936
10	3.0	0.6	3.1	2166	2133	2115	2085	2052	2019	1989	1971	1938
25	3.0	0.4	3.0	2165	2132	2114	2085	2052	2019	1990	1972	1939

Nr. of years	Uncertainty of estimate	Interanual variability	Combined uncertainty	Expected minimum | **Kadhdhoo** [kWh/m²]								
N	[±%]	N years [±%]	P90 [±%]	P01	P05	P10	P25	P50	P75	P90	P95	P99
1	3.0	2.6	4.0	2194	2150	2127	2088	2046	2003	1964	1941	1897
5	3.0	1.2	3.2	2165	2130	2111	2080	2046	2011	1980	1961	1926
10	3.0	0.8	3.1	2161	2127	2109	2079	2046	2012	1982	1964	1930
25	3.0	0.5	3.0	2159	2125	2108	2078	2046	2013	1983	1966	1932

Nr. of years	Uncertainty of estimate	Interanual variability	Combined uncertainty	Expected minimum | **Gan** [kWh/m²]								
N	[±%]	N years [±%]	P90 [±%]	P01	P05	P10	P25	P50	P75	P90	P95	P99
1	3.0	2.6	4.0	2195	2152	2129	2090	2048	2005	1966	1943	1900
5	3.0	1.2	3.2	2167	2132	2113	2082	2048	2013	1982	1963	1928
10	3.0	0.8	3.1	2163	2129	2111	2081	2048	2014	1984	1966	1932
25	3.0	0.5	3.0	2161	2128	2110	2080	2048	2015	1985	1968	1934

© 2018 Solargis

Table 6.5 Combined probability of exceedance of annual DNI for uncertainty of the estimate ±6.0%.

Nr. of years	Uncertainty of estimate	Interanual variability	Combined uncertainty	Expected minimum | **Hanimaadhoo** [kWh/m^2]								
N	[±%]	N years [±%]	P90 [±%]	P01	P05	P10	P25	P50	P75	P90	P95	P99
1	6.0	4.6	7.6	1637	1579	1549	1497	1440	1382	1331	1300	1242
5	6.0	2.1	6.3	1605	1557	1531	1488	1440	1392	1348	1322	1274
10	6.0	1.5	6.2	1601	1554	1528	1486	1440	1393	1351	1326	1278
25	6.0	0.9	6.1	1598	1552	1527	1486	1440	1394	1352	1327	1281

Nr. of years	Uncertainty of estimate	Interanual variability	Combined uncertainty	Expected minimum | **Hulhulé** [kWh/m^2]								
N	[±%]	N years [±%]	P90 [±%]	P01	P05	P10	P25	P50	P75	P90	P95	P99
1	6.0	5.2	7.9	1699	1636	1603	1547	1485	1423	1367	1333	1271
5	6.0	2.3	6.4	1659	1608	1581	1535	1485	1435	1389	1362	1311
10	6.0	1.6	6.2	1653	1604	1577	1534	1485	1436	1393	1366	1317
25	6.0	1.0	6.1	1649	1601	1575	1533	1485	1437	1395	1369	1321

Nr. of years	Uncertainty of estimate	Interanual variability	Combined uncertainty	Expected minimum | **Kadhdhoo** [kWh/m^2]								
N	[±%]	N years [±%]	P90 [±%]	P01	P05	P10	P25	P50	P75	P90	P95	P99
1	6.0	5.8	8.3	1790	1721	1684	1623	1555	1487	1426	1389	1320
5	6.0	2.6	6.5	1739	1685	1657	1609	1555	1502	1454	1425	1371
10	6.0	1.8	6.3	1732	1680	1653	1606	1555	1504	1458	1430	1378
25	6.0	1.2	6.1	1728	1677	1650	1605	1555	1505	1460	1433	1383

Nr. of years	Uncertainty of estimate	Interanual variability	Combined uncertainty	Expected minimum | **Gan** [kWh/m^2]								
N	[±%]	N years [±%]	P90 [±%]	P01	P05	P10	P25	P50	P75	P90	P95	P99
1	6.0	5.5	8.1	1846	1776	1739	1677	1609	1540	1478	1441	1371
5	6.0	2.5	6.5	1798	1742	1713	1663	1609	1554	1504	1475	1419
10	6.0	1.7	6.2	1791	1738	1709	1661	1609	1556	1508	1480	1426
25	6.0	1.1	6.1	1787	1735	1707	1660	1609	1557	1510	1483	1430

This analysis is based on the data representing a history of year 1999 to 2017, and on the expert extrapolation of the related weather variability. This report may not reflect possible man-induced climate change or occurrence of extreme events such as large volcano eruptions in the future (see the last paragraph in Chapter 6.2).

Graphical visualisation of Tables 6.4 and 6.5 on the example of the Hulhulé Airport is shown in Figures 6.1 and 6.2, where the expected probabilities of exceedance (different Pxx scenarios) are drawn on the cumulative distribution curve showing yearly GHI and DNI values.

© 2018 Solargis

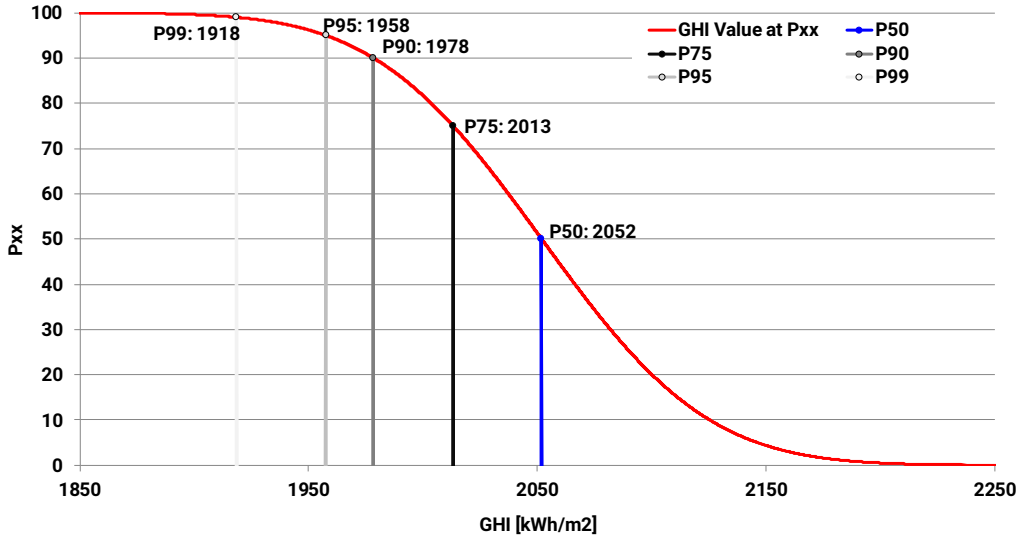

Figure 6.1: Expected Pxx values for GHI at Hulhulé Airport

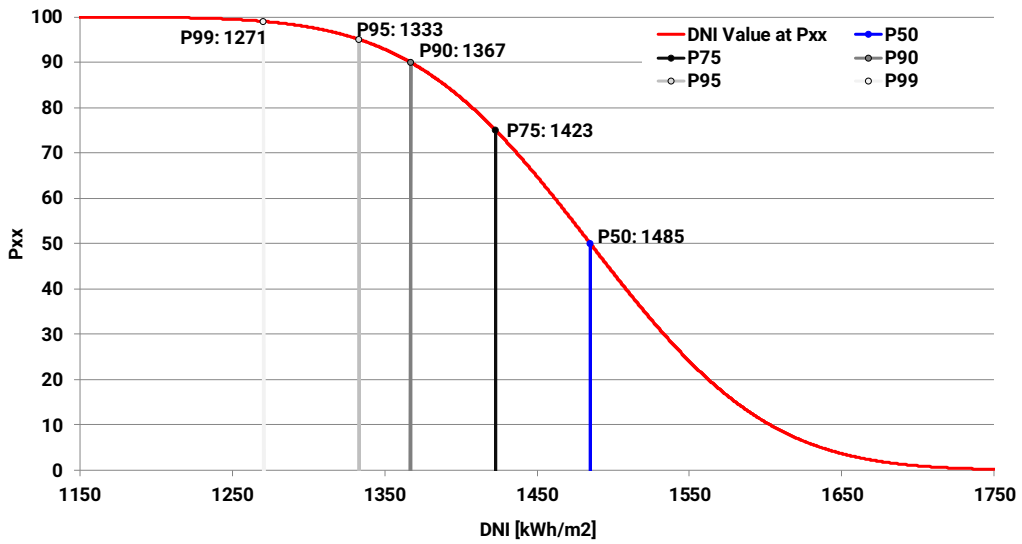

Figure 6.2: Expected Pxx values for DNI at Hulhulé Airport

© 2018 Solargis

7 TIME SERIES AND TYPICAL METEOROLOGICAL YEAR DATA

7.1 Delivered data sets

This report is accompanied by data sets delivered individually for position of each of four solar meteorological stations in Maldives. The data include (Tables 7.1 and 7.2):

- Solar and meteorological measurements, after second level quality assessment (first level was delivered by Suntrace) representing an planned minimum of 24 months of the measuring campaign;
- Time series, representing last 19+ years;
- Typical Meteorological Year data, representing last 19 years.

The data is delivered in formats ready to use in energy simulation software. This report provides detailed insight of the methodologies and results.

Table 7.1 Delivered data characteristics

Feature	Time coverage	Primary time step	Delivered files
Ground measurements (Suntrace)	Dec 2015 to Mar 2018*	1 minute	Quality controlled measurements 1- minute time step
Model data original model (Solargis)	Jan 1999 to Dec 2017	30 minutes	Time series – hourly Time series – monthly Time series – yearly
Model data site adapted model (Solargis)	Jan 1999 to Dec 2017	30 minutes	Time series – hourly Time series – monthly Time series – yearly
Model data site adapted model (Solargis)	Jan 1999 to Dec 2017	hourly	Typical Meteorological Year P50 Typical Meteorological Year P90

** April 2018 at Kadhdhoo and Gan airport site*

Table 7.2 Parameters in the delivered site-adapted time series and TMY data (hourly time step)

Parameter	Acronym	Unit	TS	TMY P50	TMY P90
Global horizontal irradiance	GHI	W/m^2	X	X	X
Direct normal irradiance	DNI	W/m^2	X	X	X
Diffuse horizontal irradiance	DIF	W/m^2	X	X	X
Global tilted irradiance (at optimum angle)	GHI	W/m^2	X	-	-
Solar azimuth	SA	°	X	X	X
Solar elevation	SE	°	X	X	X
Air temperature at 2 metres	TEMP	°C	X	X	X
Wind speed at 10 metres	WS	m/s	X	X	X
Wind direction at 10 metres	WD	°	X	X	X
Relative humidity	RH	%	X	X	X
Air Pressure	AP	hPa	X	X	X
Precipitable Water	PWAT	kg/m^2	X	X	X

© 2018 Solargis

7.2 TMY method

The Typical Meteorological Year (TMY) data sets are delivered, together with Solargis time series data and this report. TMY contains hourly data derived from the time series covering complete 19 years (1999 to 2017). The data history of 19 years is compressed into one year (Figure 7.1 to 7.3) following two criteria:

- Minimum difference between statistical characteristics (annual average, monthly averages) of TMY and long-term time series. This criterion is given about 80% weighting.
- Maximum similarity of monthly Cumulative Distribution Functions (CDF) of TMY and full-time series, so that occurrence of typical hourly values is well represented for each month. This criterion is given about 20% weighting.

TMY P50 data set is constructed on the monthly basis. For each month the long-term average monthly value and cumulative distribution for each parameters is calculated: Direct Normal Irradiance (DNI), Global Horizontal Irradiance (GHI), Diffuse Horizontal Irradiance (DIF) and Air Temperature (TEMP). Following the monthly data for each individual year from the set of 19 years are compared to the long-term parameters. The monthly data from the year, which resembles the long-term parameters more closely, is selected. The procedure is repeated for all 12 months, and the TMY is constructed by concatenating the selected months into one artificial (but representative) year.

The method for calculation **P90** data set is based on the TMY P50 method. It has been modified in a way of how a candidate month is selected. The search for set of twelve candidates is repeated in iteration until a condition of minimization of difference between annual P90 value and annual average of new TMY is reached (instead of minimization of differences in monthly means and CDFs, as applied in P50 case). Once the selection converges to minimum difference, the TMY is created by concatenation of selected months. The P90 annual values are calculated for each confidence limit – from the combined uncertainty of estimate and inter-annual variability, which can occur in any year (Chapter 6.3).

To derive TMY that fits specific needs of the selected energy application the different weights are given to individual parameters – thus highlighting important properties. In solar energy applications, the higher importance is given to GHI and DNI. In assembling TMY P50, the values of DNI, GHI, DIF and TEMP are only considered, where the weights are set as follows: 0.9 is given to DNI, 0.3 to GHI, 0.02 to diffuse horizontal irradiance, and 0.07 to air temperature (divided by the total of 1.29).

To derive solar resource parameters with an **hourly time step**, the original satellite data with time resolution of 30-minutes were aggregated by time integration. The meteorological parameters are available in the original 1-hourly time step. The TMY datasets were constructed from solar radiation and meteorological data (Chapters 4 and 5). Time zone was adjusted to Maldives Time MVT (UTC +05:00).

More about the Solargis TMY method in [22].

7.3 Results

Two data sets are derived from the Solargis historical time series for the four sites: P50 and P90. In graphs and tables below we show the values for Hulhulé meteorological site, in order to present the methodology of TMY data calculation.

Important note: Due to the inherent features of the underlying methods, monthly values in TMY data set in Tables 7.3 to 7.6 do not fit to the values generated from full time series (Figures 7.1 to 7.4).

Table 7.3 Monthly and yearly long-term GHI averages as calculated from time series and from TMY representing P50, and P90 cases at Hulhulé site

Global Horizontal Irradiation [kWh/m²]	1	2	3	4	5	6	7	8	9	10	11	12	Year
Time series (19 years)	178	182	207	185	166	157	162	169	163	177	152	155	**2052**
TMY for P50 case	180	175	206	186	164	158	165	172	156	175	160	155	**2052**
TMY for P90 case	173	178	208	176	158	153	159	170	156	169	124	152	**1978**

Table 7.4 Monthly and yearly long-term DNI averages as calculated from time series and from TMY representing P50, and P90 cases at Hulhulé site

Direct Normal Irradiation [kWh/m²]	1	2	3	4	5	6	7	8	9	10	11	12	Year
Time series (19 years)	140	147	163	143	117	105	104	107	102	131	110	117	**1485**
TMY for P50 case	141	148	162	142	118	105	103	107	101	128	112	117	**1485**
TMY for P90 case	133	143	162	134	101	99	101	103	93	117	76	105	**1367**

Table 7.5 Monthly and yearly long-term DIF averages as calculated from time series and from TMY representing P50, and P90 cases at Hulhulé site

Direct Normal Irradiation [kWh/m²]	1	2	3	4	5	6	7	8	9	10	11	12	Year
Time series (19 years)	79	73	82	76	79	78	83	86	84	79	73	75	**946**
TMY for P50 case	81	68	82	79	76	80	87	89	78	79	80	77	**956**
TMY for P90 case	77	71	82	74	80	77	81	88	81	79	69	78	**937**

Table 7.6 Monthly and yearly long-term TEMP averages as calculated from time series and from TMY representing P50, and P90 cases at Hulhulé site

Air temperature [°C]	1	2	3	4	5	6	7	8	9	10	11	12	Year
Time series (19 years)	27.5	27.6	28.2	28.7	28.7	28.4	28.2	28.0	27.9	27.9	27.7	27.5	**28.0**
TMY for P50 case	27.6	27.5	28.2	28.2	28.4	28.4	28.0	28.3	27.9	27.9	28.2	28.2	**28.1**
TMY for P90 case	27.5	27.5	28.2	28.7	28.6	28.6	28.1	28.1	27.8	28.0	27.7	27.5	**28.0**

As an example of interpretation of the tables above, the TMY data sets for P50 and P90 can be described as:

1. **P50 TMY** data set represents, for each month, the average climate conditions and the most representative cumulative distribution function, therefore extreme situations (e.g. extremely cloudy weather) are not represented in this dataset. The long-term annual summary of GHI and DNI are considered as the most critical parameters to consider, and in this data set P50 **GHI value is 2052 kWh/m²** and **DNI value is 1485 kWh/m².**
2. **P90 TMY** data set represents for each month the climate conditions, which after summarization GHI and DNI for the whole year results in the value *equal or close to P90* derived by the analysis of uncertainty of the estimate and of the interannual variability for any single year (Chapter 6.3). Thus TMY for P90 represents generally a conservative estimate, i.e. a year with the long-term value of **GHI of 1978 kWh/m²** and **DNI of 1367 kWh/m²**.

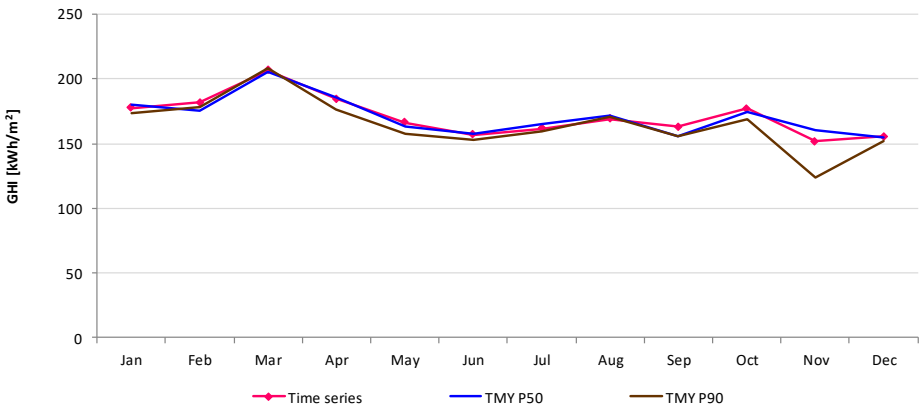

Figure 7.1: GHI monthly values derived from time series and TMY P50 and P90 at Hulhulé site.

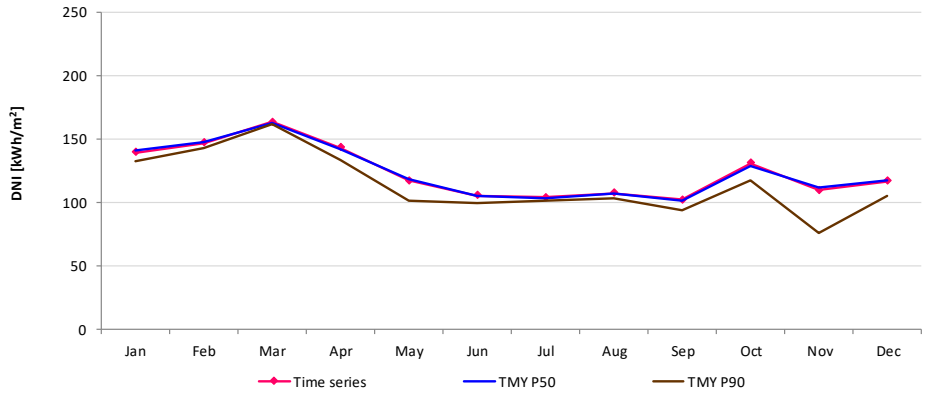

Figure 7.2: DNI monthly values derived from time series and TMY P50 and P90 at Hulhulé site.

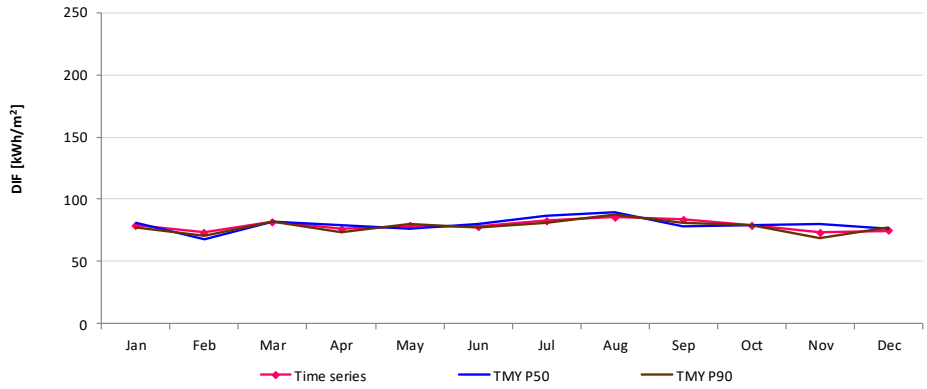

Figure 7.3: DIF monthly values derived from time series and TMY P50 and P90 at Hulhulé site

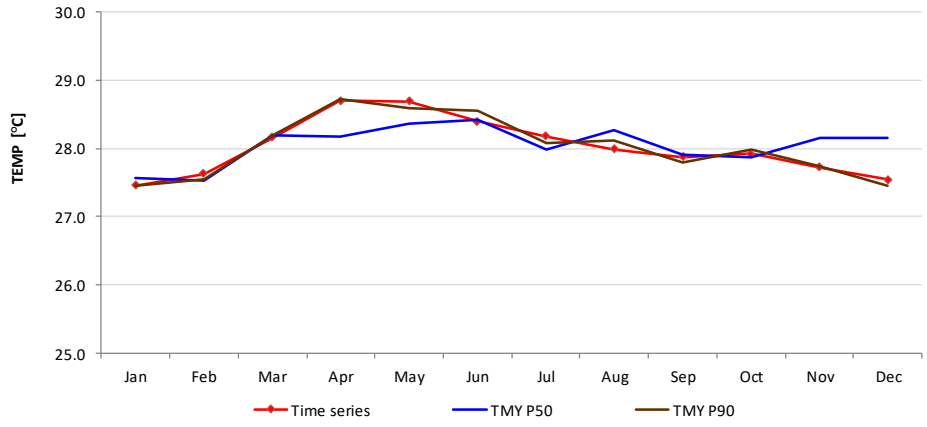

Figure 7.4: TEMP monthly values derived from time series and TMY P50 and P90 at Hulhulé site

It is important to note that the data reduction in the TMY data set is not possible without loss of information contained in the original multiyear time series. Therefore **time series data are considered as the most accurate reference suitable for the statistical analysis of solar resource and meteorological parameters of the sites.**

© 2018 Solargis

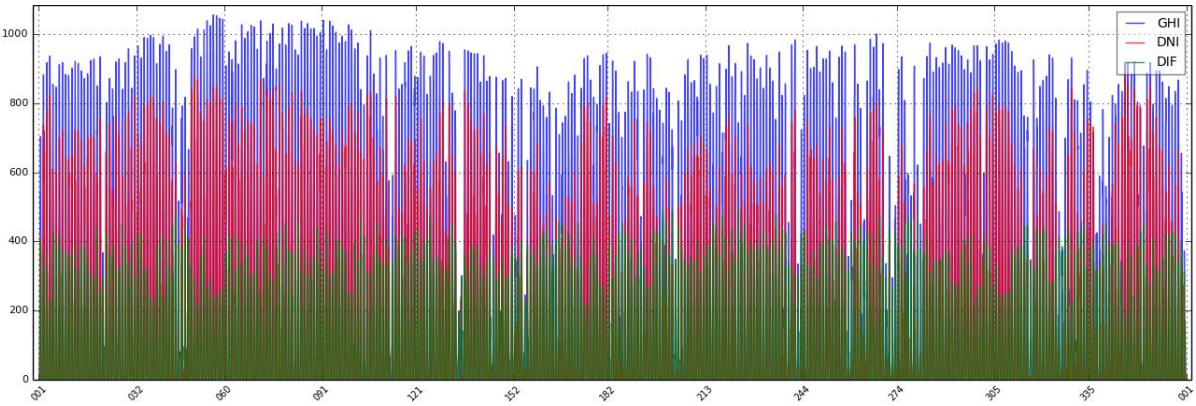

Figure 7.5: Seasonal profile of GHI, DNI and DIF for Typical Meteorological Year P50
Hulhulé site: X-axis – day of the year; Y-axis – solar irradiance W/m^2

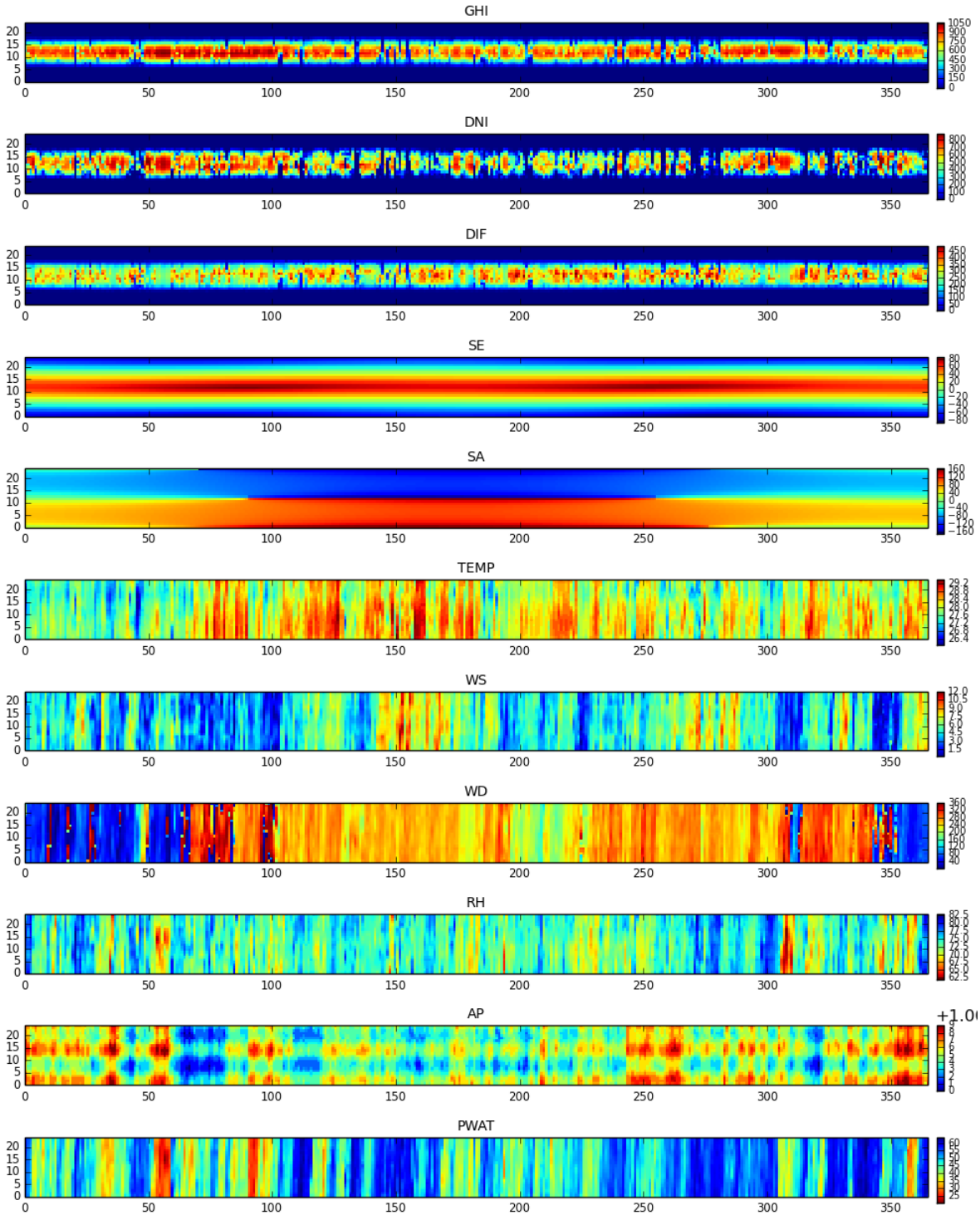

Figure 7.6: Snapshot of Typical Meteorological Year for P50 for Hulhulé

8 CONCLUSIONS

This report accompanies delivery of site-specific solar resource and meteorological data for four sites, where solar meteorological stations have been installed during December 2015 and operated originally for period of 24 months (until December 2017, when extended until March (April in Kadhdhoo and Gan) 2018. Comparing to the results obtained after period of first 12 months of measurement campaign, the data uncertainty has been reduced for GHI and remain unchanged for DNI due to some measurements issues.

The measured data is used in site-adaptation of the Solargis model. As a result, reliable historical time series and TMY data is computed and provided in formats ready to use in standard photovoltaic energy simulation software.

The reliability of the delivered data is high and it can be used for energy evaluation of any project in Maldives and also for bankable assessment.

© 2018 Solargis

ANNEX 1: SITE RELATED DATA STATISTICS

Yearly summaries of solar and meteorological parameters

Statistics for site adapted model yearly values representing 19 years (1999 to 2017).

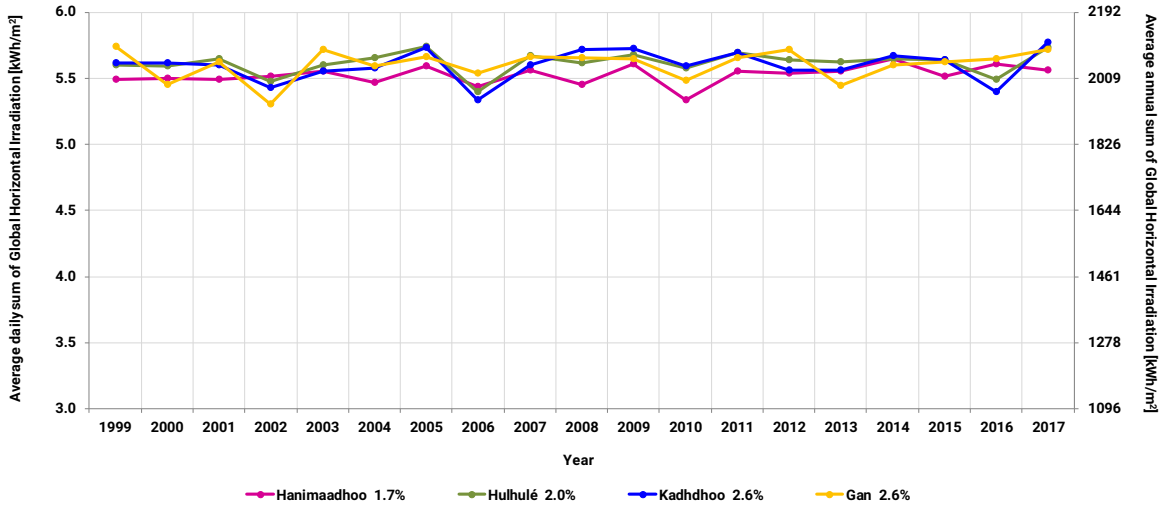

Figure I: Interannual variability of site-adapted yearly GHI [kWh/m^2].
Annual averages (*avg*, solid line) and standard deviation (value behind the names of sites).

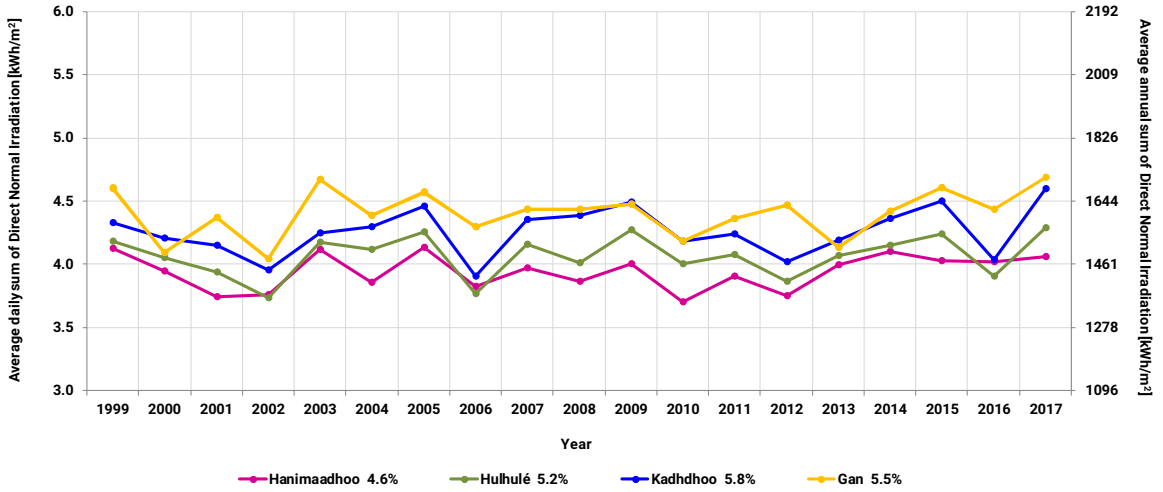

Figure II: Interannual variability of site-adapted yearly DNI [kWh/m^2].
Annual averages (*avg*, solid line) and standard deviation (value behind the names of sites).

© 2018 Solargis

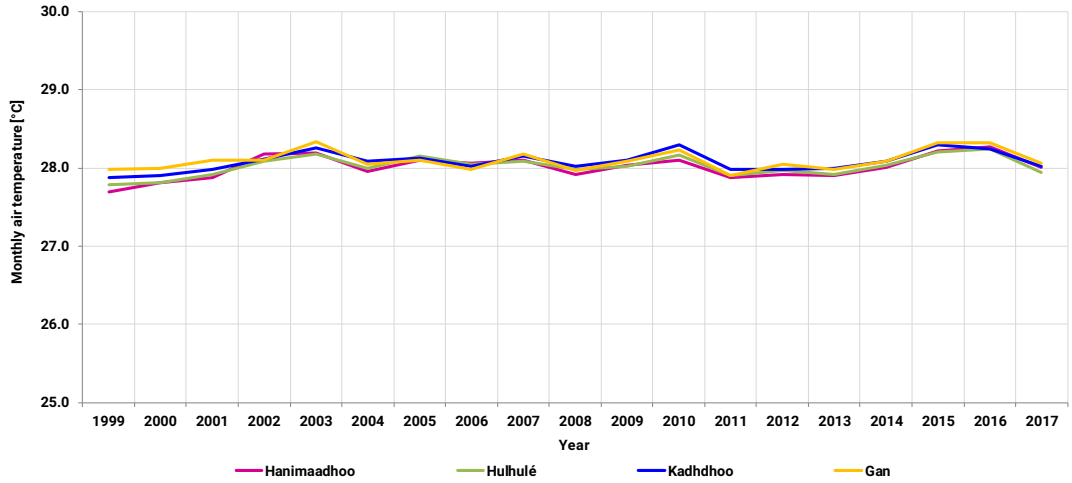

Figure III: Interannual variability of yearly TEMP [°C].
Annual averages (*avg*, solid line).

Monthly summaries of solar and meteorological parameters

The graphs compare (site-adapted) monthly model time series compared to long-term averages.

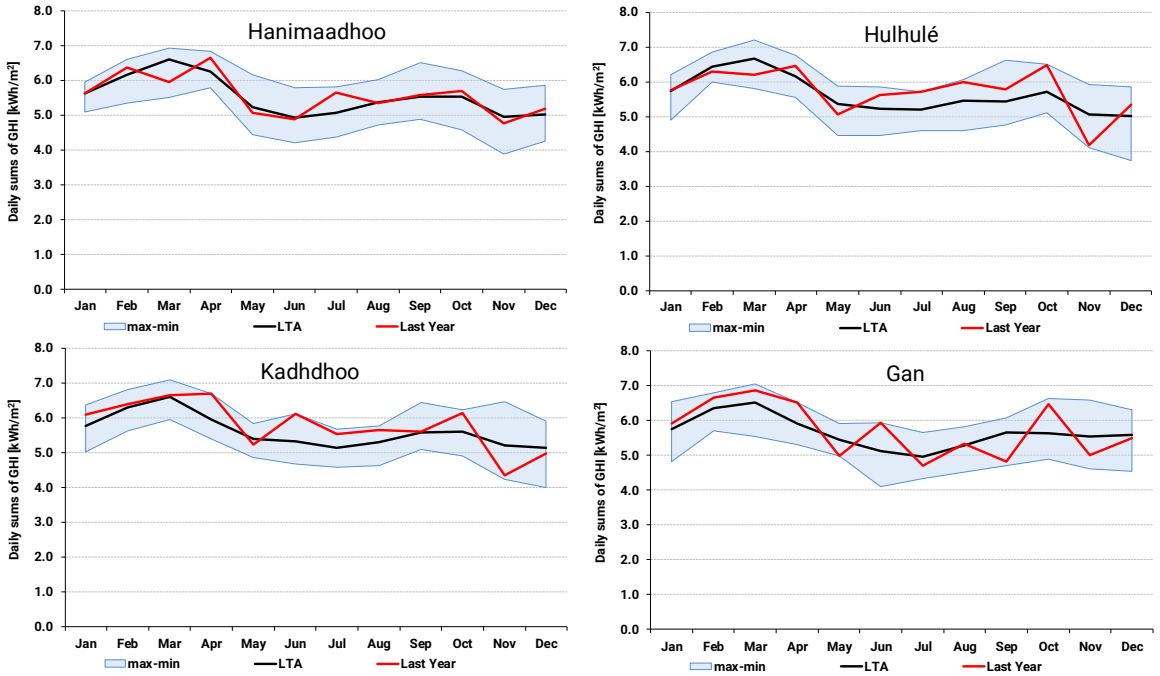

Figure IV: GHI monthly averages [kWh/m^2].
Monthly average shown as solid line; min/max monthly values as as boundary lines; last 24 months in red.

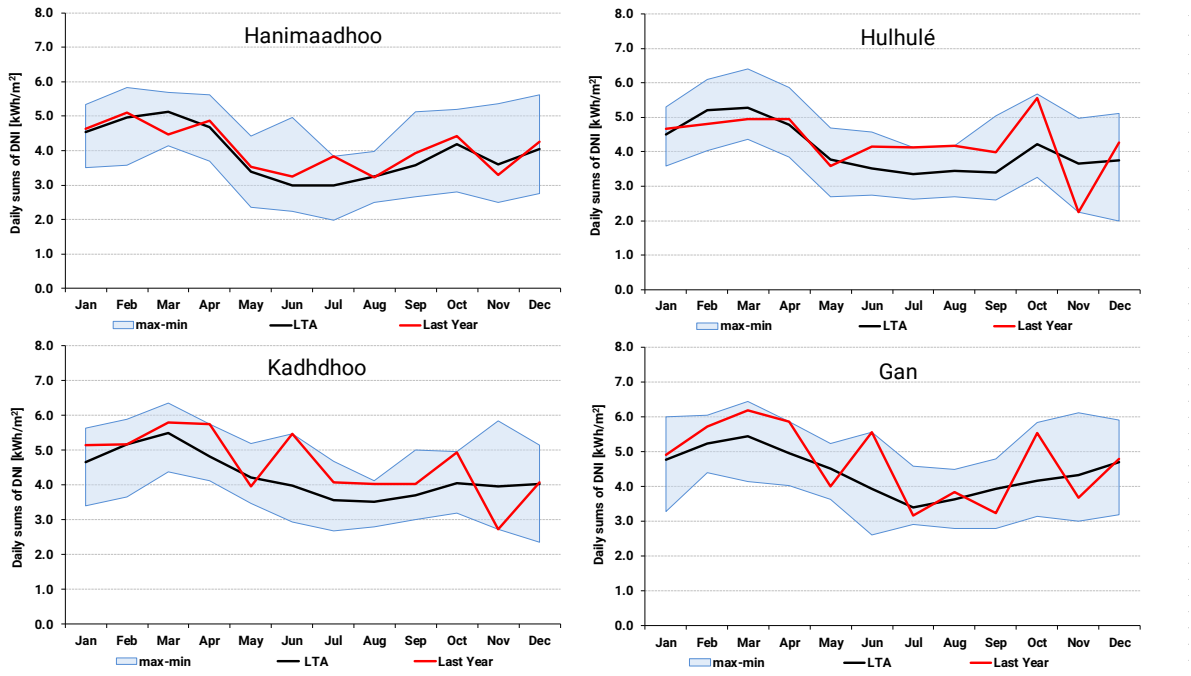

Figure V: DNI monthly averages [kWh/m^2].
Monthly average shown as solid line; min/max monthly values as boundary lines; last 24 months shown in red.

© 2018 Solargis

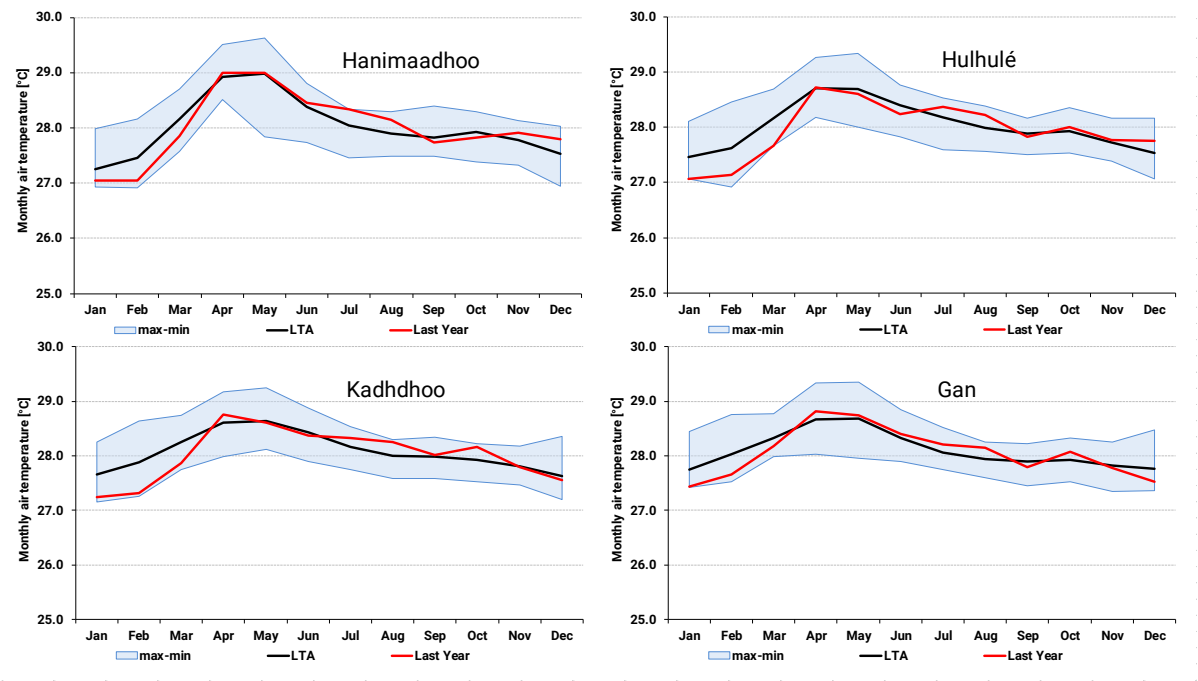

Figure VI: TEMP monthly averages [°C].
Monthly average shown as solid line; min/max monthly values as boundary lines; last 24 months shown in red.

Frequency of occurrence of GHI and DNI daily model values for a period 1999 to 2017

The histograms below show occurrence statistics of daily values derived from the satellite-based time series for GHI and DNI. The time covered in the graphs below is 19 complete calendar years (1999 to 2017). The occurrence is calculated separately for each month.

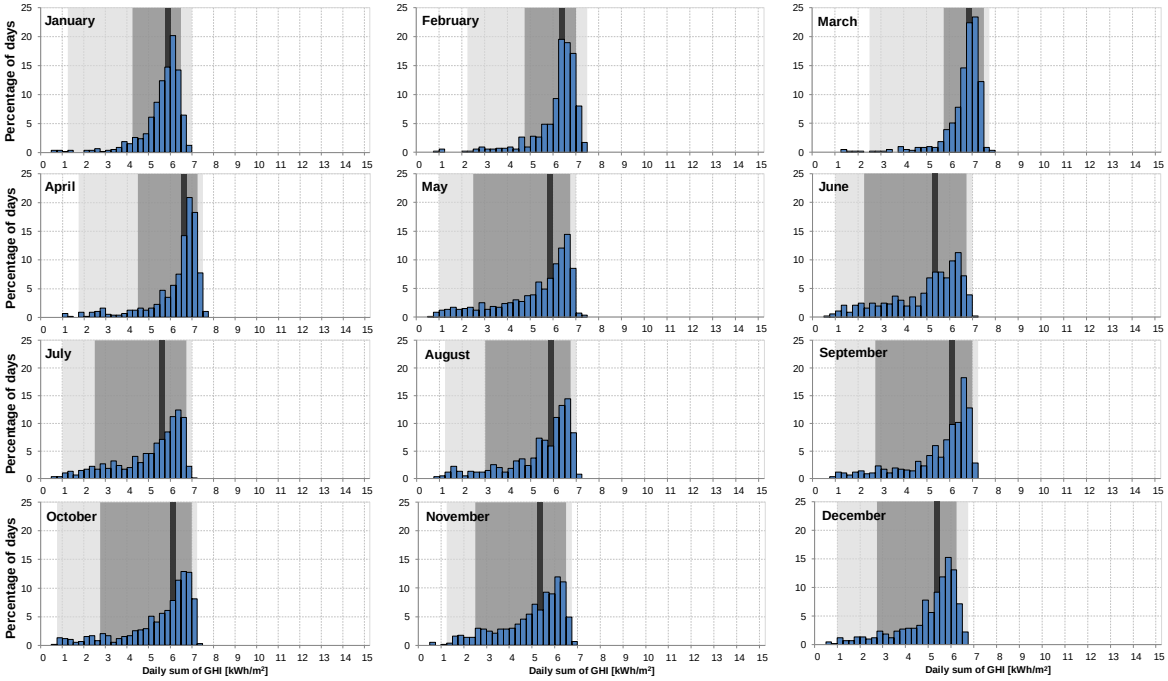

Figure VII: Histograms of daily summaries of Global Horizontal Irradiation in Hanimaadhoo.

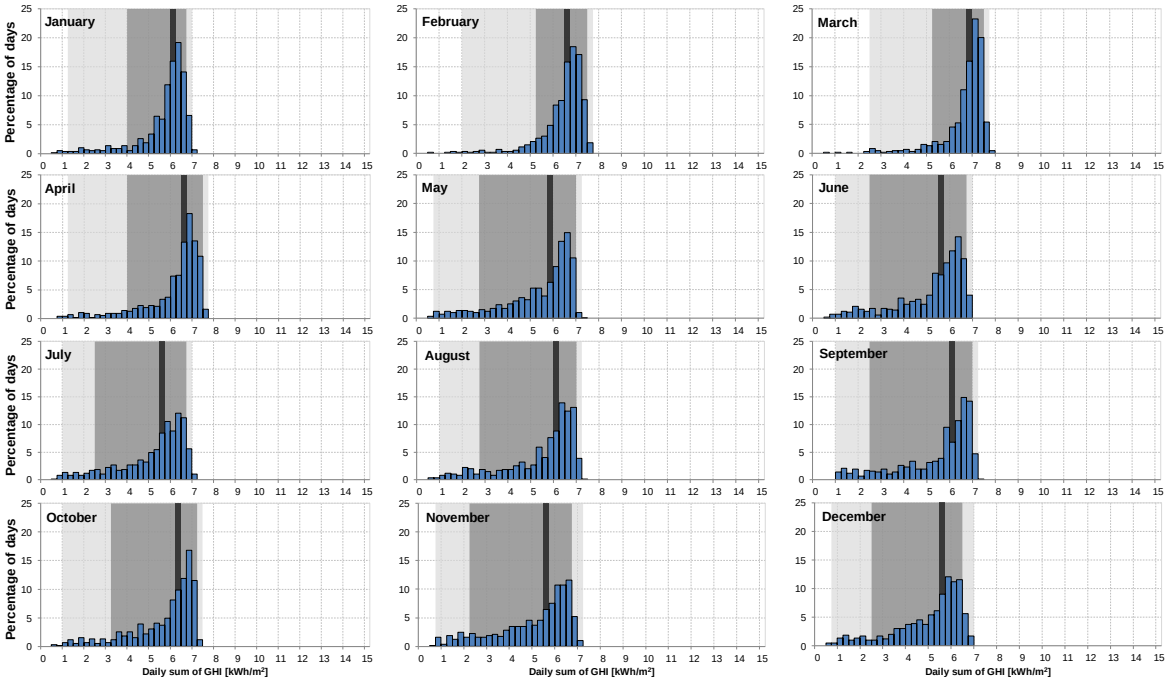

Figure VIII: Histograms of daily summaries of Global Horizontal Irradiation in Hulhulé.

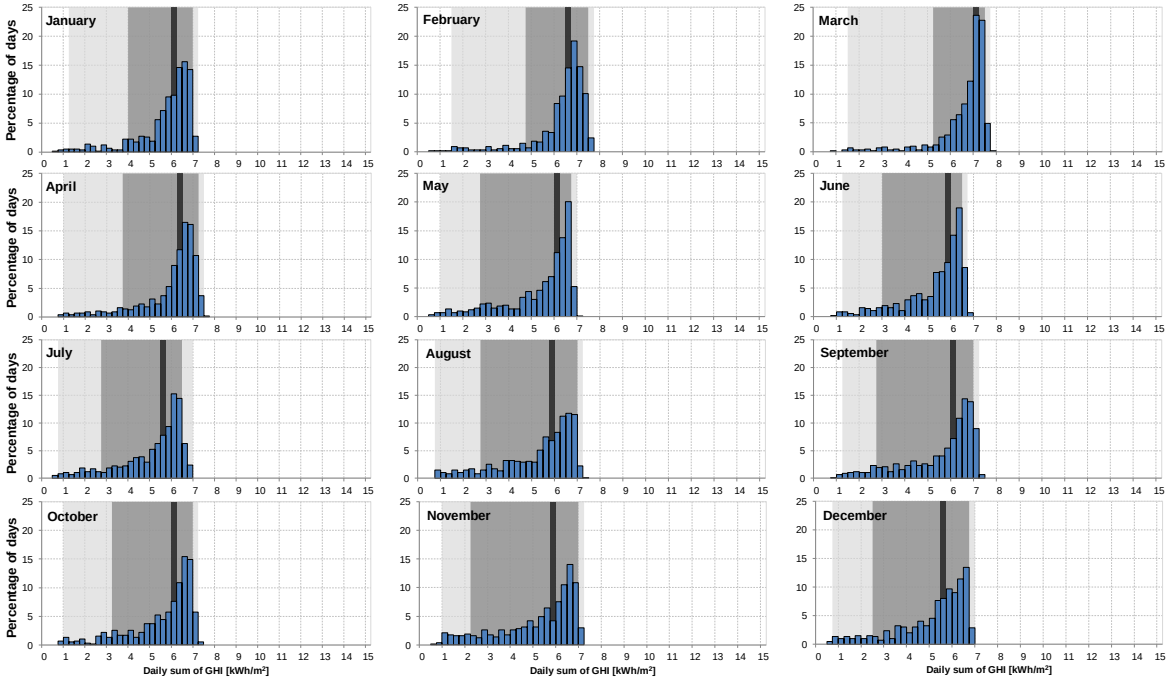

Figure IX: Histograms of daily summaries of Global Horizontal Irradiation in Kadhdhoo.

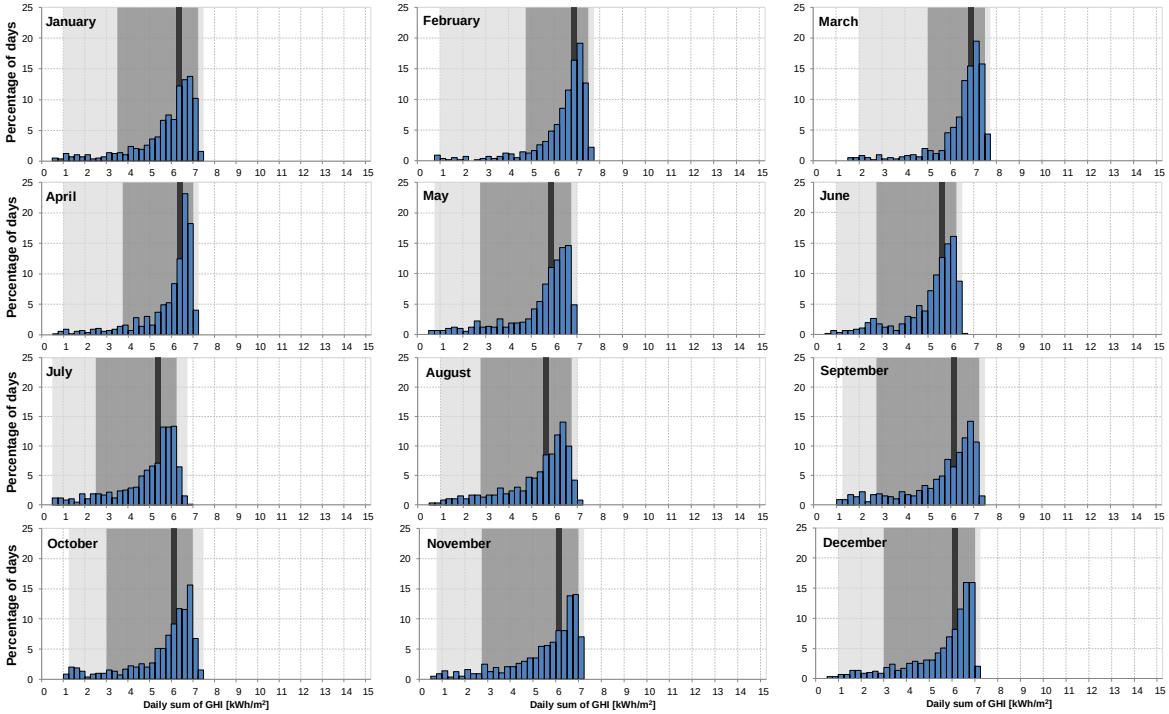

Figure X: Histograms of daily summaries of Global Horizontal Irradiation in Gan.

Figures VII to X show histograms of **daily GHI** summaries for each month as calculated from Solargis time series representing the years 1999 to 2017. The distribution of daily values is not symmetric: median is drawn by the vertical line, and percentiles P_{10}, P_{25}, and P_{75}, and P_{90} are displayed with dark grey and light grey colour bands, respectively. The percentiles P_{10} and P_{90} show 80% occurrence of daily values within each month and percentiles P_{25} and P_{75} show 50% occurrence.

© 2018 Solargis

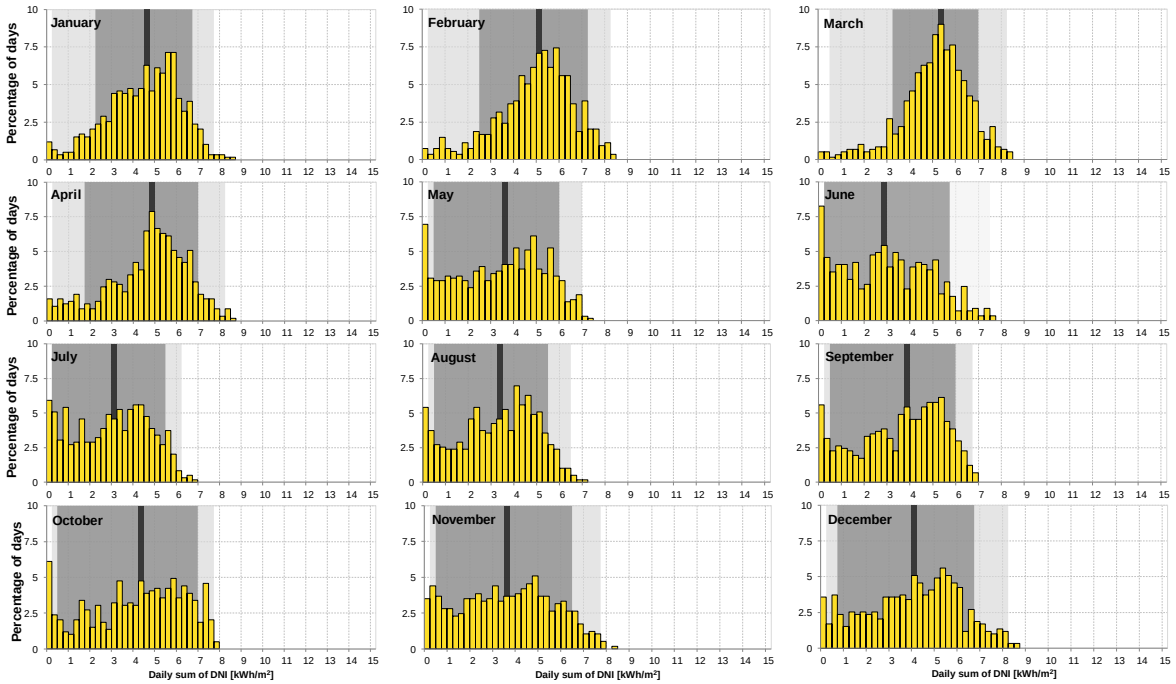

Figure XI: Histograms of daily summaries of Direct Normal Irradiation in Hanimaadhoo.

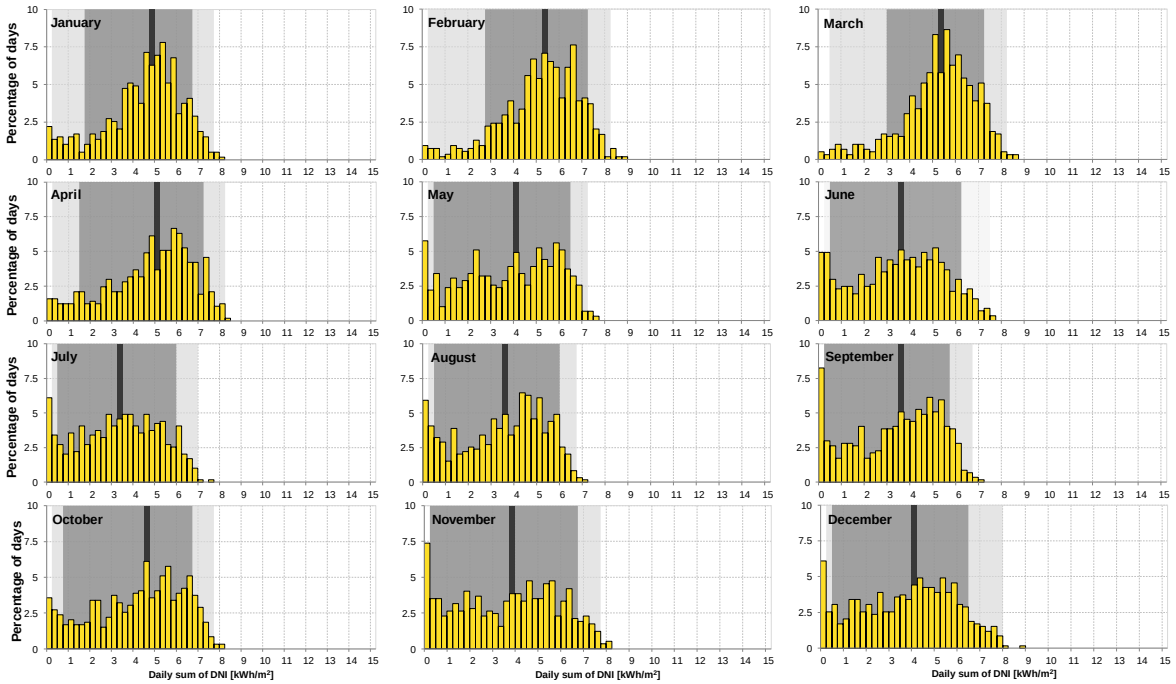

Figure XII: Histograms of daily summaries of Direct Normal Irradiation in Hulhulé.

© 2018 Solargis

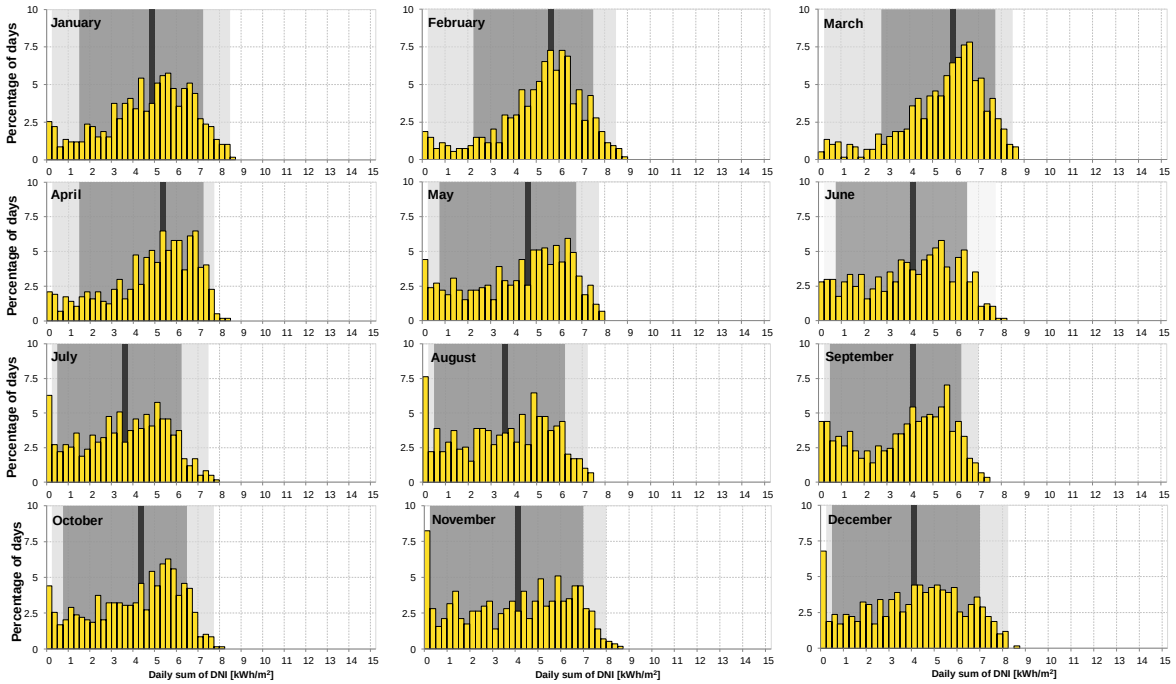

Figure XIII: Histograms of daily summaries of Direct Normal Irradiation in Kadhdhoo.

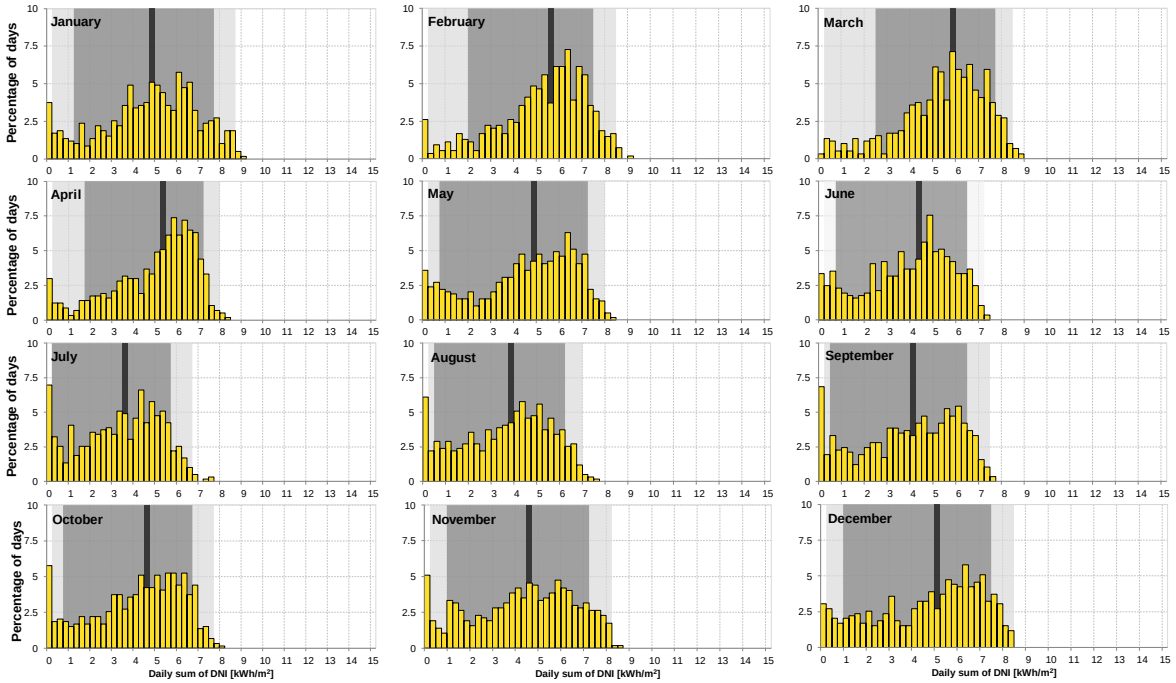

Figure XIV: Histograms of daily summaries of Direct Normal Irradiation in Gan.

Figures XI to XIV show histograms of **daily DNI** summaries for each month as calculated from Solargis time series representing the years 1999 to 2017. The distribution of daily values is not symmetric: median is drawn by the vertical line, and percentiles P_{10}, P_{25}, and P_{75}, and P_{90} are displayed with dark grey and light grey colour bands, respectively. The percentiles P_{10} and P_{90} show 80% occurrence of daily values within each month and percentiles P_{25} and P_{75} show 50% occurrence.

© 2018 Solargis

Frequency of occurrence of GHI and DNI 30-minute model values for a period 1999 to 2017

The histograms below show occurrence statistics of 30-minute values derived from the satellite-based time series for GHI and DNI. The time covered in the graphs below is 19 complete calendar years (1999 to 2017). The occurrence is calculated separately for each month.

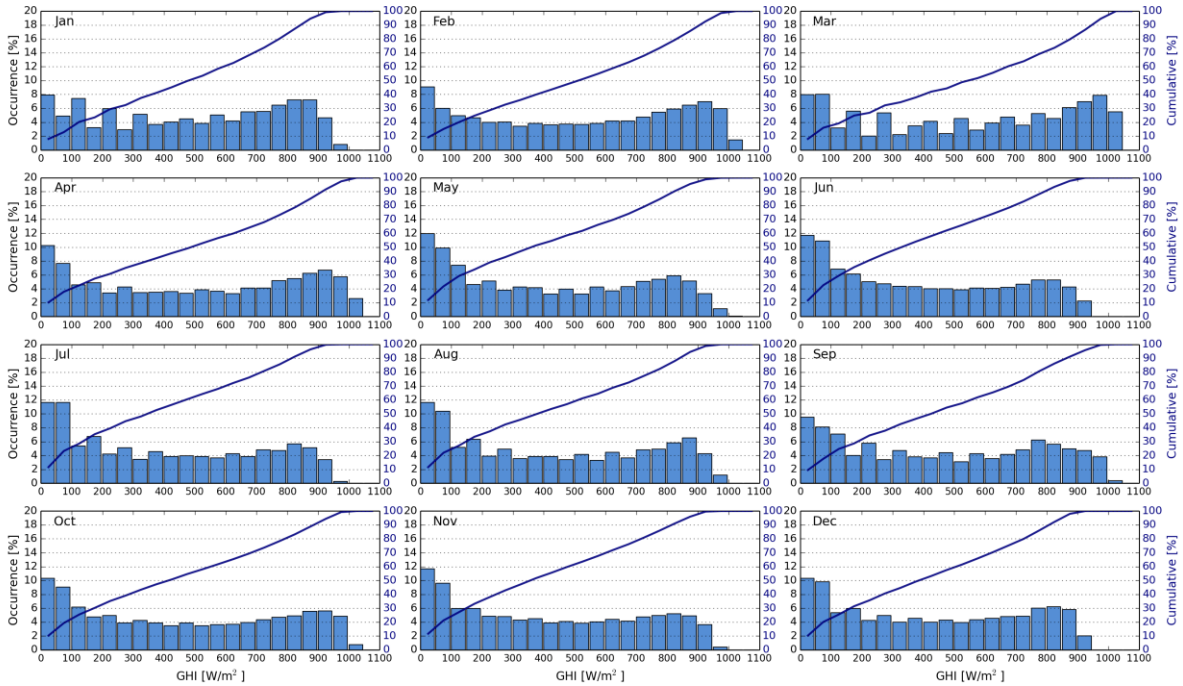

Figure XV: Histograms and cumulative distribution function of 30-minute GHI in Hanimaadhoo

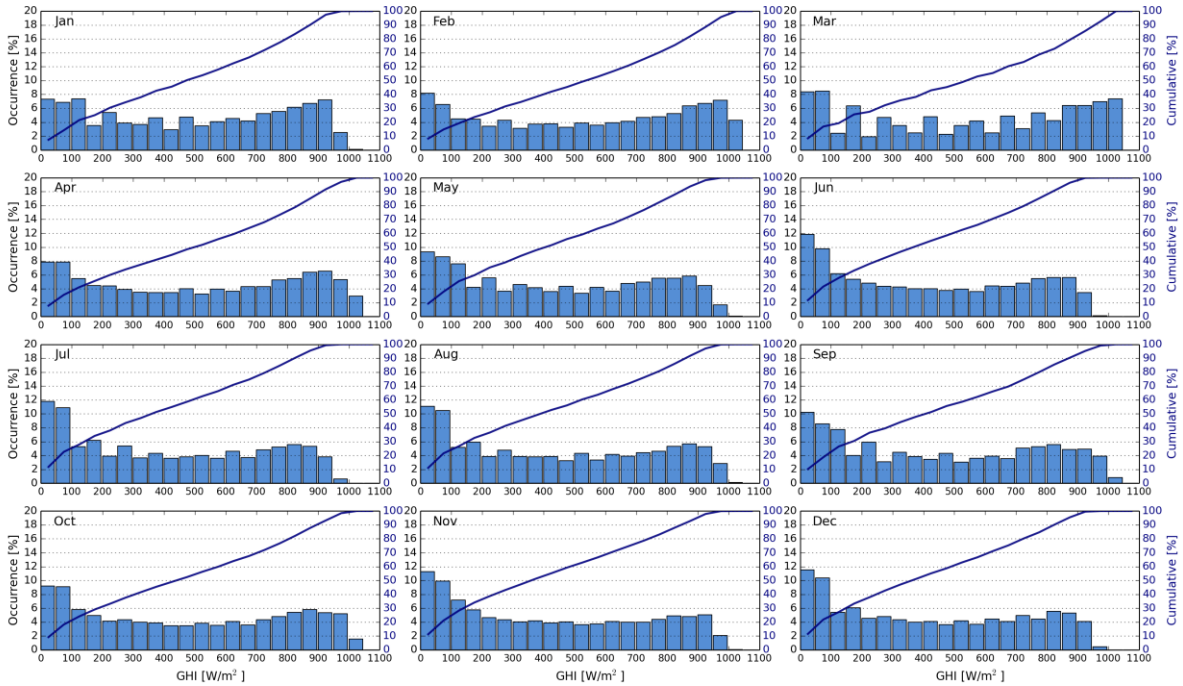

Figure XVI: Histograms and cumulative distribution function of 30-minute GHI in Hulhulé

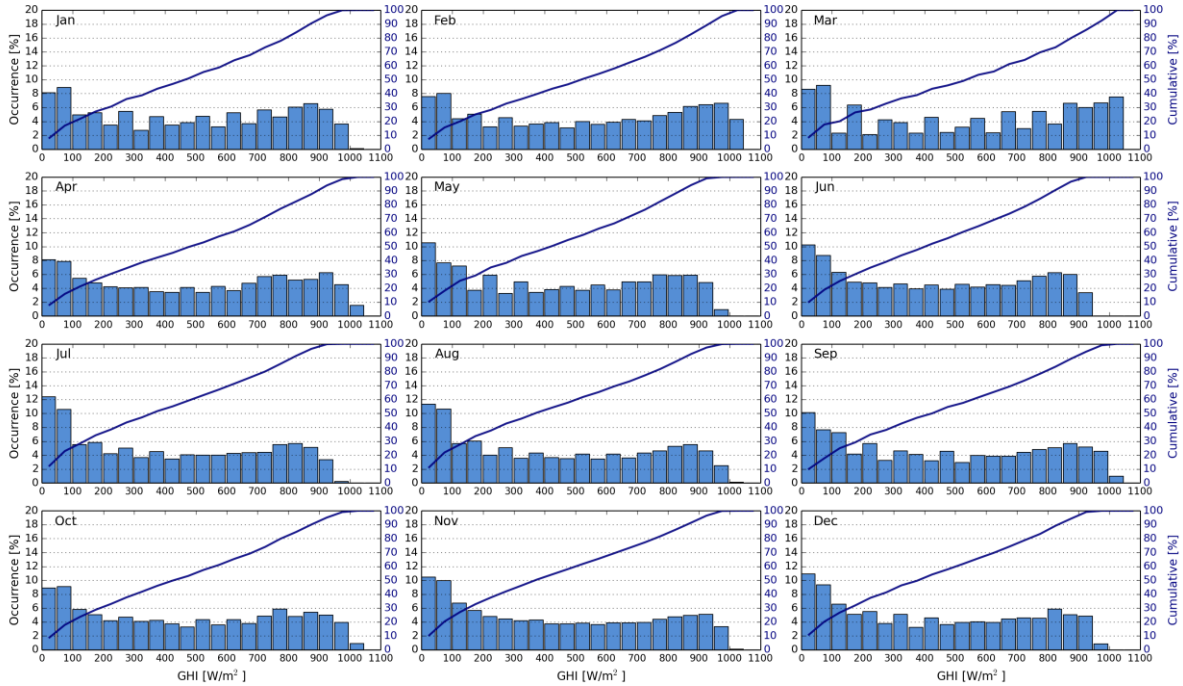

Figure XVII: Histograms and cumulative distribution function of 30-minute GHI in Kadhdhoo

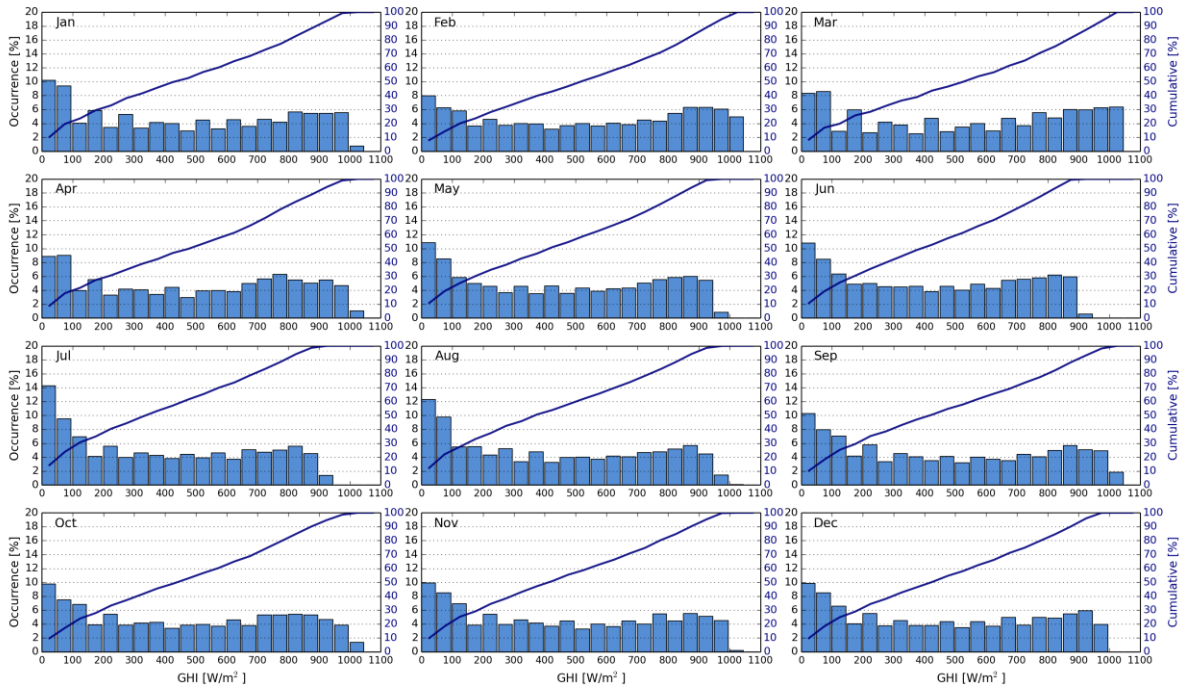

Figure XVIII: Histograms and cumulative distribution function of 30-minute GHI in Gan

Figures XV to XVIII show monthly histograms (bars) and cumulative distribution (line) of 30-minute GHI values, calculated from Solargis time series. The values represent the occurrence of GHI values within 50 W/m^2 bins, ranging from 0 to 1200 W/m^2.

© 2018 Solargis

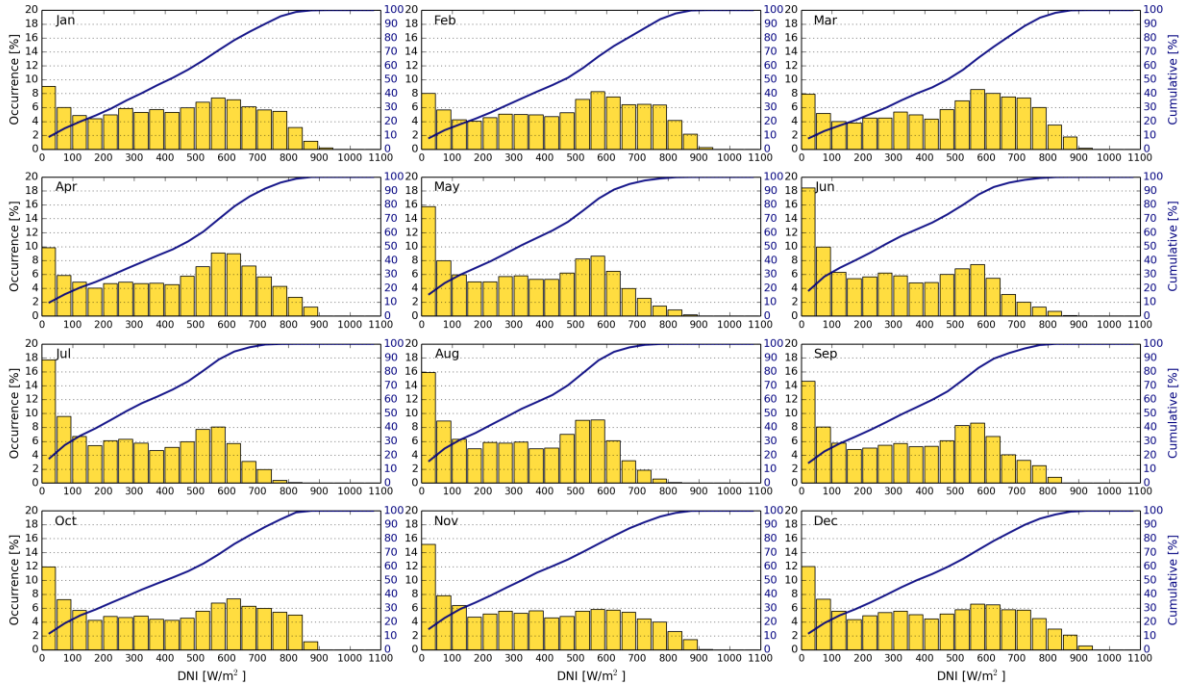

Figure XIX: Histograms and cumulative distribution function of 30-minute DNI in Hanimaadhoo

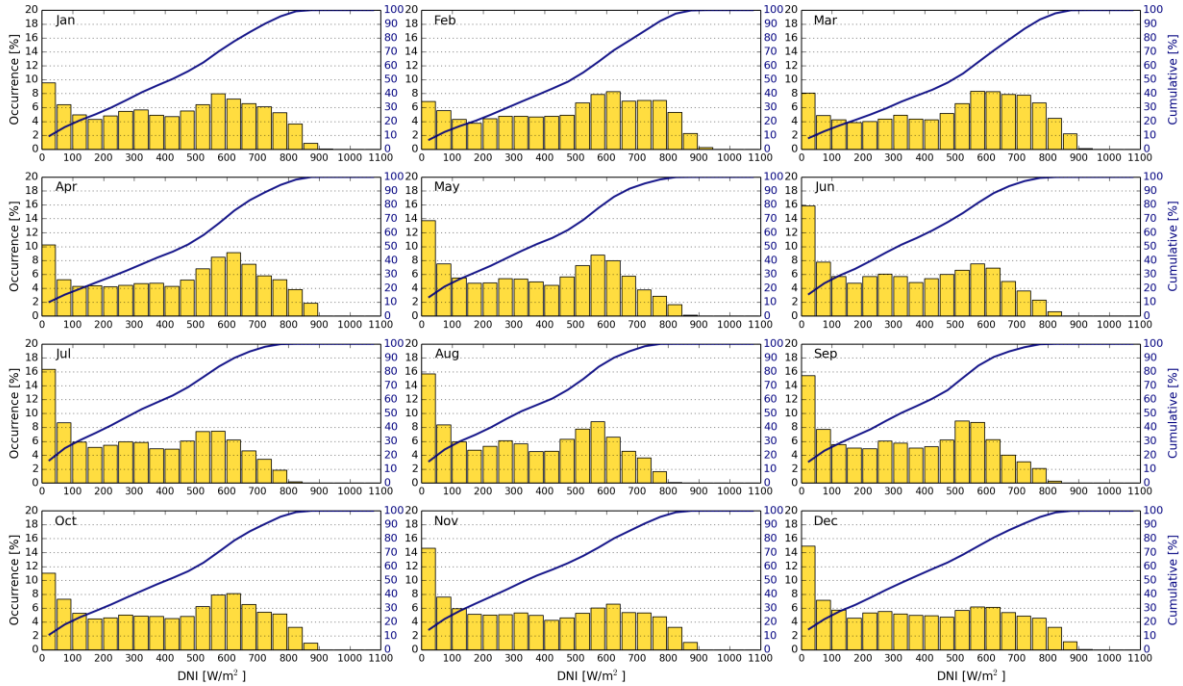

Figure XX: Histograms and cumulative distribution function of 30-minute DNI in Hulhulé

© 2018 Solargis

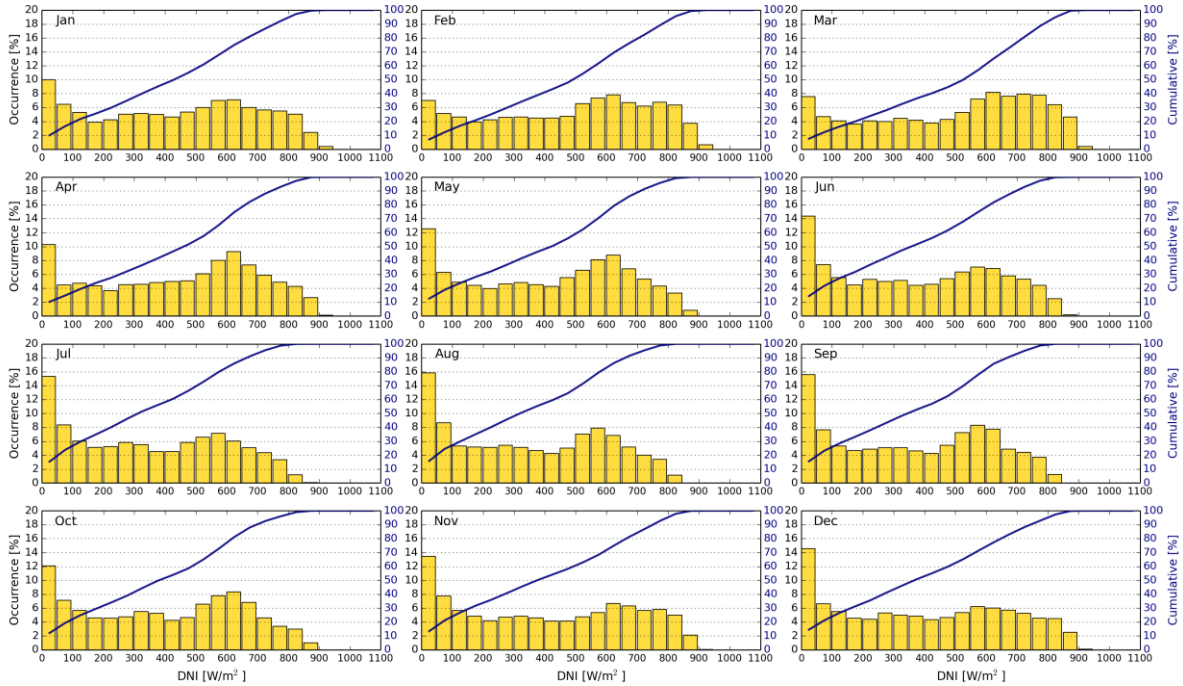

Figure XXI: Histograms and cumulative distribution function of 30-minute DNI in Kadhdhoo

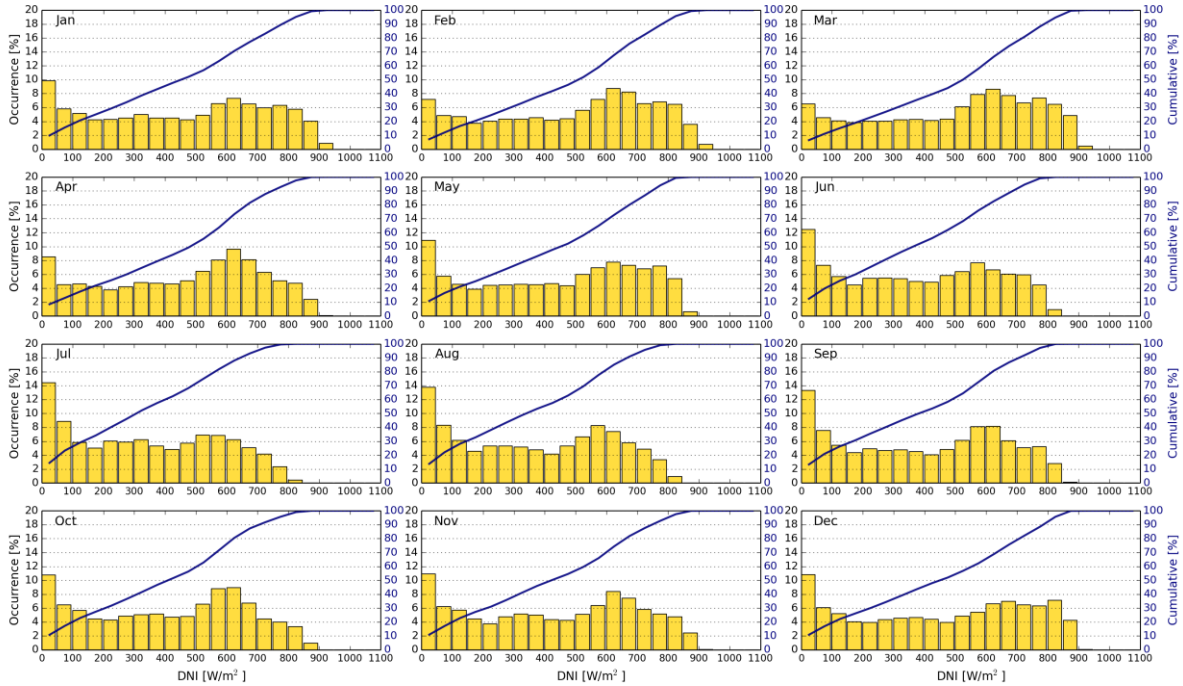

Figure XXII: Histograms and cumulative distribution function of 30-minute DNI in Gan

Figures XIX to XXII show monthly histograms (bars) and cumulative distribution (line) of 30-minute DNI values, calculated from Solargis time series. The values represent the occurrence of DNI values within 50 W/m^2 bins, ranging from 0 to 1200 W/m^2.

© 2018 Solargis

Frequency of occurrence of GHI and DNI measured and model values representing two years of ground measurements

Figures XXIII to XXX show histograms comparing the measured values with the model GHI and DNI data. The period covered in these histogram is last 24-months (two full years of data, i.e. from 1 Jan 2016 to 31 Dec 2017):

- 1-minute measured vs. 30-min satellite-based model values
- 30-minute measured (aggregated from 1-min) vs. 30-min satellite-based values
- Daily measured (aggregated from 1-min) vs. daily satellite-based model values

Aggregation process deals with the missing values in the ground measurement in three steps:

1. Only those 1-minute measured data values that passed through quality control (Chapter 3.3) is taken into account (satellite time series does not have gaps.);
2. Aggregation of 1-minute measured data values into 30-minute slots (equivalent to satellite time slots) is applied if more than 15 valid data-points is available, otherwise the 30-minute data slot is ignored in further statistical comparison;
3. Daily aggregation of measured data represents the same 30-minute time slots in a day (passing through the two steps above), as those in the satellite-based data. Incorrect data slots found in the measurements are excluded in both the measured and model data.

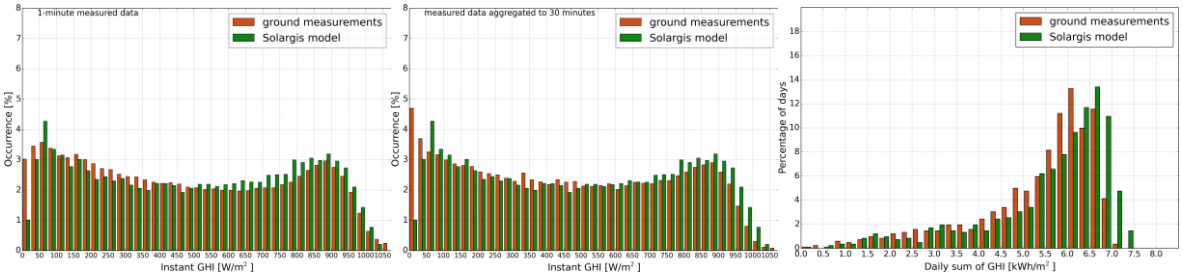

Figure XXIII: Measured vs. satellite-based GHI values in Hanimaadhoo
1-minute measured vs. 30-min satellite-based values.
30-minute measured (aggregated from 1-min) vs. 30-min satellite-based values
Daily measured (aggregated from 1-min) vs. daily satellite-based values

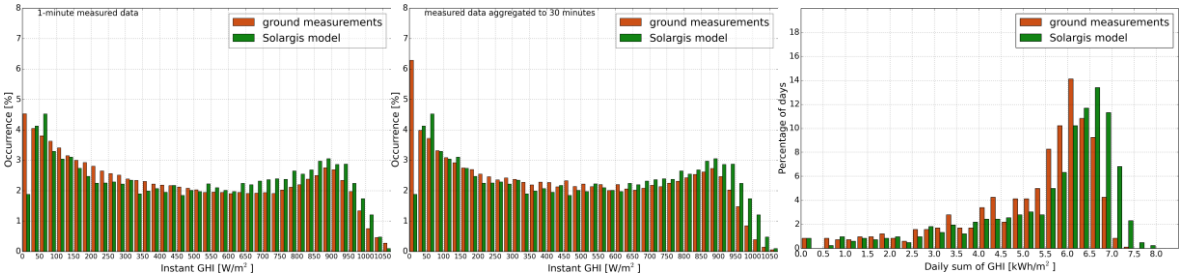

Figure XXIV: Measured vs. satellite-based GHI values in Hulhulé
1-minute measured vs. 30-min satellite-based values.
30-minute measured (aggregated from 1-min) vs. 30-min satellite-based values
Daily measured (aggregated from 1-min) vs. daily satellite-based values

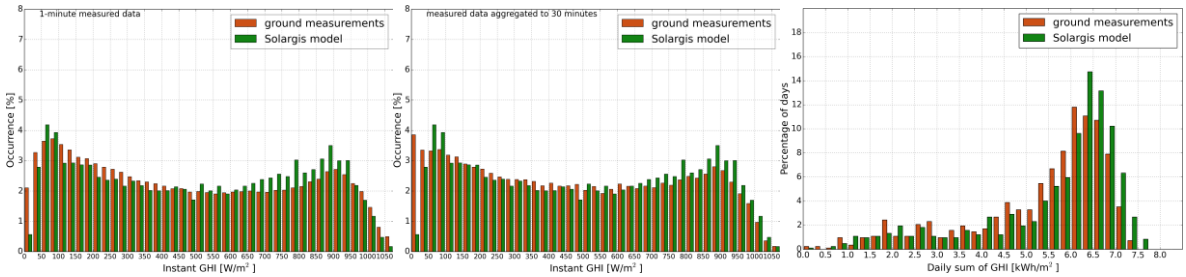

Figure XXV: Measured vs. satellite-based GHI values in Kadhdhoo
1-minute measured vs. 30-min satellite-based values.
30-minute measured (aggregated from 1-min) vs. 30-min satellite-based values
Daily measured (aggregated from 1-min) vs. daily satellite-based values

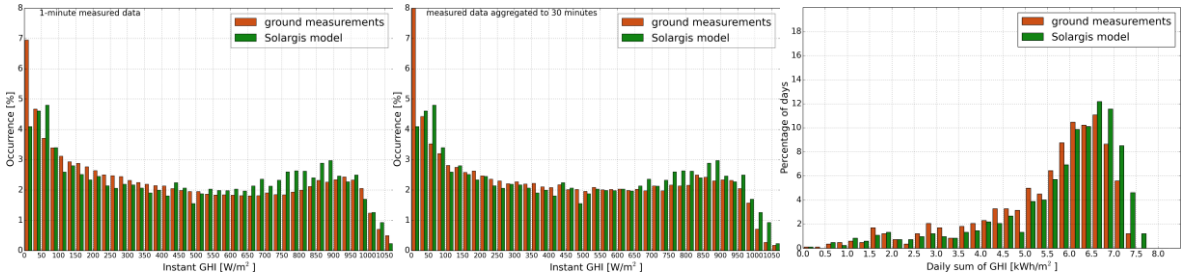

Figure XXVI: Measured vs. satellite-based GHI values in Gan
1-minute measured vs. 30-min satellite-based values.
30-minute measured (aggregated from 1-min) vs. 30-min satellite-based values
Daily measured (aggregated from 1-min) vs. daily satellite-based values

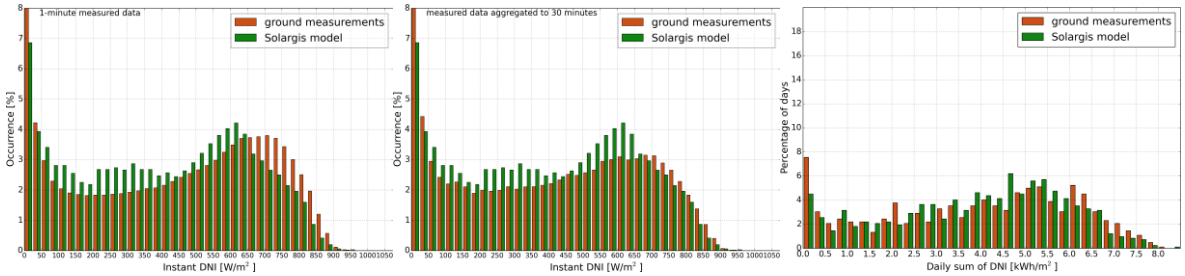

Figure XXVII: Measured vs. satellite-based DNI values in Hanimaadhoo
1-minute measured vs. 30-min satellite-based values.
30-minute measured (aggregated from 1-min) vs. 30-min satellite-based values
Daily measured (aggregated from 1-min) vs. daily satellite-based values

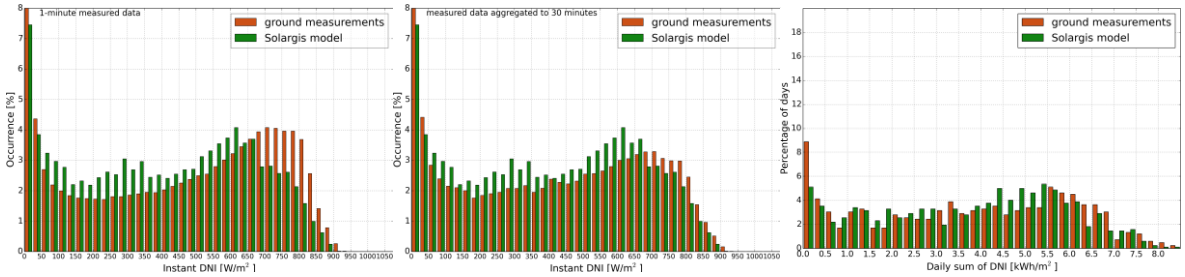

Figure XXVIII: Measured vs. satellite-based DNI values in Hulhulé
1-minute measured vs. 30-min satellite-based values.
30-minute measured (aggregated from 1-min) vs. 30-min satellite-based values
Daily measured (aggregated from 1-min) vs. daily satellite-based values

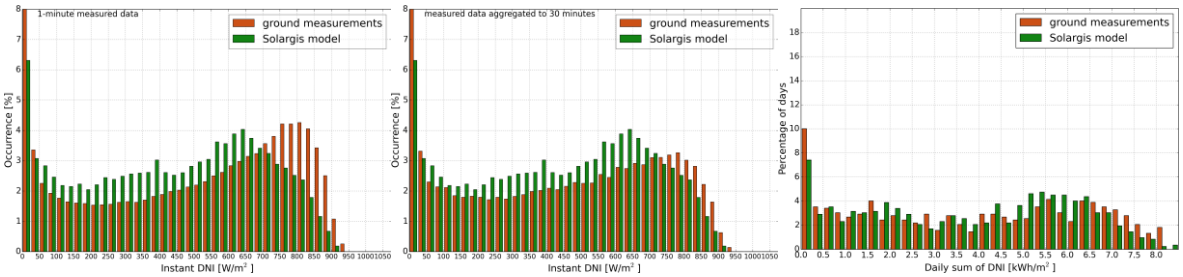

Figure XXIX: Measured vs. satellite-based DNI values in Kadhdhoo
1-minute measured vs. 30-min satellite-based values.
30-minute measured (aggregated from 1-min) vs. 30-min satellite-based values
Daily measured (aggregated from 1-min) vs. daily satellite-based values

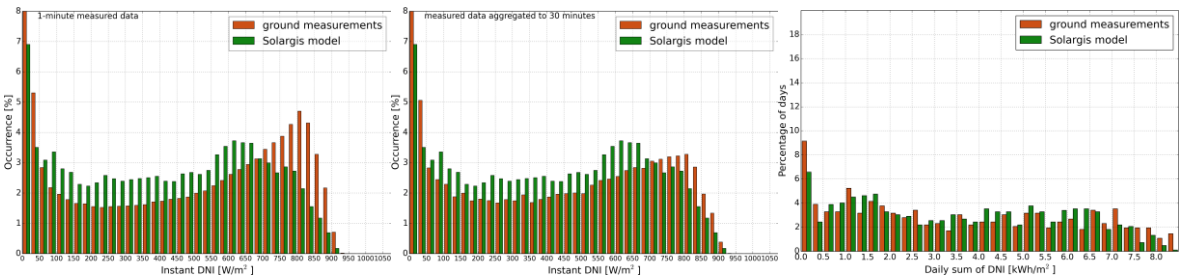

Figure XXX: Measured vs. satellite-based DNI values in Gan
1-minute measured vs. 30-min satellite-based values.
30-minute measured (aggregated from 1-min) vs. 30-min satellite-based values
Daily measured (aggregated from 1-min) vs. daily satellite-based values

© 2018 Solargis

Frequency of occurrence of GHI and DNI ramps

Figures XXXI to XXXVIII show histograms of instantaneous changes (ramps) calculated from the measurements and compared to the instantaneous changes calculated for the model data. Figures show both negative (-) and positive (+) changes. Two versions for GHI and DNI are shown:

- Ramps calculated from 1-minute measured values compared to ramps calculated from 30-minute satellite-based data (figure on the left)
- Ramps calculated from 30-minute aggregated valid measurement compared to ramps calculated from 30-minute satellite-based data (figure on the right).

Occurrence of gaps in the measurements is managed in the same way as described about in this Chapter:

1. For measurements, only those 1-minute data values (measurements) that passed through quality control (Chapter 3.3) is taken into account (satellite time series does not have gaps.);
2. For measurements, the aggregation (averaging) of 1-minute measured data values into 30-minute slots (equivalent to satellite time slots) is applied if more than 15 valid data-points is available, otherwise the 30-minute data slot is ignored in further statistical comparison;

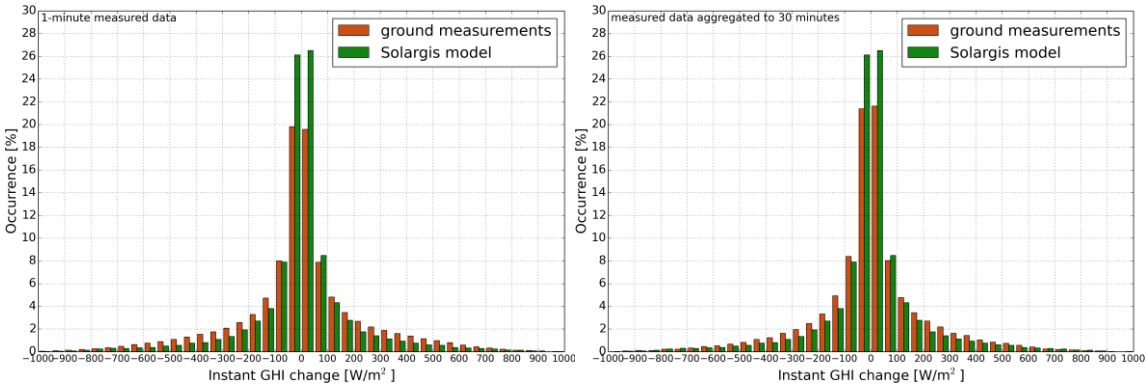

Figure XXXI: 1-minute and 30-minute GHI ramps (measured and satellite data) at Hanimaadhoo.

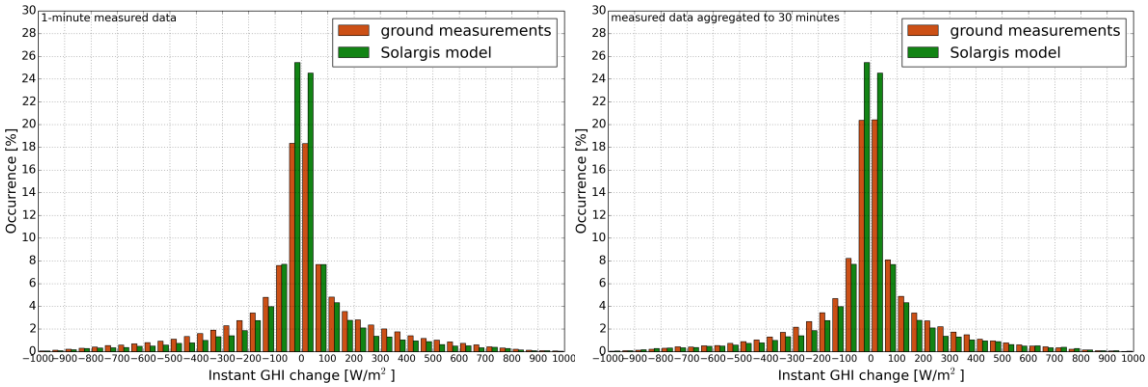

Figure XXXII: 1-minute and 30-minute GHI ramps (measured and satellite data) at Hulhulé

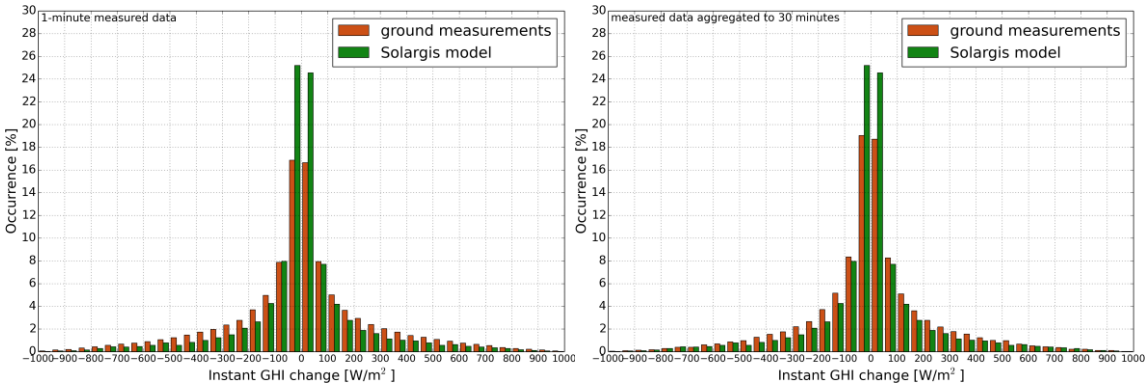

Figure XXXIII: 1-minute and 30-minute GHI ramps (measured and satellite data) at Kadhdhoo

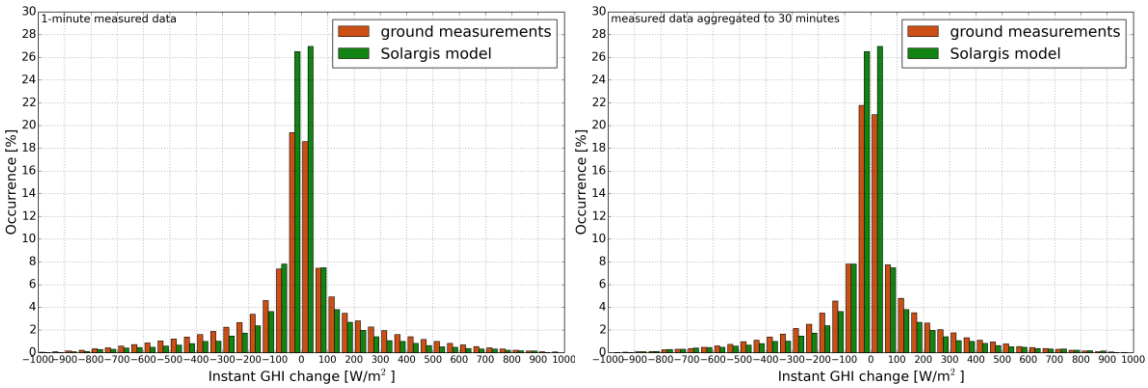

Figure XXXIV: 1-minute and 30-minute GHI ramps (measured and satellite data) at Gan

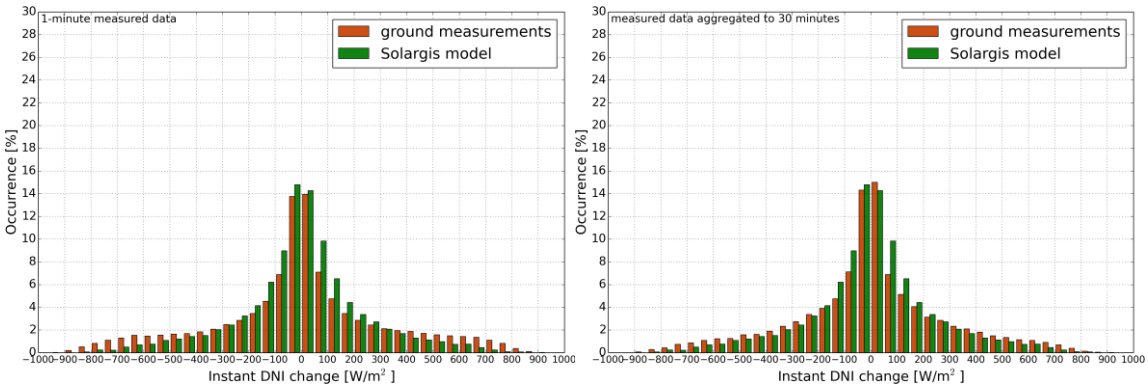

Figure XXXV: 1-minute and 30-minute DNI ramps (measured and satellite data) at Hanimaadhoo

© 2018 Solargis

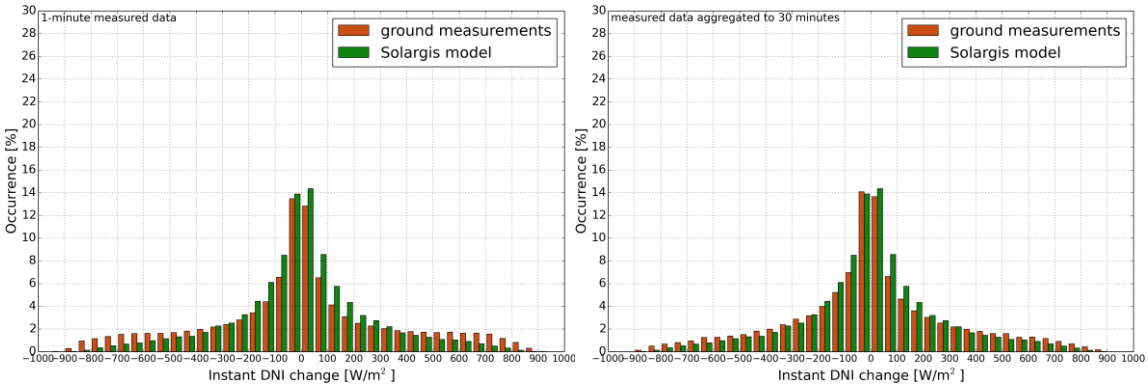

Figure XXXVI: 1-minute and 30-minute DNI ramps (measured and satellite data) at Hulhulé

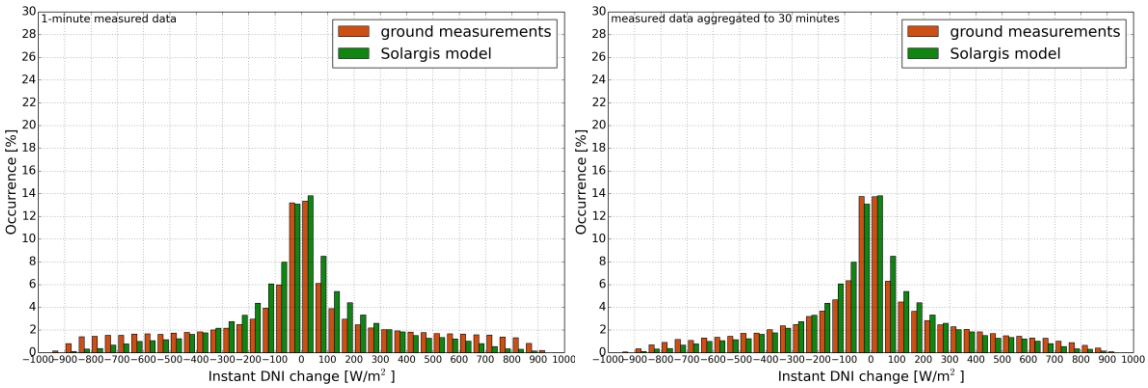

Figure XXXVII: 1-minute and 30-minute DNI ramps (measured and satellite data) at Kadhdhoo

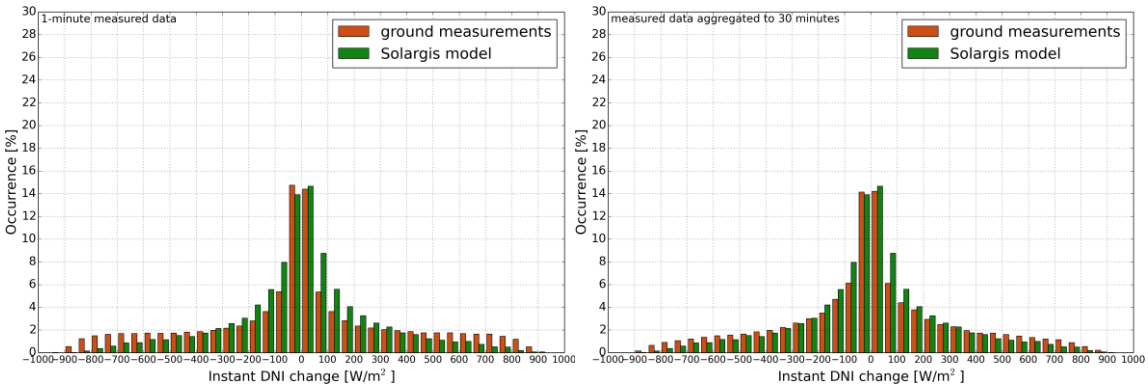

Figure XXXVIII: 1-minute and 30-minute DNI ramps (measured and satellite data) at Gan

LIST OF FIGURES

Figure 2.1: Position of solar meteorological stations in Maldives 11
Figure 3.1 Results of DNI and GHI quality control in Hanimaadhoo. 19
Figure 3.2 Systematic difference between GHI from SR20 and RSP – Hanimaadhoo. 20
Figure 3.3 Results of DNI and GHI quality control in Hulhulé. 22
Figure 3.4 Effect of RSP shadowband issues – drop of DNI in Hulhulé. 23
Figure 3.5 Systematic difference between GHI from SR20 and RSP - Hulhulé. 23
Figure 3.6 Results of DNI and GHI quality control – Kadhdhoo. 26
Figure 3.7 Effect of RSP shadowband issues – drop of DNI in Kadhdhoo. 27
Figure 3.8 Systematic difference between GHI from SR20 and RSP – Kadhdhoo. 27
Figure 3.9 Results of DNI and GHI quality control – Gan. 30
Figure 3.10 Effect of RSP shadowband issues – drop of DNI in Gan. 31
Figure 3.11 Systematic difference between GHI from SR20 and RSP - Gan. 31
Figure 3.12 Replacement of SR20 GHI by RSP GHI due to wind mast shading in Gan. 32
Figure 4.1: Sites with solar meteorological stations used for site adaptation of Solargis model in Maldives 37
Figure 4.2: Correction of DNI and GHI hourly values for Hanimaadhoo. 41
Figure 4.3: Correction of DNI and GHI hourly values for Hulhulé 42
Figure 4.4: Correction of DNI and GHI hourly values for Kadhdhoo. 43
Figure 4.5: Correction of DNI and GHI hourly values for Gan. 44
Figure 4.6: Comparison of Solargis original and site-adapted data for Hanimaadhoo site. 45
Figure 5.1: Scatterplots of air temperature at 2 m at Hanimaadhoo meteorological station. 47
Figure 5.2: Scatterplots of air temperature at 2 m at Hulhulé meteorological station. 48
Figure 5.3: Scatterplots of air temperature at 2 m at Kadhdhoo meteorological station. 48
Figure 5.4: Scatterplots of air temperature at 2 m at Gan meteorological station. 49
Figure 5.5: Scatterplots of relative humidity at 2 m at Hanimaadhoo meteorological station. 50
Figure 5.6: Scatterplots of relative humidity at 2 m at Hulhulé meteorological station. 50
Figure 5.7: Scatterplots of relative humidity at 2 m at Kadhdhoo meteorological station. 51
Figure 5.8: Scatterplots of relative humidity at 2 m at Gan meteorological station. 51
Figure 5.9: Scatterplots of wind speed at Hanimaadhoo meteorological station. 52
Figure 5.10: Scatterplots of wind speed at Hulhulé meteorological station. 53
Figure 5.11: Scatterplots of wind speed at Kadhdhoo meteorological station. 53
Figure 5.12: Scatterplots of wind speed at Gan meteorological station. 54
Figure 6.1: Expected Pxx values for GHI at Hulhulé Airport 61
Figure 6.2: Expected Pxx values for DNI at Hulhulé Airport 61
Figure 7.1: GHI monthly values derived from time series and TMY P50 and P90 64
Figure 7.2: DNI monthly values derived from time series and TMY P50 and P90 65
Figure 7.3: DIF monthly values derived from time series and TMY P50 and P90 65
Figure 7.4: TEMP monthly values derived from time series and TMY P50 and P90 65
Figure 7.5: Seasonal profile of GHI, DNI and DIF for Typical Meteorological Year P50 66
Figure 7.6: Snapshot of Typical Meteorological Year for P50 for Hulhulé 67
Figure I: Interannual variability of site-adapted yearly GHI [kWh/m^2]. 69

© 2018 Solargis

Figure II: Interannual variability of site-adapted yearly DNI [kWh/m^2]. 69
Figure III: Interannual variability of yearly TEMP [°C]. 70
Figure IV: GHI monthly averages [kWh/m^2]. 71
Figure V: DNI monthly averages [kWh/m^2]..... 71
Figure VI: TEMP monthly averages [°C]. 72
Figure VII: Histograms of daily summaries of Global Horizontal Irradiation in Hanimaadhoo. 73
Figure VIII: Histograms of daily summaries of Global Horizontal Irradiation in Hulhulé. 73
Figure IX: Histograms of daily summaries of Global Horizontal Irradiation in Kadhdhoo. 74
Figure X: Histograms of daily summaries of Global Horizontal Irradiation in Gan. 74
Figure XI: Histograms of daily summaries of Direct Normal Irradiation in Hanimaadhoo. 75
Figure XII: Histograms of daily summaries of Direct Normal Irradiation in Hulhulé. 75
Figure XIII: Histograms of daily summaries of Direct Normal Irradiation in Kadhdhoo. 76
Figure XIV: Histograms of daily summaries of Direct Normal Irradiation in Gan. 76
Figure XV: Histograms and cumulative distribution function of 30-minute GHI in Hanimaadhoo 77
Figure XVI: Histograms and cumulative distribution function of 30-minute GHI in Hulhulé 77
Figure XVII: Histograms and cumulative distribution function of 30-minute GHI in Kadhdhoo 78
Figure XVIII: Histograms and cumulative distribution function of 30-minute GHI in Gan 78
Figure XIX: Histograms and cumulative distribution function of 30-minute DNI in Hanimaadhoo 79
Figure XX: Histograms and cumulative distribution function of 30-minute DNI in Hulhulé 79
Figure XXI: Histograms and cumulative distribution function of 30-minute DNI in Kadhdhoo 80
Figure XXII: Histograms and cumulative distribution function of 30-minute DNI in Gan 80
Figure XXIII: Measured vs. satellite-based GHI values in Hanimaadhoo 81
Figure XXIV: Measured vs. satellite-based GHI values in Hulhulé 81
Figure XXV: Measured vs. satellite-based GHI values in Kadhdhoo 82
Figure XXVI: Measured vs. satellite-based GHI values in Gan 82
Figure XXVII: Measured vs. satellite-based DNI values in Hanimaadhoo 82
Figure XXVIII: Measured vs. satellite-based DNI values in Hulhulé 82
Figure XXIX: Measured vs. satellite-based DNI values in Kadhdhoo 83
Figure XXX: Measured vs. satellite-based DNI values in Gan 83
Figure XXXI: 1-minute and 30-minute GHI ramps (measured and satellite data) at Hanimaadhoo. 84
Figure XXXII: 1-minute and 30-minute GHI ramps (measured and satellite data) at Hulhulé 84
Figure XXXIII: 1-minute and 30-minute GHI ramps (measured and satellite data) at Kadhdhoo 85
Figure XXXIV: 1-minute and 30-minute GHI ramps (measured and satellite data) at Gan 85
Figure XXXV: 1-minute and 30-minute DNI ramps (measured and satellite data) at Hanimaadhoo 85
Figure XXXVI: 1-minute and 30-minute DNI ramps (measured and satellite data) at Hulhulé 86
Figure XXXVII: 1-minute and 30-minute DNI ramps (measured and satellite data) at Kadhdhoo 86
Figure XXXVIII: 1-minute and 30-minute DNI ramps (measured and satellite data) at Gan 86

© 2018 Solargis

LIST OF TABLES

Table 1.1 Delivered data characterstics ... 9
Table 1.2 Parameters in the delivered site-adapted time series and TMY data (hourly time step) ... 10
Table 2.1 Overview information on the solar meteorological stations installed in Maldives ... 12
Table 3.1 Overview information on measurement stations operated in the region ... 13
Table 3.2 Instruments installed at the solar meteorological stations ... 13
Table 3.3 Technical parameters and accuracy class of the instruments ... 13
Table 3.4 Overview information on solar meteorological stations operating in the region ... 14
Table 3.5 Data recovery statistics of the two-year measurement campaign period ... 14
Table 3.6 Data recovery statistics of the measurement campaign period including prolongation ... 15
Table 3.7 Period of measurements analysed in this report ... 15
Table 3.8 Meteorological stations maintenance and instruments field verification ... 15
Table 3.9 Occurrence of data readings for Hanimaadhoo meteorological station ... 17
Table 3.10 Excluded ground measurements after quality control (Sun above horizon) in Hanimaadhoo ... 17
Table 3.11 Quality control summary – Hanimaadhoo ... 20
Table 3.12 Occurrence of data readings for Hulhulé meteorological station ... 21
Table 3.13 Excluded ground measurements after quality control (Sun above horizon) in Hulhulé ... 21
Table 3.14 Quality control summary – Hulhulé ... 24
Table 3.15 Occurrence of data readings for Kadhdhoo meteorological station ... 25
Table 3.16 Excluded ground measurements after quality control (Sun above horizon) in Kadhdhoo ... 25
Table 3.17 Quality control summary – Kadhdhoo ... 28
Table 3.18 Occurrence of data readings for Gan meteorological station ... 29
Table 3.19 Excluded ground measurements after quality control (Sun above horizon) in Gan ... 29
Table 3.20 Quality control summary – Gan ... 32
Table 3.21 Updated re-calibration schedule proposed by Suntrace ... 34
Table 3.22 Overview of instruments to be re-calibrated and/or exchanged ... 35
Table 4.1 Input data used in the Solargis and related GHI and DNI outputs for Maldives ... 36
Table 4.2 Direct Normal Irradiance: bias and KSI before and after model site-adaptation ... 39
Table 4.3 Global Horizontal Irradiance: bias and KSI before and after model site-adaptation ... 40
Table 4.4 Direct Normal Irradiance: RMSD before and after model site-adaptation ... 40
Table 4.5 Global Horizontal Irradiance: RMSD before and after model site-adaptation ... 40
Table 4.6 Comparison of long term average of yearly summaries of original and site-adapted values ... 45
Table 5.1 Original source of Solargis meteorological data: models CFSR and CFSv2 ... 46
Table 5.2 Solargis meteorological parameters delivered within this project ... 46
Table 5.3 Air temperature at 2 m: accuracy indicators of the model outputs [°C] ... 47
Table 5.4 Relative humidity: accuracy indicators of the model outputs [%] ... 49
Table 5.5 Wind speed: accuracy indicators of the model outputs [m/s] ... 52
Table 5.6 Expected uncertainty of modelled meteorological parameters at the project site ... 55
Table 6.1 Uncertainty of the model estimates for original and site-adapted annual long-term values ... 56
Table 6.2 Annual GHI that should be exceeded with 90% probability in the period of 1 to 10 (25) years ... 57
Table 6.3 Annual DNI that should be exceeded with 90% probability in the period of 1 to 10 (25) years ... 58

© 2018 Solargis

Table 6.4 Combined probability of exceedance of annual GHI for uncertainty of the estimate ±3.0%. 59
Table 6.5 Combined probability of exceedance of annual DNI for uncertainty of the estimate ±6.0%. 60
Table 7.1 Delivered data characteristics 62
Table 7.2 Parameters in the delivered site-adapted time series and TMY data (hourly time step) 62
Table 7.3 Monthly and yearly long-term GHI averages as calculated from time series and from TMY 63
Table 7.4 Monthly and yearly long-term DNI averages as calculated from time series and from TMY 64
Table 7.5 Monthly and yearly long-term DIF averages as calculated from time series and from TMY 64
Table 7.6 Monthly and yearly long-term TEMP averages as calculated from time series and from TMY 64

© 2018 Solargis

REFERENCES

[1] NREL, 1993. User's Manual for SERI_QC Software-Assessing the Quality of Solar Radiation Data. NREL/TP-463-5608. Golden, CO: National Renewable Energy Laboratory.

[2] Younes S., Claywell R. and Muneer T, 2005. Quality control of solar radiation data: Present status and proposed new approaches. Solar Energy 30, 1533-1549.

[3] Perez R., Cebecauer T., Šúri M., 2013. Semi-Empirical Satellite Models. In Kleissl J. (ed.) Solar Energy Forecasting and Resource Assessment. Academic press. http://www.sciencedirect.com/science/article/pii/B9780123971777000024

[4] Cebecauer T., Šúri M., Perez R., High performance MSG satellite model for operational solar energy applications. ASES National Solar Conference, Phoenix, USA, 2010. http://solargis.com/assets/publication/2010/Cebecauer-Suri-Perez--ASES2010--High-performance-MSG-satellite-model-for-operational-solar-energy-applications.pdf

[5] Šúri M., Cebecauer T., Perez P., 2010. Quality Procedures of Solargis for Provision Site-Specific Solar Resource Information. Conference SolarPACES 2010, September 2010, Perpignan, France. http://solargis.com/assets/publication/2010//Suri-Cebecaue--Perez-SolarPACES2010--Quality-procedures-of-solargis-for-provision-site-specific-solar-resource-information.pdf

[6] Cebecauer T., Suri M., Gueymard C., Uncertainty sources in satellite-derived Direct Normal Irradiance: How can prediction accuracy be improved globally? Proceedings of the SolarPACES Conference, Granada, Spain, 20-23 Sept 2011.

http://solargis.com/assets/publication/2011/Cebecauer-Suri-Gueymard--SolarPACES2011--Uncertainty-sources-in-satellite-derived-direct-normal-irradiance--How-can-prediction-accuracy-be-improved-globally.pdf

[7] Suri M., Cebecauer T., 2014. Satellite-based solar resource data: Model validation statistics versus user's uncertainty. ASES SOLAR 2014 Conference, San Francisco, 7-9 July 2014. http://solargis.com/assets/publication/2014//Suri-Cebecauer--ASES-Solar2014--Satellite-Based-Solar-Resource-Data--Model-Validation-Statistics-Versus-User-Uncertainty.pdf

[8] Ineichen P., A broadband simplified version of the Solis clear sky model, 2008. Solar Energy, 82, 8, 758-762.

[9] Benedictow A. et al. 2012. Validation report of the MACC reanalysis of global atmospheric composition: Period 2003-2010, MACC-II Deliverable D83.1.

[10] Molod, A., Takacs, L., Suarez, M., and Bacmeister, J., 2015: Development of the GEOS-5 atmospheric general circulation model: evolution from MERRA to MERRA2, Geosci. Model Dev., 8, 1339-1356, doi:10.5194/gmd-8-1339-2015

[11] GFS model. http://www.nco.ncep.noaa.gov/pmb/products/gfs/

[12] CFSR model. https://climatedataguide.ucar.edu/climate-data/climate-forecast-system-reanalysis-cfsr/

[13] CFSv2 model http://www.cpc.ncep.noaa.gov/products/CFSv2/CFSv2seasonal.shtml

[14] Cano D., Monget J.M., Albuisson M., Guillard H., Regas N., Wald L., 1986. A method for the determination of the global solar radiation from meteorological satellite data. Solar Energy, 37, 1, 31–39.

[15] Perez R., Ineichen P., Maxwell E., Seals R. and Zelenka A., 1992. Dynamic global-to-direct irradiance conversion models. ASHRAE Transactions-Research Series, pp. 354-369.

[16] Perez, R., Seals R., Ineichen P., Stewart R., Menicucci D., 1987. A new simplified version of the Perez diffuse irradiance model for tilted surfaces. Solar Energy, 39, 221-232.

[17] Ruiz-Arias J.A., Cebecauer T., Tovar-Pescador J., Šúri M., 2010. Spatial disaggregation of satellite-derived irradiance using a high-resolution digital elevation model. Solar Energy, 84,1644-57. http://www.sciencedirect.com/science/article/pii/S0038092X10002136

[18] Zelenka A., Perez R., Seals R., Renne D., 1997. Effective Accuracy of Satellite-Derived Hourly Irradiances. Theoretical Appl. Climatology, 62, 199-207.

[19] Espinar B., Ramírez L., Drews A., Beyer H. G., Zarzalejo L. F., Polo J., Martín L., Analysis of different comparison parameters applied to solar radiation data from satellite and German radiometric stations. Solar Energy, 83, 1, 118-125, 2009.

© 2018 Solargis

[20] Lohmann S., Schillings C., Mayer B., Meyer R., 2006. Long-term variability of solar direct and global radiation derived from ISCCP data and comparison with reanalysis data, Solar Energy, 80, 11, 1390-1401.

[21] Gueymard C., Solar resource assessment for CSP and CPV. Leonardo Energy webinar, 2010. http://www.leonardo-energy.org/webfm_send/4601

[22] Cebecauer T., Šúri M., 2015. Typical Meteorological Year Data: Solargis Approach. Energy Procedia, Volume 69, 1958-1969. http://dx.doi.org/10.1016/j.egypro.2015.03.195

[23] Meyer, R., Butron, J. T., Marquard, G., Schwandt, M., Geuder, N., Hoyer-Klick, C., et al. (2008). Combining solar irradiance measurements and various satellite-derived products to a site-specific best estimate. In 14th biennial SolarPACES Symposium. Retrieved from http://elib.dlr.de/53849/

[24] Jessen, W., Wilbert, S., Nouri, B., Geuder, N., & Fritz, H. (2016). Calibration methods for rotating shadowband irradiometers and optimizing the calibration duration. Atmospheric Measurement Techniques, 9(4), 1601–1612. https://doi.org/10.5194/amt-9-1601-2016

[25] Wilbert, S., Röger, M., Csambor, J., Breitbach, M., Klinger, F., Nouri, B., et al. (2017). Sunshape Measurements with Conven-tional Rotating Shadowband Irradiometers. In Proc. of the SolarPACES Conference 2017 (p. 8). Santiago, Chile: SolarPACES

[26] Lezaca, J., Meyer, R., & Heinemann, D. (2018). Towards an in-situ calibration of Rotating Shadowband Irradiometers (RSI) using simultaneous pyranometer measurements. In Proc. of the SolarPACES Conference 2017 (p. 10). Santiago, Chile: SolarPACES, reviewed and accepted for publication

© 2018 Solargis

SUPPORT INFORMATION

Background on Solargis

Solargis is a technology company offering energy-related meteorological data, software and consultancy services to solar energy. We support industry in the site qualification, planning, financing and operation of solar energy systems for more than 18 years. We develop and operate a new generation high-resolution global database and applications integrated within Solargis® information system. Accurate, standardised and validated data help to reduce the weather-related risks and costs in system planning, performance assessment, forecasting and management of distributed solar power.

ISO 9001
LL-C (Certification)

Solargis is ISO 9001:2015 certified company for quality management.

This report has been prepared by Tomas Cebecauer, Marcel Suri, Branislav Schnierer, Nada Suriova, Juraj Betak, and Artur Skoczek from Solargis

All maps in this report are prepared by Solargis

Solargis s.r.o., Mytna 48, 811 07 Bratislava, Slovakia

Reference No. (Solargis): 129-08/2018

http://solargis.com

© 2018 Solargis